Dynamic Maximum Power Point Tracking and Robust Voltage Regulation for Photovoltaic Systems

Written by

©Rasool Kahani

A Thesis Submitted to the School of Graduate Studies in partial fulfillment of the requirements for the degree of

Master of Engineering

Faculty of Engineering and Applied Science
Memorial University of Newfoundland

January 2023

St. John's Newfoundland and Labrador Canada

Abstract

This research proposes a Maximum Power Point Tracking (MPPT) and voltage regulation method based on model reference adaptive control (MRAC). The MPPT algorithm which is presented in this work is a modified perturb and observe (P&O) algorithm. The new algorithm prevents oscillation around maximum power point (MPP) by approximating the peak of photovoltaic (PV) array power curve. This goal is achieved by comparing the change in output power during each cycle with change in array terminal power during the previous cycle. When array terminal power decreases following an increase in the previous cycle or the opposite, a decrease in array terminal power is followed by an increase, it means the power curve has reached its peak. Therefore, the duty cycle of the boost converter should remain the same. When irradiance changes, the proposed technique produces an MPPT algorithm's average efficiency (η_{MPPT}) of nearly 3.1 percent greater than the conventional P&O and the Incremental conductance (InC) algorithm. In addition, under strong partial shading conditions (PSC) and drift avoidance tests, the proposed technique produces an average η_{MPPT} of nearly 9 percent and 8 percent greater than the conventional algorithms, respectively. To inject the generated PV power into the grid with high quality, this work designs voltage regulation controller based on MRAC to ensure the output voltage of the PV system is at the desired level. To achieve this goal, we propose a DC–DC boost converter that stabilizes output voltage variations by using MIT rule controllers. An output voltage is stabilized using two control loops, PID controllers are capable of regulating output voltage at fixed levels, and for the outer loop, it's intended to implement the direct model reference adaptive controller (DMRAC) MIT rule. In comparison with DC–DC boost converters connected to the micro-grid (MG), the controller presented here, manages disturbances and unknown parameter fluctuations more effectively. The proposed controller and the model are tested in MATLAB/SIMULINK for load

disturbances. The load was changed by ~50% of its original value, and the worst-case settling time and maximum overshoot were less than ~0.1 s and 0.5 V (0.3%), respectively. Comparison with the PID methods, the lowest overshoot among three different PID tuning methods, namely the Ziegler–Nichol's frequency-domain method, damped oscillation method, and Good Gain method, is 34%. Therefore, it is evident from results that the proposed algorithm has better performance in dealing with the maximum overshoot issues. The hardware validation is also carried out to show the performance of the proposed controller.

Acknowledgments

I want to express my sincere gratitude to my supervisor Dr. Mohsin Jamil, whose immense knowledge and expertise in electrical power and renewable energy proved to be generous support and a great help throughout my master's degree. He was very helpful, accommodating, and responsive whenever I turned to him for advice regarding my research. His support during COVID-19 times in terms of being flexible was the one that allowed me to carry out my research work without feeling overwhelmed.

I also would like to thank my co-supervisor Dr. Iqbal, for his support. This support enabled me to utilize all my efforts in research without concern about achieving my goals.

Moreover, I want to thank the School of Graduate Studies, Engineering, and Applied Sciences department, and all my teachers at Memorial University of Newfoundland, class fellows.

Finally, I want to thank my wife, who has always been my encouragement and go-to person throughout my life so far; her inspiration kept me floating even during these difficult times.

Table of Contents

List of Tables

List of Figures

List of Abbreviations and Symbols

PV	Photovoltaic
MATLAB	Matrix Laboratory
DMRAC	Direct Model References Adaptive Controller
MPPT	Maximum Power Point Tracking
MPP	Maximum power point
P&O	Perturb and Observe
InC	Incremental Conductance
HC	Hill Climbing
PSC	Partial Shading Condition
MG	Micro-grid
PVG	Photovoltaic Generator
PSO	Particle Swarm Optimization
GA	Genetic Algorithms
ANN	Artificial Neural Networks
FLBC	Fuzzy Logic-Based Controllers
VSS	Variable Step Size
DPGM	Derated Power Generation Mode
ZVS	Zero Voltage Switching
IBC	Interleaved Boost Converter
GWO	Grey Wolf Optimization

Chapter 1

Introduction

1.1 Introduction

Among the most popular renewable energy, solar photovoltaic (PV) systems are, easy to install, and require little maintenance. A PV power generation system converts solar energy into electricity. Irradiation and temperature can affect PV power, however. Due to the poor conversion efficiency of solar panels, solar electricity remains more expensive than fossil fuels. Maximum power point tracking (MPPT) is well known as one of the main solutions to increase efficiency in PV systems. A variety of control techniques are presented in numerous papers pertaining to PV MPPT. In general, they can be divided into two categories: conventional and soft computing.

The most popular algorithms are conventional algorithms due to their ease of implementation and low cost. Consequently, most scientists recommend modifying conventional approaches over complex modern theories because they are easier to apply. Although traditional methods are easy to use, they respond slowly to changes in ambient temperature or solar radiation power. Among traditional MPPTs, perturb and observe (P&O) has excellent convergence and is the simplest.

There are, however, two significant flaws in the algorithm. First, there is constant oscillation in the vicinity of the maximum power point (MPP). As a second consideration, if the irradiance increases rapidly or is not uniform partial shading condition (PSC), the P&O tends to lose its orientation

when tracking. Consequently, the system's deviation from its MPP results in a power loss that is proportional to the size of the installed solar array [1].

Besides, the power maximizing issue for PV systems, there is voltage regulation problem when they are getting connected to the grid. Due to the low system inertia and fast changes in the output power of solar power sources, frequency and voltage can vary greatly from nominal operating conditions.

When we have a DC grid, the DC–DC converters are the most significant part of the system. Many DC–DC converter topologies, such as the boost topology, the buck topology, buck-boost converters, and single-ended primary inductor converter (SEPIC) topology [2, 3], have been discussed in the literature. DC–DC boost converters are the simplest converters for effective reproduction of output amplification for a given input voltage. Many applications have been developed using it, including those related to the automotive industry, power amplifications, adaptive control applications, battery power systems, robotics, wind power, and PV systems [4].

1.2 Literature Review

1.2.1 A background discussion of MPPT algorithms

Several studies have been carried out on conventional MPPT methods such as P&O [5], [6], [7], incremental conductance (InC) algorithm [8], [9], and a hill-climbing (HC) algorithm [10], [11]. Besides conventional algorithms, there are many other solutions, such as bioinspired algorithms, which are much more efficient in some special cases when compared to conventional ones. They are capable enough to quickly converge to a global maximum and hence can save power loss even in a partially shaded environment [12]. Particle swarm optimization (PSO) is a bioinspired

algorithm that is employed successfully in [13]. A genetic algorithm (GA) is one such algorithm that solves the obstacle of partial shading [14], [15]. Moreover, there are two artificial intelligence (AI) based algorithms, fuzzy logic-based controllers (FLBCs) and artificial neural network (ANN)-based MPPT [16], [17]. Although the mentioned algorithms show less settling time, less overshoot, and better performance about MPPT, they require data set in the beginning to train the input-output relation. In [18], [19], a sliding mode and Lyapunov function-based algorithms were presented for achieving MPPT control of a solar-PV array tied with the grid. In addition, nonlinear optimal feedback control is employed in [1] to deal with oscillations around the MPP of the system. Although there exist various techniques in the literature that try to improve the drawbacks of conventional MPPT approaches, they are substantially slower, and the implementation is still in priority when control methods are put into practice. As the conventional MPPT algorithms are suitable for low-cost applications, easier to implement, and need lower data set, there are many works tried to modify the conventional algorithms in the case of PSC [20-23] and drift avoidance issues [24-25]. Complex computations and large memory requirements are the drawbacks of mentioned works. Moreover, they are not multi-purpose solutions and only consider specific issues such as: drift effect or PSC or slow and fast irradiation changes of conventional algorithms.

1.2.2 An overview of converters and voltage regulation of PV systems

Many studies compare different types of converters' performances. In [26], research has been conducted over step-up DC–DC converters in various configurations. In [27], the authors analyzed boost and SEPIC converters, considering output voltage ripple, total harmonic distortion, power factor for both converters, and boost converters produced better results. Besides mentioned features, boost converters are easier to use. So, the boost-type converter is frequently used because of its superior performance. In this research, we use MOSFET as a switch that can consistently

turn ON and OFF based on the generated duty cycle, because the voltage drop across the MOSFET, when on, is lower than the voltage drop across a BJT.

Because the converters display poor voltage regulation and inadequate dynamic response when run in an open loop, they are often equipped with closed-loop control for output voltage regulation [28]. Due to the nonlinear dynamics of boost converters and non-minimum phase (NMP) behavior, controller design for boost converters is more complex and challenging than for buck converters.

Many control techniques have been presented to regulate the switch ON/OFF (duty cycle) to achieve the required output voltage. The most common controllers are linear PID controllers. The PID control design is based on linear control theory, such as the Ziegler–Nichol's method [29], the root locus approach [30], the circle-based criterion [31], and the hysteresis method [32], the bode plot. These control methods perform well around the linearized model's operating points. The small-signal model of a boost converter, on the other hand, changes when the operating point changes. It is important to mention here that the duty cycle determines the poles and a right-half-plane zero and the amplitude of the frequency response. As a result, PID controllers have a hard time respecting changes in operating points, and they function poorly when the system is subjected to frequent load fluctuations.

Despite the necessity of changes in input, the Ziegler–Nichol's technique for PID tuning is an experimental one that is extensively utilized. One downside of this technique is that it necessitates a prior understanding of plant models. A decent but not optimal system response is achieved when the controller is adjusted using the Ziegler–Nichol's technique. If the operational parameters of the plant change, the transient reaction might be considerably worse. It should be noted that many plants have time-varying dynamics due to external/environmental factors, such as temperature and pressure. The controller must respond to changes in the dynamics of the plant features to provide a robust system. Nonlinear control techniques [33–36], such as fuzzy logic and sliding mode

control, have recently offered good static and dynamic responsiveness. The disadvantage of the fuzzy logic technique is that all available data are needed. Also, the algorithm has to be trained, by human knowledge, which is incomplete as opposed to systematic methods available, before use. The sliding mode controller is suffering from a chattering issue.

1.3 Research Objectives

To compensate for the steady-state oscillation of MPP tracking, this research proposes a modified P&O algorithm.

A new approach is presented here to recognize the peak power point when the PV array output reaches its maximum. In this study, MPPT efficiency tests, PSC tests, and drift effect tests are used to evaluate both conventional and modified P&Os under varying environmental conditions. Also, the modified P&O algorithm compares with the InC algorithm. The performance boost from the suggested method is clarified when the results for the conventional algorithms and modified P&O have been compared in all mentioned environmental conditions. In this way, the proposed algorithm can be considered a multi-purpose solution for crucial MPPT conditions.

A second goal of this work is to regulate the voltage of PV systems DC-DC converter's output in island micro-grid (MG). Voltage and frequency variability are very sensitive in islanded microgrids; for this reason, a robust and adaptive controller is always desirable.

Here we propose a DC-DC boost converter with a modified MIT rule controller that stabilizes output voltage variations in island MG. Here, two control loops are used to achieve a stable output voltage; a PID controller can regulate the output voltage at a fixed level, and the outer loop is designed to implement the MIT rule for a direct model reference adaptive controller (DMRAC). To ensure that the actual system is following the desired reference model, using only an output

voltage feedback sensor, a DMRAC is devised to update the PID controller parameters in real-time. Compared to a DC–DC boost converter connected to the MG, a controller, such as the one introduced in this paper, is more successful in dealing with unknown parameter fluctuations and disturbance changes.

The significant contributions of the proposed work are summarized as follows:

- The conventional and modified P&Os are thoroughly benchmarked in this study under varying environmental conditions utilizing the steady state and dynamic MPPT efficiency tests, PSC tests, and drift effect tests.
- A novel MPPT algorithm with a set of features such as: improving the efficiency of conventional P&O algorithm by 0.5 percent for both slow and fast irradiance changes, and improving the efficiency of the traditional methods on average by about 9% and 8% under strong partial shading situations (PSC) and drift avoidance tests, respectively.
- An adaptive controller is designed to regulate the output voltage of the DC–DC converters in a PV system.
- This thesis proposes a novel output voltage regulation approach that can adjust the parameters of the PID controller in real-time to ensure that the actual system is following the desired reference model.
- The PID controller regulates the output voltage at a fixed level, essential for correct power injection when the DC–DC boost converter is connected to the MG.
- The proposed controller does not require using any current sensor, and the control scheme is only obtained using the voltage feedback of the boost converter. So, the proposed design is cost-effective.

1.4 Thesis Structure

This thesis is divided into six chapters. The details of what each chapter would cover are given below.

Chapter 1 starts with an introduction of the PV systems, MPPT algorithms, converters, and voltage regulation of PV systems. The chapter also includes a detailed literature review or all the research and development that has been done in this field. Further, the chapter identifies the gap in the literature and talks about our motivation to pursue this research.

Chapter 2 of the thesis is a survey on the MPPT modified algorithms. This chapter is submitted to the Journal of Renewable and Sustainable Energy Reviews.

Chapter 3 is focuses on a novel dynamic MPPT algorithm for photovoltaic power systems. A version of this chapter has been peer-reviewed and accepted for publishing in the Journal of Modern Power Systems and Clean Energy (MPCE), September 2022.

Chapter 4 of the thesis will focus on the direct model reference adaptive control of a boost converter for voltage regulation in microgrids. A version of this chapter has been published in Energies, July 2022.

Chapter 5 of the thesis will focus on the design of a super-fast sliding mode control of a boost converter for voltage tracking in microgrids. A draft of this chapter will be submitted to Energies.

Chapter 6 of the thesis will discuss the conclusions drawn from the previous chapters and will propose future areas of research that can be undertaken as an extension to this research.

References

[1] M. Farsi and J. Liu, "Nonlinear Optimal Feedback Control and Stability Analysis of Solar Photovoltaic Systems," IEEE Transactions on Control Systems Technology, vol. 28, no. 6, pp. 2104-2119, Nov. 2020.

[2] Forouzesh, M.; Siwakoti, Y.P.; Gorji, S.A.; Blaabjerg, F.; Lehman, B. A survey on voltage boosting techniques for step-up DC-DC converters. In Proceedings of the IEEE Energy Conversion Congress and Exposition (ECCE), Milwaukee, WI, USA, 2016; pp. 1–8.

[3] Mamarelis, E.; Petrone, G.; Spagnuolo, G. Design of a sliding mode controlled SEPIC for PV MPPT applications. *IEEE Trans. Ind. Electron.* **2014**, *61*, 3387–3398.

[4] Yanarates, C.; Zhou, Z. Design and Cascade PI Controller-Based Robust Model Reference Adaptive Control of DC-DC Boost Converter. *IEEE Access* **2022**, *10*, 44909–44922.

[5] N. Femia, G. Petrone, G. Spagnuolo, and M. Vitelli, "Optimization of perturb and observe MPPT method," IEEE Transactions on Power Electronics, vol. 20, no. 4, pp. 963-973, July 2005.

[6] H. A. Sher, A. F. Murtaza, A. Noman, K. E. Addoweesh, K. Al-Haddad, and M. Chiaberge, "A new sensorless hybrid MPPT algorithm based on fractional short-circuit current measurement and P&PO MPPT," IEEE Transactions on Sustainable Energy, vol. 6, no. 4, pp. 1426-1434, Oct. 2015.

[7] M. A. Elgendy, B. Zahawi, and D. J. Atkinson, "Assessment of perturb and observe MPPT algorithm implementation techniques for PV pumping applications," IEEE Transactions on Sustainable Energy, vol. 3, no. 1, pp. 21-33, Jan. 2012.

[8] J. H. Lee, H. Bae, and B. H. Cho, "Advanced incremental conductance MPPT algorithm with a variable step size," Proc. 12th International Power Electronics and Motion Control Conference, Aug./Sep. 2006, pp. 603-607.

[9] M. Qiang, S. Mingwei, L. Liying, and J. M. Guerrero, “A novel improved variable step-size incremental-resistance MPPT method for PV systems,” IEEE Transactions on Industrial Electronics, vol. 58, no. 6, pp. 2427-2434, Jun. 2011.

[10] Weidong Xiao and W. G. Dunford, “A modified adaptive hill climbing MPPT method for photovoltaic power systems,” IEEE 35th Annual Power Electronics Specialists Conference (IEEE Cat. No.04CH37551), Aachen, Germany, Jun. 2004, pp. 1957-1963.

[11] E. Koutroulis, K. Kalaitzakis, and N. C. Voulgaris, “Development of a microcontroller-based, photovoltaic MPPT control system,” IEEE Transactions on Power Electronics, vol. 16, no. 1, pp. 46-54, Jan. 2001.

[12] R. Iftikhar, I. Ahmad, M. Arsalan, N. Naz, N. Ali, and H. Armghan, “MPPT for Photovoltaic System Using Nonlinear Controller,” International Journal of Photoenergy, vol. 2018, pp. 1-11, Apr. 2018.

[13] F. M. de Oliveira, F. R. Durand, V. D. Bacon, S. A. O. da Silva, L. P. Sampaio, and L. B. G. Campanhol, “Grid-tied photovoltaic system based on PSO MPPT technique with active power line conditioning,” IET Power Electronics, vol. 9, no. 6, pp. 1180-1191, May. 2016.

[14] M. B. Smida and A. Sakly, “Genetic based algorithm for MPPT (MPPT) for grid connected PV systems operating under partial shaded conditions,” 7th International Conference on Modelling, Identification and Control (ICMIC), Tunisia, Dec. 2015, pp.1-6.

[15] A. A. S. Mohamed, A. Berzoy, and O. A. Mohammed, “Design and Hardware Implementation of FL-MPPT Control of PV Systems Based on GA and Small-Signal Analysis,” IEEE Transactions on Sustainable Energy, vol. 8, no. 1, pp. 279-290, Jan. 2017.

[16] M. Dehghani, M. Taghipour, G. B. Gharehpetian and M. Abedi, “Optimized Fuzzy Controller for MPPT of Grid-connected PV Systems in Rapidly Changing Atmospheric Conditions,” Journal of Modern Power Systems and Clean Energy, vol. 9, no. 2, pp. 376-383, Mar. 2021.

[17] R, Kumar, N, Tadikonda, J, Kumar, RN, Mahanty, “An ANN-Based MPPT Technique for Partial Shading Photo Voltaic Distribution Generation,” In Control Applications in Modern Power Systems, Springer, Singapore. 2022, pp. 391-403.

[18] M. Rezkallah, S. K. Sharma, A. Chandra, B. Singh, and D. R. Rousse, “Lyapunov Function and Sliding Mode Control Approach for the Solar-PV Grid Interface System,” IEEE Transactions on Industrial Electronics, vol. 64, no. 1, pp. 785-795, Jan. 2017.

[19] S, Golzari, F, Rashidi, HF, Farahani, “A Lyapunov function-based model predictive control for three phase grid connected photovoltaic converters” Solar Energy, vol. 15, no. 181pp. 222-233, Mar. 2019.

[20] S, Rezazadeh, A, Moradzadeh, SM, Hashemzadeh, K, Pourhossein, B, Mohammadi-Ivatloo, SH, Hosseini, “A novel prime numbers-based PV array reconfiguration solution to produce maximum energy under partial shade conditions,” Sustainable Energy Technologies and Assessments, vol. 1, no. 47, pp. 101498, Oct. 2021.

[21] M. Madhukumar, T. Suresh, and M. Jamil, “Investigation of PV Integrated Grid System Under NonUniform Irradiance Conditions” Electronics, Special Issue on Power Electronics, Vol. 9, no. 9 Aug. 2020.

[22] SM, Hashemzadeh, “A new model-based technique for fast and accurate tracking of global maximum power point in photovoltaic arrays under partial shading conditions,” Renewable energy, vol. 1, no. 139, pp. 1061-76, Aug. 2019.

[23] V, kumar Vethanayagam, KK, Prabhakaran, V, Balasubramanian, “A Novel Algorithm based on Voltage and Current Perturbation to track Global peak under Partial Shading Conditions,” IEEE Transactions on Energy Conversio, 2022 May 27.

[24] M. Killi and S. Samanta, “Modified Perturb and Observe MPPT Algorithm for Drift Avoidance in Photovoltaic Systems,” IEEE Transactions on Industrial Electronics, vol. 62, no. 9, pp. 5549-5559, Sep. 2015.

[25] V. Jately, S. Bhattacharya, B. Azzopardi, A. Montgareuil, J. Joshi and S. Arora, "Voltage and Current Reference Based MPPT Under Rapidly Changing Irradiance and Load Resistance," IEEE Transactions on Energy Conversion, vol. 36, no. 3, pp. 2297-2309, Sep. 2021.

[26] Young, M. *The Technical Writer's Handbook*; University Science: Mill Valley, CA, USA, 1989.

[27] Rajakumari R. F.; Deshpande, M. Comparative Analysis of DC-DC Converters. In Proceedings of the 2nd International Conference on Power and Embedded Drive Control (ICPEDC), Chennai, India, 2019; pp. 504–509.

[28] Zaitu, R. *Voltage Mode Boost Converter Small Signal Control Loop Analysis Using the TPS61030*; Application Report; Texas Instruments: Dallas, TX, USA, 2007.

[29] Perry, A.G.; Feng, G.; Liu, Y.F.; Sen, P.C. A design method for PI-like fuzzy logic controller for DC-DC converter. I*EEE Trans. Ind. Electron.* **2007**, *54*, 2688–2695.

[30] Aldo, B.; Corsanini, D.; Landi, A.; Sani, L. Circle based Criteria for performance evaluation of controlled DC-DC Switching Converters. *IEEE Trans. Ind. Electron.* **2006**, *53*, 1862–1869.

[31] Zhang, J.; Shu-Hung Chung, H.; Lo, W.L. and Ron Hui, S.Y. Implementation technique for design of switching Regulators Using Genetic Algorithm. *IEEE Trans. Power Electron.* **2001**, *16*, 752–763.

[32] Hung, J.Y.; Gao, W.; Hung, J.C. Variable structure control: A survey. *IEEE Trans. Ind. Electron.* **1993**, *40*, 2–22.

[33] Tang, K.L., and Mulholland, R.J. Comparing Fuzzy logic with classical controller design. *IEEE Trans. Syst. Man Cybern.* **1987**, *6*, 1085–1087.

[34] Nelms, R.M.; Guo, L.; Hung, J.H. Digital Controller design for Buck and Boost Converters Using Root Locus Technique. In Proceedings of the 29th Annual Conference of the IEEE Industrial Electronics Society, Roanoke, VA, USA, 2003; Volume 2, pp. 1864–1869.

[35] Rashid, U.; Jamil, M.; Gilani, S.O.; Niazi, I.K. LQR based Training of Adaptive Neuro-Fuzzy Controller. In Proceedings of the 25th Italian Workshop on Neural Networks, Salerno, Italy, 20–22 May 2015; pp. 311–322.

[36] Schmidt S, Richter M, Oberrath J, Mercorelli P. Control oriented modeling of DCDC converters. *IFAC-Pap. Line* **2018**, *51*, 331–336.

Chapter 2

Maximum Power Point Tracking Modified Algorithms Survey

Preface

A version of this chapter has been submitted in the Journal of Renewable and Sustainable Energy Reviews, October 2022. I am the primary author, and I carried out most of the research work performed the literature reviews, carried out the system design, implementations, and analysis of the results. I also prepared the first draft of the manuscript. The Co-authors, Dr. Mohsin Jamil and Dr. M. Tariq Iqbal supervised the research, provided the research guide, reviewed, and corrected the manuscript, and contributed research ideas to the actualization of the manuscript.

Abstract

Due to the energy crisis in the world, the use of solar photovoltaic (PV) as a source of renewable energy is demanding today. The main problem with the PVs is the output power fluctuation in case of temperature and irradiance change. Maximum power point tracking (MPPT) methods based on conventional algorithms such as perturb and observe (P&O), and incremental conductance (InC) are popular applications to deal with mentioned issues. The conventional MPPT methods are famous for their ease of implementation and understanding. This study focuses on the effectiveness of 24 modified algorithms in the three most environment change cases: irradiance changes, drift avoidance, and partial shading condition (PSC). Modified algorithms' efficiency and response time are compared in the mentioned environment conditions.

Keywords: Conventional Maximum Power Point Tracking algorithms, P&O algorithm, InC algorithm, Drift free, Partial shading condition

2.1 Introduction

Solar energy is one of the most significant energy sources in the world. As a renewable and non-conventional energy source, solar energy is very clean, safe, and freely available in nature. The PV energy absorbs the attention of many researchers due to its advantages and applications. In recent years, PV systems have become increasingly popular since they are environmentally friendly and can be installed in residential and remote environments. PV systems produce their maximum output power at a maximum power (MPP) point, and its location continuously varies depending on irradiance and temperature.

Consequently, an operation point should be located at the MPP to extract the most power from the photovoltaic generator (PVG). Thus, MPP must be continuously monitored by the MPPT algorithms. There are many factors to consider when designing a PV system's MPPT, such as how much it costs, how efficient it is, how much energy is lost, and how it is implemented [1, 2]. There are many research publications with various control techniques for PV MPPT systems, which are mainly divided into two categories: conventional and soft computing approaches. Several studies have been conducted on conventional MPPT methods, such as P&O [3], [4], [5], InC algorithm [6], [7], and hill-climbing (HC) algorithm [8], [9].

A conventional algorithm is the most used since it is easiest to implement, thus making it more suitable for low-cost applications. Even though traditional methods can be easily used, they have shown a sluggish response to changes in ambient temperature and solar radiation. Therefore, the system's deviation from its MPP results in power losses that are proportional to the size of the installed solar array [1]. In addition to conventional algorithms, there are several bioinspired algorithms that are generally more efficient in some special cases than conventional methods. Even in partially shaded environments, they can quickly converge to a global maximum [10]. A

bioinspired particle swarm optimization (PSO) algorithm is successfully applied in [11]. Genetic algorithms (GA) are a type of algorithm that solves partial shading challenges [8, 12]. Moreover, there are two algorithms based on artificial intelligence (AI), fuzzy logic-based controllers (FLBCs) and artificial neural networks (ANN)-based MPPTs [13]. These algorithms have lower settling times, less overshoot, and better performance than MPPT, but they require input data at the beginning to train the output-input relationship. A sliding mode and Lyapunov function-based algorithm were presented in [14] for achieving MPPT control of a solar-PV array connected to the grid. While there are several strategies in the literature that attempt to improve the drawbacks of conventional MPPT approaches, they tend to be considerably slower, and the implementation remains a priority when control methods are put into practice. Thus, many scientists believe that modified conventional approaches are more efficient to apply than complicated modern theories. Therefore, many MPPT algorithms focus on improving the conventional algorithm's efficiency and response time. Some of the mentioned algorithms [15], [20-21], [22-23] enhanced the efficiency of conventional algorithms in PSCs, and some others introduced modified algorithms in slow and fast irradiance changing [18-19], [25], and other worked on drift issue [16-17], [45]. This work presents the most recently modified P&O and InC algorithms.

- This review of MPPT techniques has been classified into three essential groups: drift-free algorithms, modified algorithms for slow and fast irradiance changes, and PSC algorithms.
- This study compares 12 modified P&O algorithms and 12 modified InC algorithms in the case of efficiency and response time.
- The comparison is done based on mathematical analysis.

2.2 Methodology

This study conducts comparative research over the modified P&O and InC algorithms to present more efficient MPPT algorithms to a PV system. We compare 24 MPPT techniques in case of their performance over fast irradiance changes, drift issues, PSC, and temperature changes. Besides, the efficiency and response time of the modified algorithms are considered and compared with the conventional algorithms.

2.3 P&O Modified Algorithms

2.3.1 Overview of the conventional P&O algorithm

The P&O algorithm is the most often used MPPT method because of its simplicity. The P&O algorithm is based on perturbing the PV array output voltage by tuning the duty cycle of a power converter and then checking the changes in the output power of the array. This implies that the PV panel's output power in each cycle must be compared with PV power in the antecedent perturbation cycle. The flowchart of the P&O algorithm is displayed in Figure 2.1. ΔP, ΔV , and ΔI are the differences of power, voltage, and current in two antecedent perturbation cycles. If ΔP is positive, it means we are approaching the maximum panel power, and the perturbation must be made in the same direction. Conversely, if the output power decreases, the perturbation must be made in reverse order. $\Delta P = 0$ is shown that the MPP is reached.

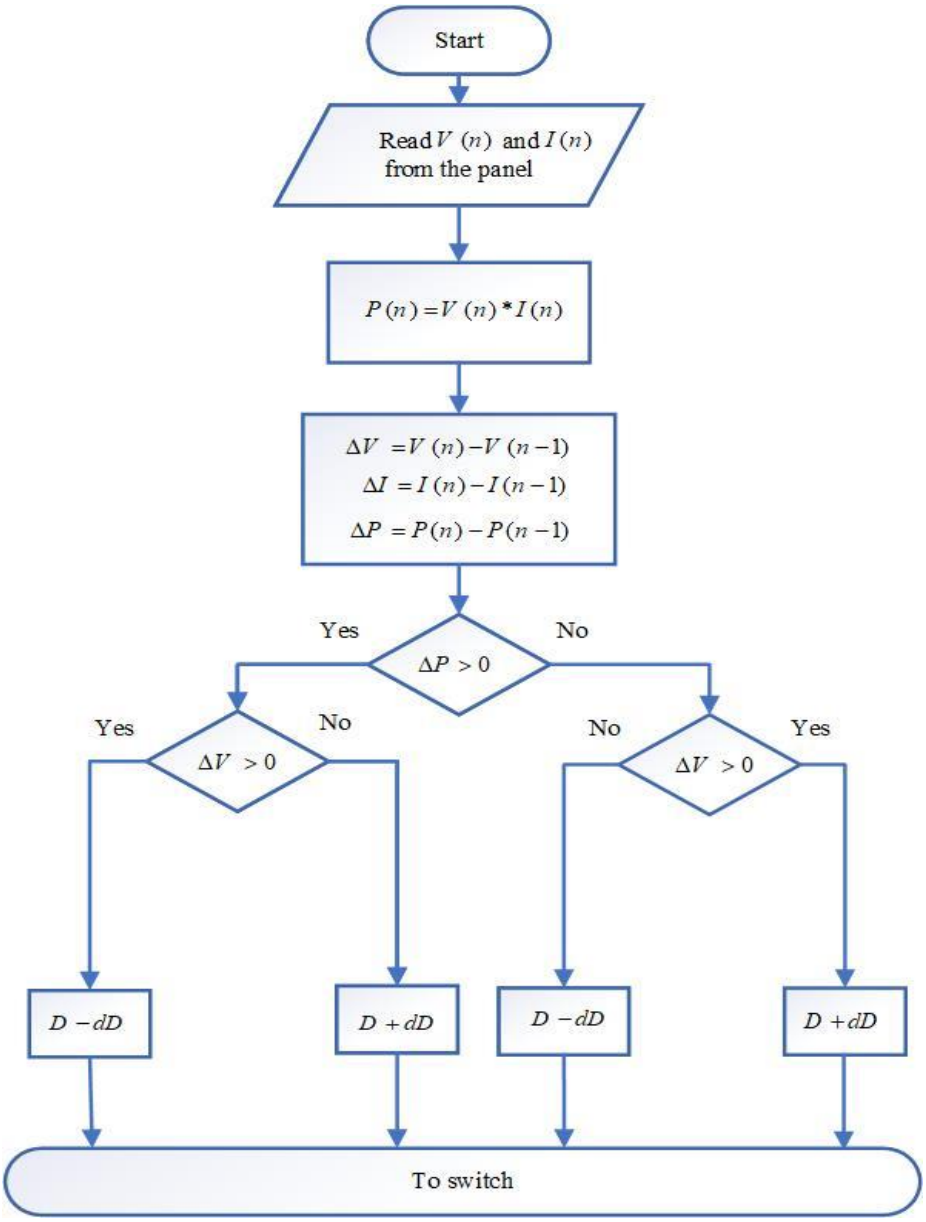

Fig. 2.1 The flowchart of the conventional P&O algorithm.

The perturbation step size plays an undeniable role in reaching the MPP, as the large step size may lead to a fast-tracking response, but the amplitude of the steady-state oscillations will be high. On the other hand, if the step size has a small value, the tracking is slower, and still, a small oscillation will be seen. Although this method has indubitable merits, such as its high efficiency, being cheap for implementation, and needing only two sensors to sense the current and voltage of the PV array,

nonstop oscillation around the MPP is the main drawback P&O algorithm. Unfortunately, this hindrance is bold because it leads to energy losses.

2.3.2 Drift-free P&O algorithm

In [16], by changing the current (ΔI), the voltage (ΔV), and power (ΔP) in the decision process, a modified P&O algorithm has been proposed, which avoids the drift drawback in P&O algorithms. A modification may be necessary to the algorithm if drift occurs as solar irradiation increases. Drift problem can be eliminated by changing current (ΔI) parameter & increases the duty-cycle.

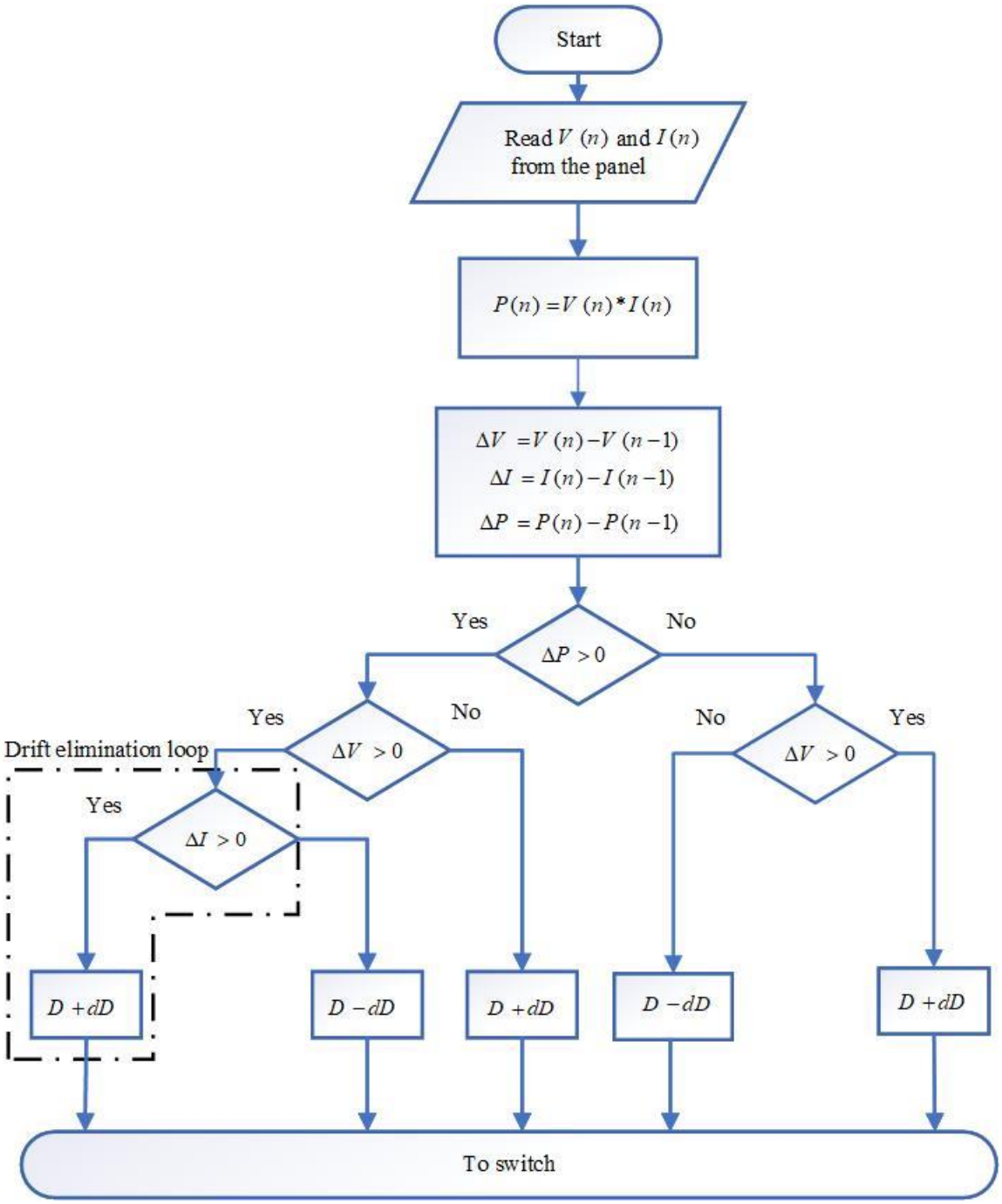

Fig. 2.2. The flowchart of the modified P&O algorithm in [16]

In [17], the authors presented a modified P&O MPPT based on a mathematic solution which is called the Pythagorean theorem and constant voltage (CV) MPPT to deal with the weather condition issues such as the drift problem when the irradiation changes very fast in the conventional P&O algorithm.

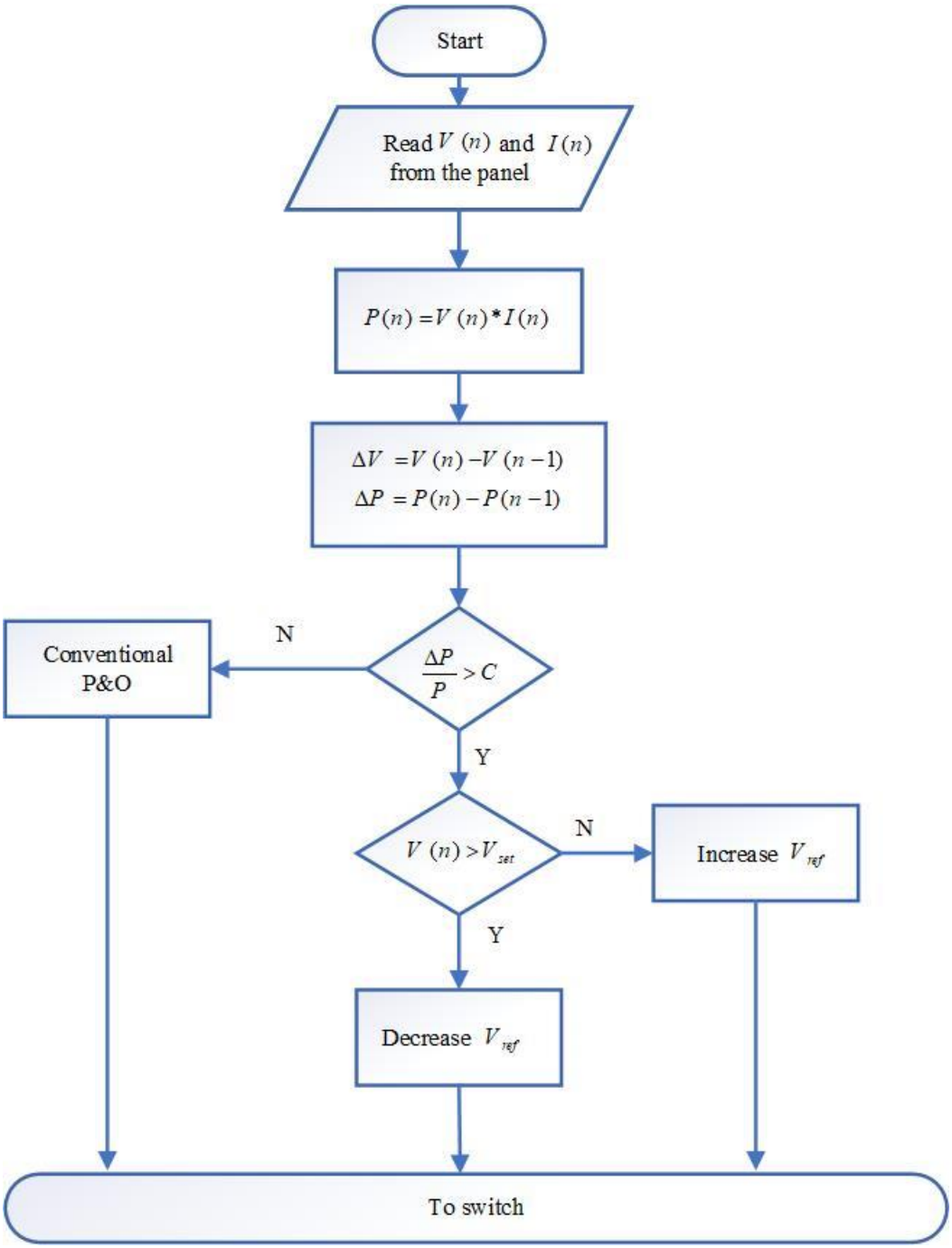

Fig. 2.3. The flowchart of the modified P&O algorithm in [17].

The proposed modification consists of two sections. Firstly, an innovative and easy to use variable step size (VSS) is developed, improving tracking, and reducing oscillations around the MPP. VSS is indicated by using the Pythagorean theorem, which says that the square opposite the right angle equals the square of the other two sides. In the proposed algorithm C is the length of the hypotenuse

of the triangle of movement of dP and dV in the P-V curve. Part two of this modification is the adoption of a new duty cycle selection for conventional P&O to deal with drift problems early. The insolation of solar panels depends on the weather condition is divided into two different types: slow change and fast change. In this case the parameter C in the flowchart shows the rate of solar irradiance changes, so it addresses the drift problem.

[45] presents an active power curtailment control strategy based on derated power generation mode (DPGM). In addition, a drift-free P&O technique is also proposed to enhance the MPPT algorithm's performance. With the proposed modified algorithm, MPP's power loss and time to search are reduced. Furthermore, it gives the system drift-free run-in conditions of variable irradiance. The proposed algorithm in [45] operates in two modes: the modified MPPT and DPGM, which are depicted in Figure 2.4. As a result, during the peak periods of power generation, the DPGM control scheme with the intermediate boost converter reduces the excess active power. The improved MPPT algorithm also takes into account irradiance variations during non-peak hours. As a result, the suggested control method results in a system that is more effective during the peak periods of power generation. Additionally, it decreases power loss and settling time during non-peak hour irradiance variation.

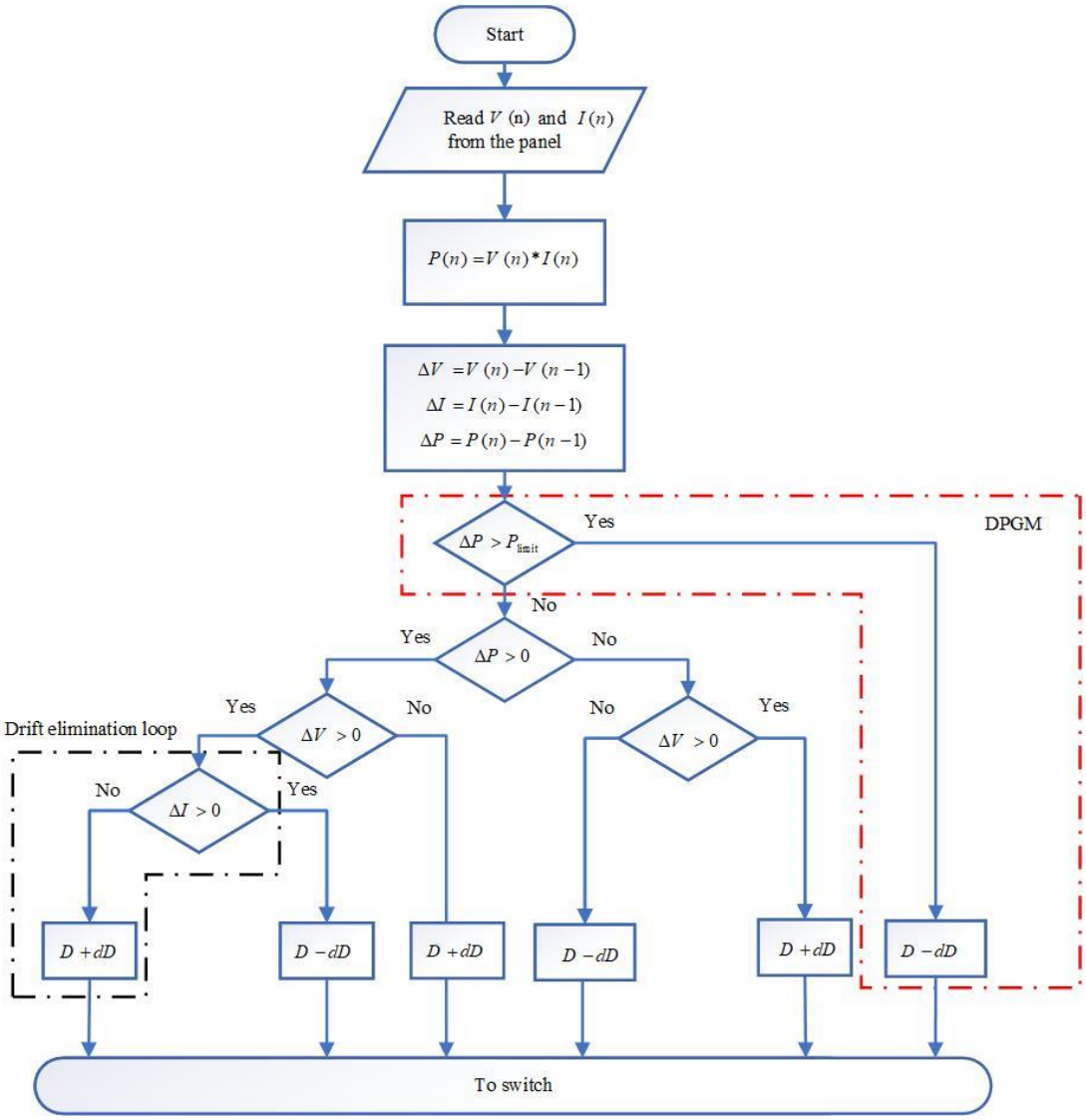

Fig. 2.4. The flowchart of the modified P&O algorithm in [45].

Table 2.1

Drift-Free Modified P&O Algorithms Comparison

Algorithm	Error	Response Time (*s*)
[16] Drift-free P&O	**4.1%**	**<0.05**
[17] P&O based on Pythagorean theorem	**3.9%**	**<0.5**
[45] DPGM	**2.05%**	**<0.6**

2.3.3 Slow and fast irradiance changes modified P&O

In [18], at first, the irradiance (G) is considered to vary as follows: 1) slow change in irradiance, i.e., $G < 10\ w/m2$) fast changes in irradiance means that G is higher than $10\ w/m2$. These two irradiance profiles have been given special consideration in term of an initial perturbation size (ΔV). In the case of small gradients of G, conventional P&O can track MPP without divergence. In the second, a soft switched converter based on zero voltage switching (ZVS) is proposed to minimize losses caused by switching, turn-on loss, and conduction loss in the Buck-Boost converter. Upon turning on the switch, the voltage falls to zero then the current starts increasing so as to have the least switching loss. Conversely, when the switch is OFF, the voltage goes to the maximum from zero and the current goes to a minimum. A ZVS converter can be constructed by adding an inductor $L_2$and a capacitor C_2, as shown in the following figure.

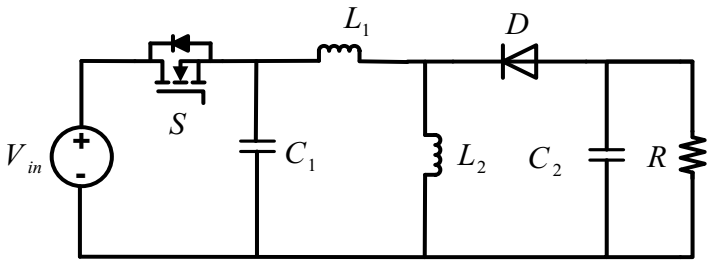

Fig. 2.5. ZVS-based soft switched buck-boost converter.

The efficiency of the described P&O with the ZVS converter in [18] is 96.3%.

Table 2.2

Slow and Fast Irradiance Changes Modified P&O Algorithms Comparison

Algorithm	Error	Response Time (*s*)
[18] Zero voltage switching	**3.7%**	**0.4**
[19] Adaptive P&O	**2.05%**	**<0.001**
[25]GA P&O	**3.33%**	**<0.06**
[44] Linear tangent (LT) P&O	**0.25%**	**<0.05**

[19] presents an adaptive P&O MPPT algorithm that can track the MPP rapidly and with less steady-state oscillation as compared to conventional P&O MPPT algorithms. This method's perturbation amplitude is robust to accelerate the tracking process and reduce steady-state oscillations. This technique results in a large perturbation amplitude if the operating point is far from the MPP and a small perturbation amplitude if the operating point is close to the MPP. To improve track performance, current perturbation is considered instead of voltage perturbation. The flowchart of this algorithm is illustrated in Figure 2.6. The oscillation of the adaptive P&O algorithm is improved by 0.26% in [19].

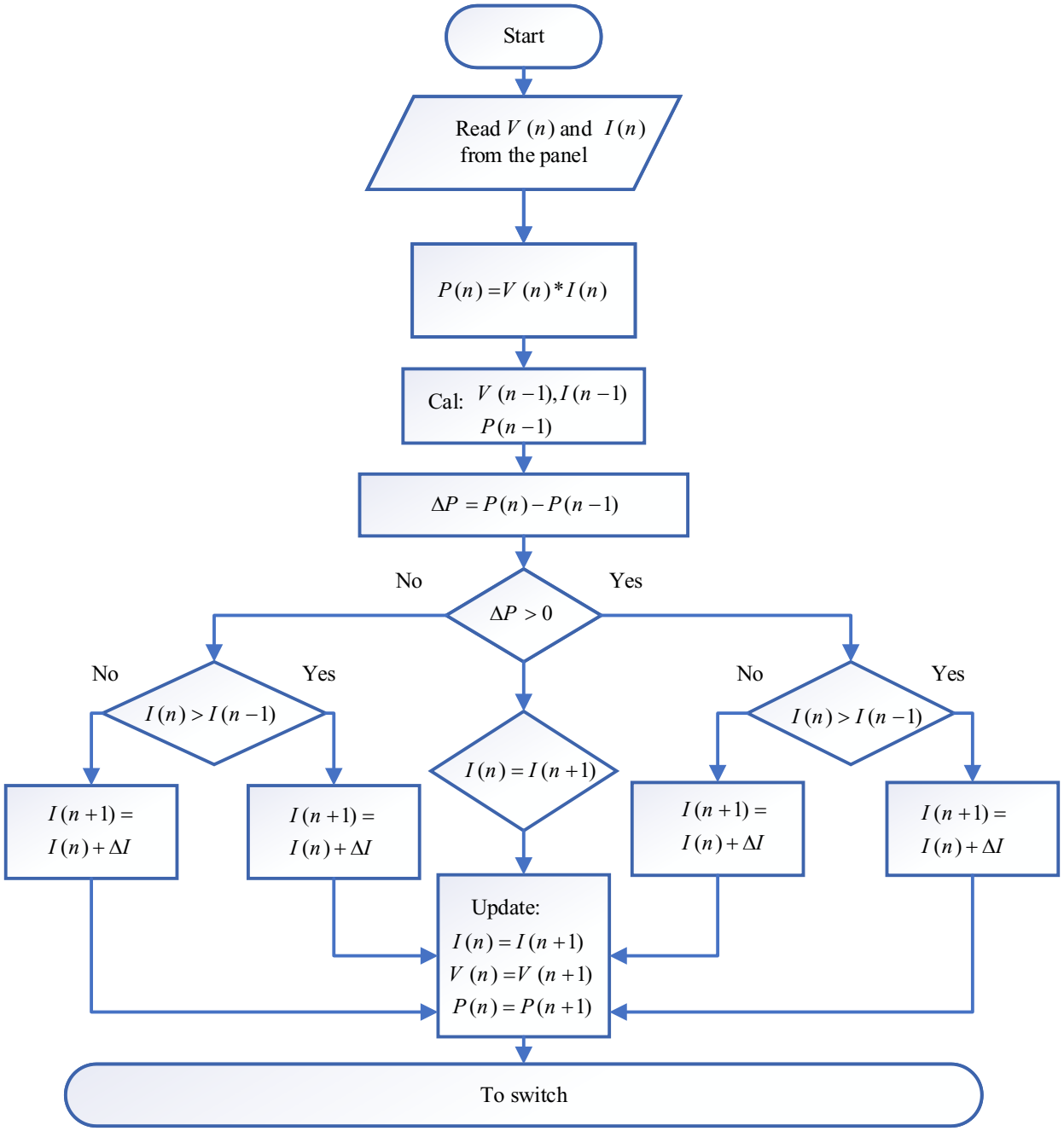

Fig. 2.6. The flowchart of the modified P&O algorithm in [19].

In [25], the authors presented a modified P&O MPPT algorithm using a PID controller based on genetic algorithms (GA). GA is also considered in many other MPPT papers [23-40]. GA tune the PID controller in [25] to optimize the P&O variable step. To optimize DC/DC converter power transfer, GA selects the value of K_p, K_i, and K_d PID parameters. There are two modes of operation

for the system: (1) the offline mode for testing different PID parameters to find the optimal controller, and (2) the online mode for tracking the MPP point after the optimal PID is found. Figure 2.7 depicts the block diagram of the proposed genetic variable step P&O MPPT in [25].

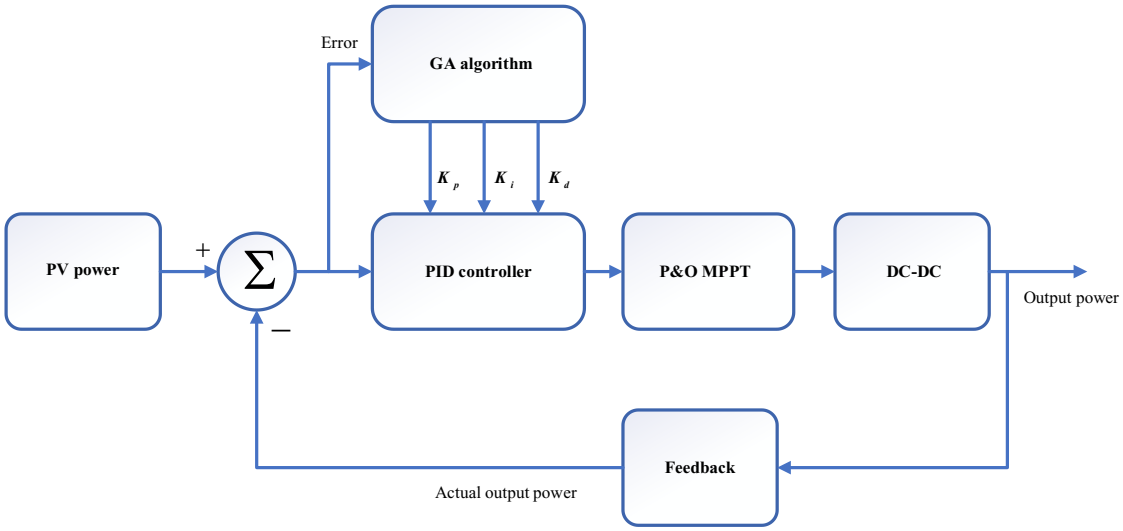

Fig. 2.7. The block diagram of the proposed genetic variable step P&O MPPT in [25].

A LT P&O is proposed in [44] as a new MPPT scheme. MPPT is proposed as a three-step process in [44], the first step is projection of tangents over P-V curve, second step is estimation of MPP on P-V curve, and the third is calculation of the actual MPP based on the perturbation from the estimated MPP.

2.3.4 PSC P&O

[23] proposes a modified MPPT method that only uses one parameter to tune. Compared to P&O MPPT, this method overcomes the problems of steady-state oscillations and lower efficacy.

The duty ratio can be calculated by equating the difference between the voltage obtained and the reference voltage, multiplied by variable M, which represents a step-change. M is selected here according to its performance and rate of convergence in order to achieve the best results. Usually, it is between e^{-1} and e^{-12}. With a particular value of M, the system had difficulty tracking the

MPP with very little distortion, but the performance of the selected value of M is similar to that of the lowest value of M, with a significantly higher convergence rate.

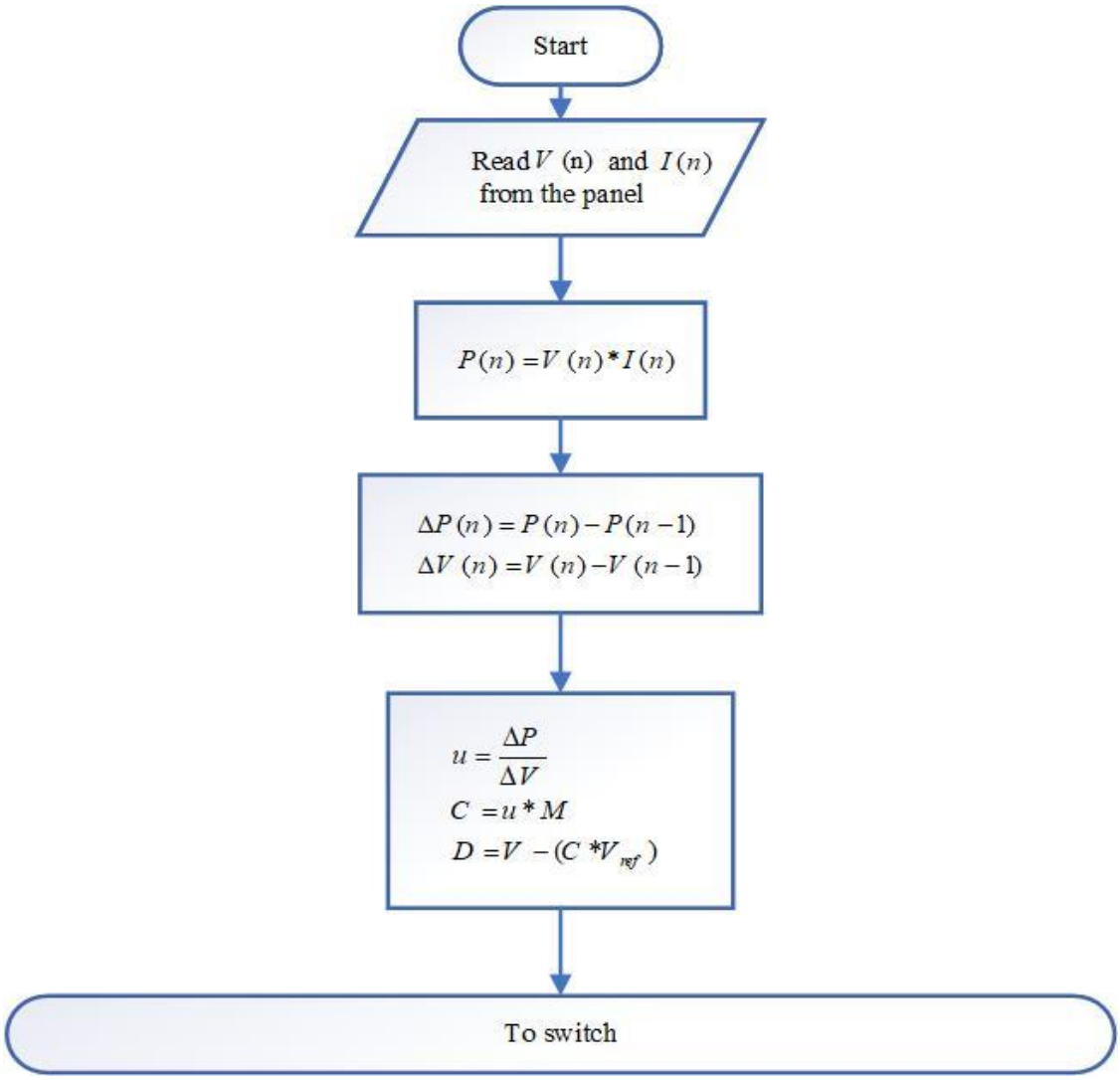

Fig. 2.8. The flowchart of the modified P&O algorithm in [23].

In [15], the authors proposed to modify P&O to track the MPP even under the PSC, without having to oscillate around the MPP. The paper proposes two methods to solve the PSC issues: (1) Using a function to identify if the PSC is occurring. Set the track direction flag to search the P-V curve if it occurs. The information of global maximum power point (GMPP) should be updated if any local maximum power point (LMPP) can output higher power. (2) After finding the maximum point, stop the oscillation.

A Modified variable step size (MVSS) P&O MPPT algorithm was proposed in [21] in order to implement a peak tracking system for solar photovoltaic (SPV) systems with two-phase Interleaved Boost Converters (IBCs). It is possible for MPPT to handle PSC in a very efficient manner.

In another work [24], the authors proposed a modified P&O method for PV systems under PSC. This modified algorithm combines an adjustable step size algorithm and an inspection algorithm to determine the global MPP by comparing all multiple MPPs. In order to increase efficiency and achieve the benefits of both systems, this paper merges the two algorithms. A step size algorithm is employed in this work to determine whether the saved MPP is local or global. Several measured operating points are compared with the saved MPP value. The minimum distance between MPPs must be closer to the previously measured MPP to ensure a higher MPP. The closest voltage to the short circuit current is also measured. A power comparison is carried out using the measured voltage, current, and saved MPP. A new operating point is calculated if the estimated MPP exceeds the saved value. Therefore, the P-V curve is continuously monitored until the peak power is measured. With the MPPs being updated, the adjustable step size algorithm comes into play to determine the most accurate MPP value.

In [22] authors proposed an improved adaptive step size P&O MPPT method that effectively achieves the MPP under PSC. They also optimized all other aspects of high-performance MPPT to make it novel, easier to use, quicker, and more accurate.

Table 2.3

PSC Modified P&O Algorithms Comparison

Algorithm	Error	Response Time (*s*)
[15] MP&O	**1.36%**	**<0.02**
[23] PSC P&O	**0.3%**	**<0.01**
[21] MVSS P&O	**2.1%**	**<0.03**
[24] Adjustable step size and inspection algorithm	**0.16%**	**<0.03**
[22] adaptive step size P&O	**1.33%**	**<0.13**

2.3.5 Modified P&O algorithms comparison

In this section, we take a look at all modified P&O algorithms mentioned in previous sections. As illustrated in Table 2.4, most of the modified P&O algorithms considered slow and fast irradiance changes, and a few considered drift issues, PSC, and temperature changes. The best modified P&O algorithm in the case of efficiency is the adjustable step size and inspection algorithm [24], and in the case of response time, the most stable algorithm is adaptive P&O [19].

Table 2.4

P&O algorithms Comparison Table

Algorithm	Error	Response Time (*s*)	Application				
			Slow irradiance changes	Fast irradiance changes	Drift	PSC	Temperature changes
Conventional P&O	4.1%	0.4	✓	-	-	-	-
[15] MP&O	1.36%	<0.02	✓	-	-	✓	-
[16] Drift-free P&O	4.1%	<0.05	✓	✓	✓	-	-
[17] P&O based on the Pythagorean theorem	3.9%	<0.5	✓	✓	✓	-	-
[18] Zero voltage switching	3.7%	0.4	✓	✓	-	-	-
[19] Adaptive P&O	2.05%	<0.001	✓	✓	-	-	-
[23] PSC P&O	0.3%	<0.01	✓	✓	-	✓	-
[24] Adjustable step size and inspection algorithm	0.16%	<0.03	✓	✓	-	✓	-
[25]GA P&O	3.33%	<0.06	✓	✓	-	-	-
[44] LT P&O	0.25%	<0.05	✓	-	-	-	✓
[45] DPGM	2.05%	<0.6	✓	✓	✓	-	-
[21] MVSS P&O	2.1%	<0.03	✓	✓	-	✓	-
[22] adaptive step size P&O	1.33%	<0.13	✓	✓	-	✓	-

2.4 Incremental Conductance Modified Algorithms

2.4.1 Overview of the conventional InC algorithm

The InC method relies on the observation that the first derivative of the PV function, i.e., $\Delta P / \Delta V$ becomes zero at maximum. Due to PV current's dependence on voltage, power = voltage*current = $I(V) \times V$. Thus, $V \times (\Delta I / \Delta V) + I(V) = \Delta P / \Delta V$. We get the following equation when we set the value of the variable equal to zero:

$$\frac{\Delta I}{\Delta V} = -\frac{I(\mathrm{V})}{V} \qquad (1)$$

Hence, the MPP occurs when InC equals instantaneous conductance. The MPP voltage is defined as the voltage corresponding to the point where, $\Delta I / \Delta V = -I(V)/V$. This voltage is maintained until the solar irradiation changes and the procedure is repeated [43]. The mentioned steps are shown in Figure 2.9.

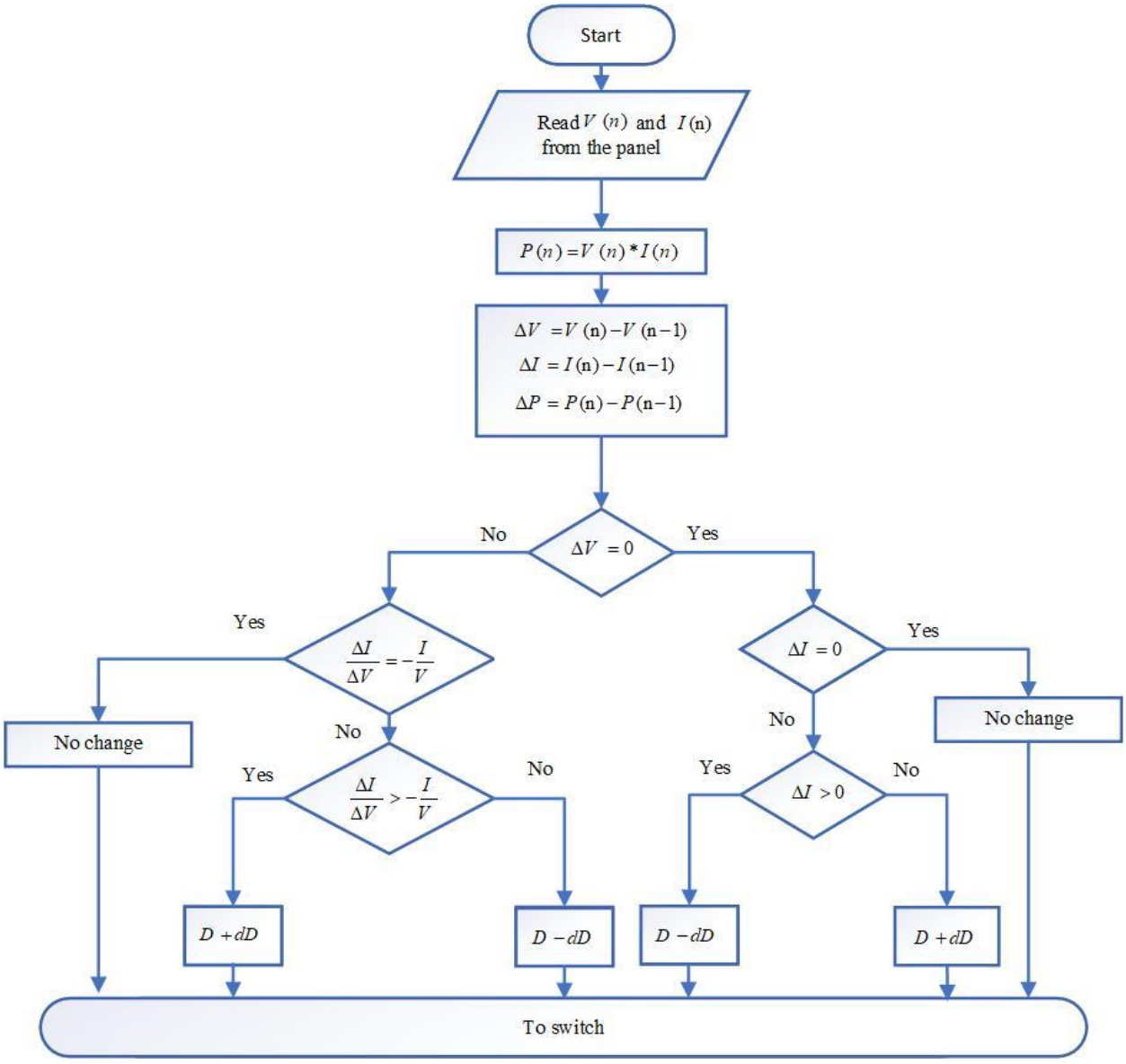

Fig. 2.9. The flowchart of the conventional InC algorithm.

2.4.2 Drift-free InC algorithm

For solving the conventional InC algorithm problems, [46] proposed a new variation of the InC algorithm with a VSS. A slope angle variation algorithm and an autonomous scaling factor are proposed as parts of the proposed algorithm.

Using the autonomous scaling factor, the step size is continuously adjusted without using a constant tracking precision and convergence speed must be balanced.

By implementing the slope of the angle variation algorithm, the PV voltage change effect is mitigated, especially during conditions of variable irradiance, thus improving MPPT efficiency.

To bypass the limitations of traditional conductance increments with variable step lengths, [47] proposed a VSS MPPT algorithm, which is based on analyzing the dP/dU slope to determine the scaling factor (N). Where dP is the variation of power and dU is the variation of voltage.

The slope of dP/dU is checked for the modified VSS algorithm. The system assumes that the operating power is far from the MPP if dP/dU is higher than the previous dP/dU, thus using a higher N value to achieve the MPP more quickly. As an alternative, if dP/dU slopes lower than dP/dU, the system assumes the operating power is already close to the MPP.

In [48], the InC algorithm is enhanced to eliminate the division calculations. Consequently, algorithm implementation complexity is minimized, thereby making it possible to use a low-cost microcontroller to reduce system costs. Moreover, the system response time during sudden changes is improved due to a reduction in the real processing time.

[48] proposed to use a modified variable step-size, which is solely dependent on PV power, as the step-size.

While partial shading is present, the latter model offers enhanced transient performance and minimal steady-state power oscillations around the MPP.

An InC MPPT algorithm with VSS is presented in [49] to track MPP with direct control solar arrays without the proportional-integral control loop.

MPPT response speed and accuracy can be significantly improved with the proposed method compared to conventional InC and variable step-size InC methods.

Table 2.5

Drift-Free Modified InC Algorithms Comparison

Algorithm	Error	Response Time (*s*)
InC	**5.85%**	**0.5**
[46] VSS InC	**0.16%**	**<0.013**
[47] Variable step lengths InC	**1.65%**	**<0.03**
[48] Modified VSS InC	**0.82%**	**<0.02**
[49] Direct control VSS InC	**1.8%**	**<0.013**

2.4.3 Slow and fast irradiance changes modified InC

In [50], the authors propose an InC with direct control and a dual-scaled adaptive step-size method to overcome the shortcoming of the InC MPPT algorithm.

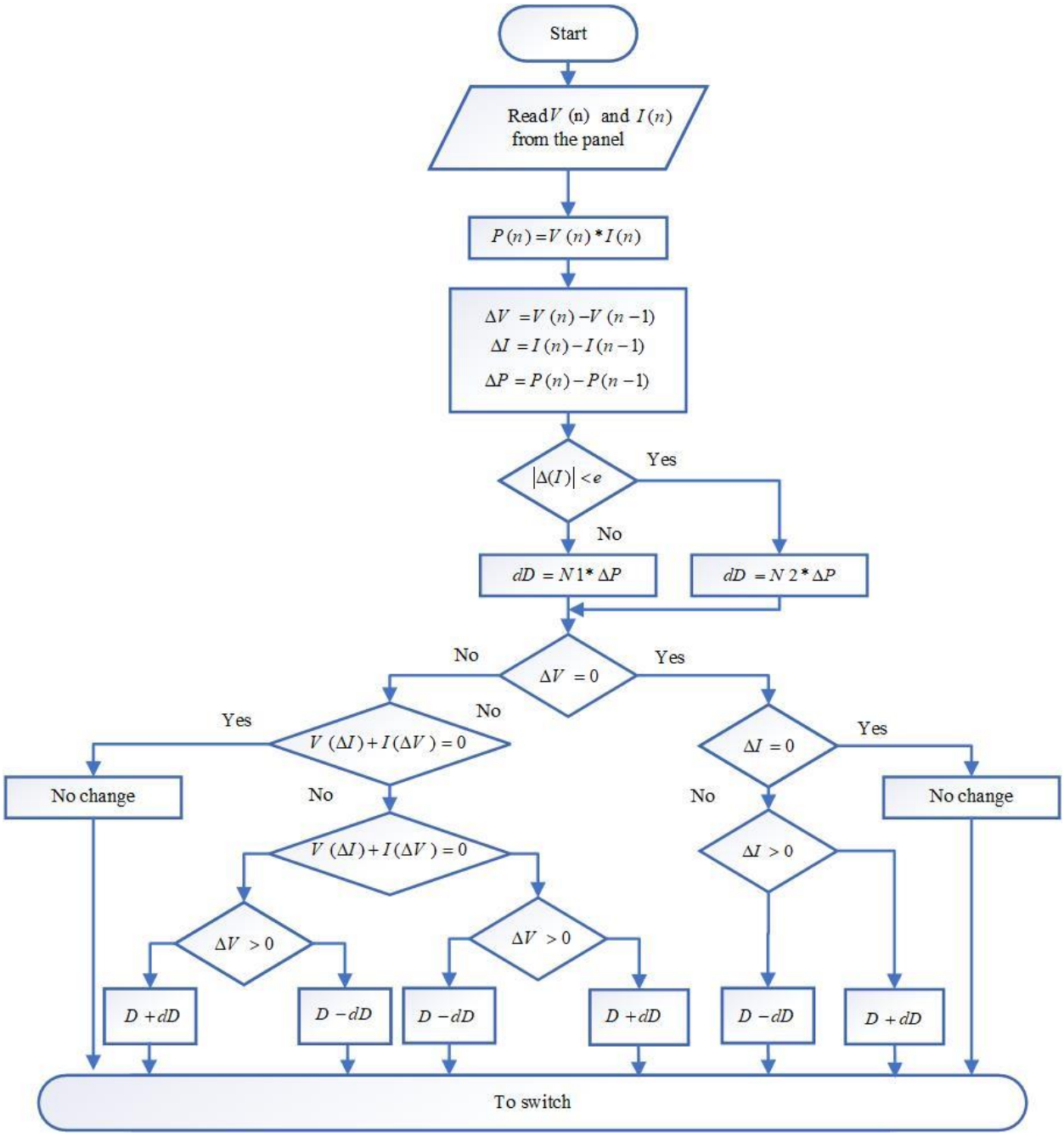

Fig. 2.10. The flowchart of the modified InC algorithm in [50].

In [50], instead of using the Incremental conventional equations for adjusting the duty cycle, the following equations are used to define the MPP and update the duty cycle.

$$\frac{V(\Delta I)+I(\Delta V)}{V(\Delta V)}=0 \qquad \text{MPP} \qquad (2)$$

$$\frac{V(\Delta I)+I(\Delta V)}{V(\Delta V)}>0 \qquad \text{The left side of the MPP}$$

$$\frac{V(\Delta I)+I(\Delta V)}{V(\Delta V)}<0 \qquad \text{The right side of the MPP}$$

Besides removing division complexity, this simplification also reduces steady-state error. As Figure 2.10 depicts, the dual-scaled adaptive step size is designed to deal with the overshoot and slow voltage response instead of using the constant scaling factor.

In [51], MPPT tracking speed is increased by using the VSS InC method. To reduce the oscillation at maximum power conditions, the mentioned paper presented the design of MPPT with buck-boost Converter that uses the filter VSS modified InC method. PV panels generate voltage and current as a starting point for MPPT calculations. Based on these parameters, the power generated can be determined. In its tracking step, the algorithm attempts to calculate voltage and current deviations.

A tracking condition is always determined by the changing value of voltage (ΔV). A zero change in current is determined if the algorithm checks the existing current in case $\Delta V = 0$. An algorithm determines if an error increases or decreases based on the current; otherwise, if it's not changing ($\Delta I = 0$), an error is equal to zero. Whenever ΔV is not zero, the algorithm will check the value of the comparison between equation (1) and use the filter limit to filter the calculation. This result provides a basis for determining that the error should be calculated using the following equation.

$$D_{(t)} = D_{(t-1)} + (N \times error) \qquad (3)$$

Where N is the scaling factor that determines the performance of MPPT, and D is the duty cycle that is used to generate PWM. An MPP is reached in the PV curve, and the algorithm tries a steady state after reaching an MPP.

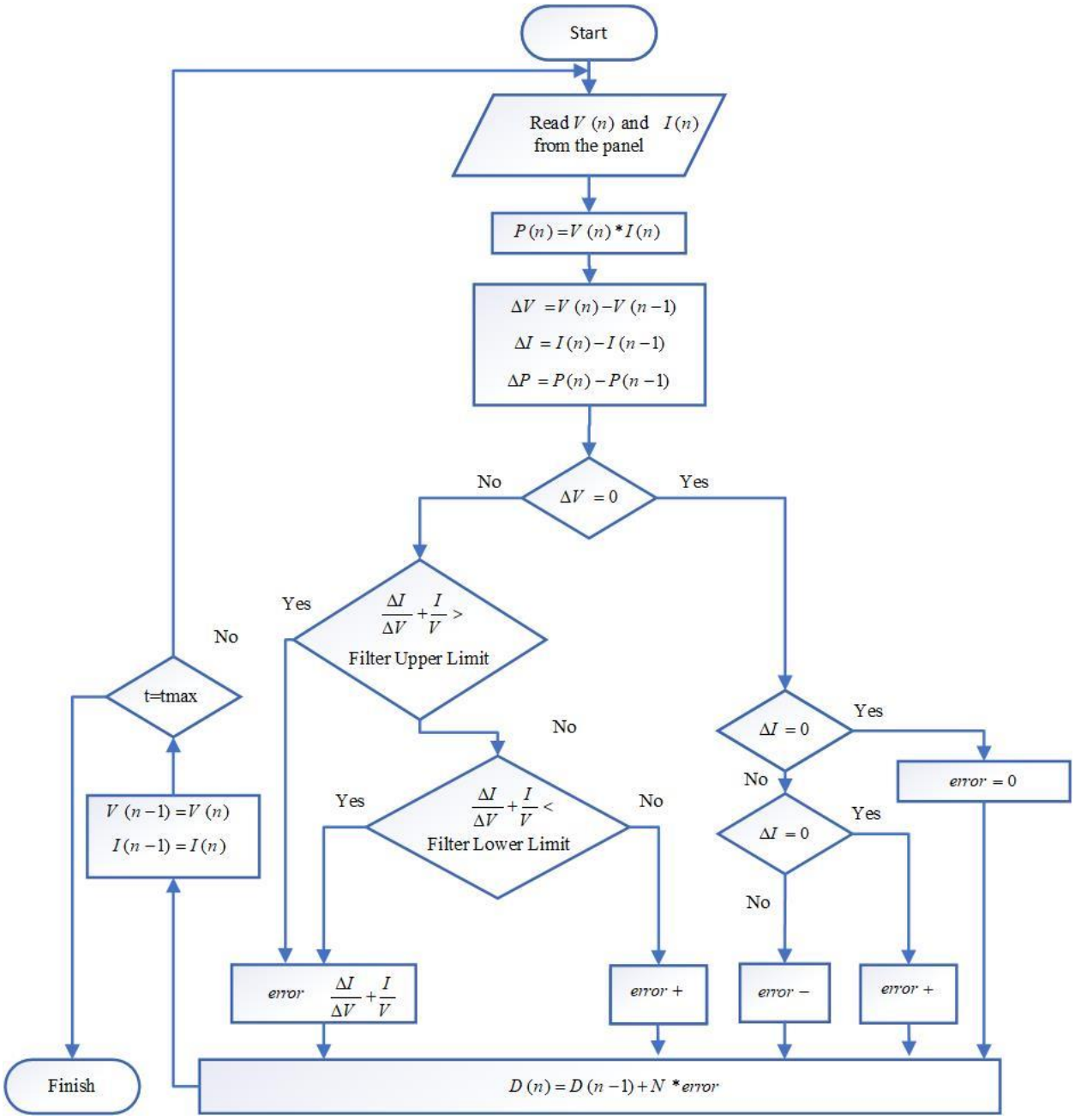

Fig. 2.11. The flowchart of the modified Inc algorithm in [51].

In [52], the steady-state error signal is reduced in conventional algorithm design by using a proportional integral. Error signals (e) are the result of multiplying an instantaneous conductance (I/V) by InC ($\Delta I/\Delta V$).

$$e=\frac{I}{V}+\frac{\Delta I}{\Delta V} \qquad (4)$$

The integral regulator multiplies the integral gain by accumulating the instantaneous error and adds it to the controller output. To reach maximum power, it is essential to make the output impedance equal to the source impedance.

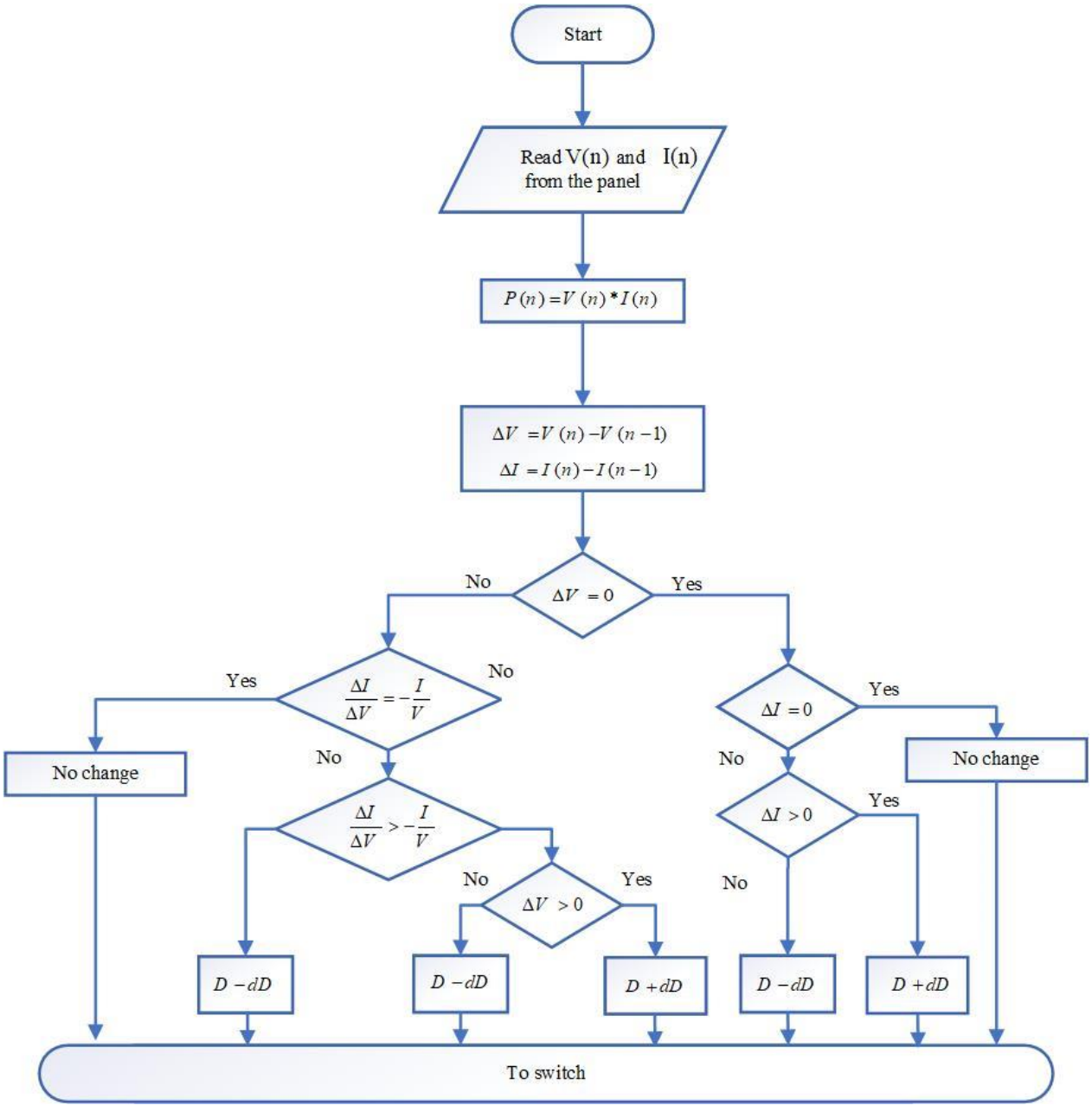

Fig. 2.12. The flowchart of the modified Inc algorithm in [52].

In [53], an improved InC MPPT controller, i.e., InC-PID, is proposed that is the combination of the advantages of the traditional InC algorithm and proportional-integral-derivative controller. The proposed method circumvents the conventional InC algorithm drawbacks while also preserving its simplicity. The parameters of the controller are optimized using grey wolf optimization (GWO). Conventionally, the rate of current change with respect to voltage dI/dV is proportional to the conductance in the instantaneous phase, i.e.

$$\frac{\Delta I}{\Delta V}+\frac{I}{V}=0 \qquad (5)$$

$\Delta P/\Delta V$ will be zero at MPP, i.e., the power will change with voltage equally. In order to decrease the steady-state fluctuations at the MPP, the error signal resulted by the mentioned condition is applied to an MPPT controller to minimize the error. Control gains can be optimized using gray wolf optimization. Grey wolf optimization minimizes the fitness function by adjusting the controller parameter. Here is the fitness function that is applied to the problem.

$$J=\sum_{k=1}^{N}\left|0-(\frac{dI}{dV}+\frac{I}{V})\right| \qquad (6)$$

A new approach to improve MPPT in PV systems with InC MPPTs and VSS was explained in [54]. This modification allows for gradual variation of the initial step so that the MPP can be approached quickly. Once complete, the step can be fractionated after each slope. By dividing each time after exceeding the slope around the PPM according to the desired precision, the step size of the duty cycle ratio (DCR) decreases, and the step value becomes very small. As a result of this technique, the PPM search dynamics are effectively improved. However, the small step value does not contribute to additional searches when a new change occurs. To resolve this issue, the search module must be reset to its initial state.

In [57], taking into account the slope of the power-voltage relationship allows us to estimate the size of a variable voltage step. Introducing an overview of a few effective regions around the PV point of maximum power is proposed as a novel treatment for this goal. As a result, a fuzzy logic system is developed based on the locations of the fuzzy inputs in relation to the five regions to vary the step size of the duty cycle. Then, the fuzzy inputs are inspired by the slope of the current-voltage relation, and its derivatives, while membership functions and fuzzy rules are designed based on the slope of the current-voltage relationship.

Table 2.6

Slow and Fast Irradiance Changes Modified InC Algorithms Comparison

Algorithm	Error	Response Time (*s*)
InC	**5.85%**	**0.5**
[50] Dual-scaled adaptive step-size InC	**4.29%**	**<0.02**
[51] Filter variable modified InC	**1.188%**	**<0.01**
[52] Integral regulator InC	**5%**	**<0.5**
[53] InC-PID	**0.4%**	**0.055**
[54] Fast InC	**0.6%**	**<0.04**
[57] Fuzzy logic based InC	**4.77%**	**<0.013**

2.4.4 PSC InC

Using a modified InC method, [55] proposed a fast and efficient solution to track the global peak under uniform irradiance conditions (UIC) and PSC. By analyzing the relationship between the minimum current at other peaks and the short circuit current, this method detects PSC. It detects if

other peaks need to be tracked under it. This method can improve tracking speed by increasing the sensitivity to the minimum current during other peaks.

The table below compares the main modified InC algorithms discussed in this research. In [56], the objective is to improve the tracking time of the simulated annealing (SA) method by combining the SA method with the modified incremental conductance (MInC) method. Adaptive step sizes are employed in the modified MInC in order to improve speed and accuracy.

Table 2.7

PSC Modified InC Algorithms Comparison

Algorithm	Error	Response Time (*s*)
InC	**5.85%**	**0.5**
[55] PSC InC	**1.18%**	**<0.4**
[56] SA and MInC	**2.95%**	**<3**

2.4.5. Modified InC algorithms comparison

In this section, we look at all modified InC algorithms mentioned in previous sections. As summarized in Table 2.8, most of the modified InC algorithms considered slow and fast irradiance changes, and a few considered drift issues, PSC, and temperature changes. The best modified InC algorithm in case of efficiency is the InC-PID algorithm [53], and in case of response time, the filter variable is modified [51].

Table 2.8

Modified InC MPPT Algorithms Comparison

Algorithm	Error	Response Time (*s*)	Application				
			Slow irradiance changes	Fast irradiance changes	Drift	PSC	Temperature changes
InC	5.85%	0.5	✓	-	-	-	-
[46] VSS InC	0.16%	<0.013	✓	✓	✓	-	
[47] Variable step lengths InC	1.65%	<0.03	✓	✓	✓	-	-
[48] Modified VSS InC	0.82%	<0.02	✓	✓	✓	-	-
[49] Direct control VSS InC	1.8%	<0.013	✓	✓	✓	-	-
[50] Dual-scaled adaptive step-size InC	4.29%	<0.02	✓	✓	-	-	-
[51] Filter variable modified InC	1.188%	<0.01	✓	-	-	-	-
[52] Integral regulator InC	5%	<0.5	✓	✓	-	-	-
[53] InC-PID	0.4%	0.055	✓	✓	-	-	-
[54] Fast InC	0.6%	<0.04	✓	✓	-	-	-
[55] PSC InC	1.18%	<0.4	✓	✓	-	✓	-
[56] SA and MInC	2.95%	<3	✓	✓	-	✓	-
[57] Fuzzy logic based InC	4.77%	<0.013	✓	✓	-	-	✓

2.5 Challenges and Further Studies

Although many substantial works improved the efficiency of conventional P&O and InC algorithms, the modified algorithms are not as easy as conventional algorithms to implement. Therefore, they are still not suitable for low-cost applications. Due to the complexity of some modified algorithms [17], [45], and [52], the response time is not improved or is worse than the conventional algorithms, and those are considerably slower. Moreover, they are not multi-purpose solutions and only consider specific issues of conventional algorithms. It means the mentioned modified algorithms focused on particular environmental conditions such as drift issues, slow or fast irradiance, and PSC.

In future works, the efficiency and response time can be improved. Also, it is still possible to consider the algorithms in case of cost, hardware implementation, and applications. Moreover, the computations should not be that complex to lead to large memory requirements. Besides, the industry still needs a general solution for different cases of environmental conditions. So, the future modified algorithms should have high efficiency in different ambient factors.

2.6 Conclusion

In our study, we focused on analyzing and comparing the modified algorithms of two conventional MPPT methods: InC and P&O. The paper includes a list of various MPP techniques that are reviewed and discussed. Different MPPT techniques have been reviewed based on different applications, such as fast and slow irradiance changes, drift elimination, and PSC. The P&O technique and InC technique are two of the most popular conventional techniques. The best modified InC algorithm in case of efficiency is the InC-PID algorithm [53], and in case of response time, the filter variable is modified [51]. On the other side, the best modified P&O algorithm in the

case of efficiency is the adjustable step size and inspection algorithm [24], and in the case of response time, the most reliable algorithm is adaptive P&O [19].

References

[1] B. Bendib, H. Belmili, and F. Krim, "A survey of the most used MPPT methods: Conventional and advanced algorithms applied for (PV) systems, "Renew. Sustain. Energy Rev., vol. 45, pp. 637–648, 2015.

[2] Z. Salam, J. Ahmed, and B. S. Merugu, "The application of soft computing methods for MPPT of PV system: A technological and status review," Appl. Energy, vol. 107, pp. 135–148, 2013.

[3] N. Femia, G. Petrone, G. Spagnuolo, and M. Vitelli, "Optimization of P&O MPP tracking method," IEEE Transactions on Power Electronics, vol. 20, no. 4, pp. 963–973, July 2005.

[4] H. A. Sher, A. F. Murtaza, A. Noman, K. E. Addoweesh, K. Al-Haddad, and M. Chiaberge, "A new sensorless hybrid MPPT algorithm based on fractional short-circuit current measurement and PPO MPPT," IEEE Trans. Sustainable energy, vol. 6, no. 4, pp. 1426–1434, Oct. 2015.

[5] M. A. Elgendy, B. Zahawi, and D. J. Atkinson, "Assessment of P&O MPPT algorithm implementation techniques for PV pumping applications," IEEETrans. Sustainable energy, vol. 3, no. 1, pp. 21–33, Jan.2012.

[6] J. H. Lee, H. Bae, and B. H. Cho, "Advanced InC MPPT algorithm with a variable step size," in Proc. 12th Int. Power Electron. Motion Control Conf., Aug./Sep. 2006, pp. 603–607.

[7] M. Qiang, S. Mingwei, L. Liying, and J. M. Guerrero, "A novel improved variable step-size incremental-resistance MPPT method for PV systems," IEEE Trans. Ind. Electron., vol. 58, no. 6, pp. 2427–2434, Jun. 2011.

[8] Weidong Xiao and W. G. Dunford, "A modified adaptive hill climbing MPPT method for (PV) power systems," IEEE 35th Annual Power Electronics Specialists Conference (IEEE Cat. No.04CH37551), Aachen, Germany, pp. 1957–1963, 2004.

[9] M. Rezkallah, S. K. Sharma, A. Chandra, B. Singh and D. R. Rousse, "Lyapunov Function and Sliding Mode Control Approach for the Solar-PV Grid Interface System," in IEEE Transactions on Industrial Electronics, vol. 64, no. 1, pp. 785–795, Jan. 2017.

[10] R. Iftikhar, I. Ahmad, M. Arsalan, N. Naz, N. Ali, and H. Armghan, "MPPT for (PV) System UsingNon-linear Controller," Int. J. Photoenergy, vol. 2018, pp. 1–11, 2018.

[11] F. M. de Oliveira, F. R. Durand, V. D. Bacon, S. A. O. da Silva, L. P. Sampaio, and L. B. G. Campanhol, "Grid-tied (PV) system based on PSO MPPT technique with active power line conditioning," IET Power Electronics, vol. 9, no. 6, pp. 1180–1191, 2016.

[12] A. A. S. Mohamed, A. Berzoy and O. A. Mohammed, "Design and Hardware Implementation of FL-MPPT Control of PV Systems Based on GA and Small-Signal Analysis," in IEEE Transactions on Sustainable Energy, vol. 8, no. 1, pp. 279-290, Jan. 2017.

[13] M. Dehghani, M. Taghipour, G. B. Gharehpetian, and M. Abedi, "Optimized Fuzzy Controller for MPPT of Grid-connected PV Systems in Rapidly Changing Atmospheric Conditions," in Journal of Modern Power Systems and Clean Energy, vol. 9, no. 2, pp. 376-383, March 2021.

[14] E. Koutroulis, K. Kalaitzakis, and N. C. Voulgaris, "Development of a microcontroller-based, (PV) MPPtracking control system," IEEE Trans. Power Electron., vol. 16, no. 1, pp. 46–54, Jan. 2001.

[15] C. -C. Hua and Y. -m. Chen, "Modified (P&O) MPPT with zero oscillation in steady-state for PV systems under partial shaded conditions," *2017 IEEE Conference on Energy Conversion (CENCON)*, 2017, pp. 5-9, doi: 10.1109/CENCON.2017.8262448.

[16] V. B. Waghmare and C. N. Swapnali, "A drift free perturb & observe MPPT in PV system," *2017 Second International Conference on Electrical, Computer and Communication Technologies (ICECCT)*, 2017, pp. 1-5.

[17] S. D. Al-Majidi, M. F. Abbod and H. S. Al-Raweshidy, "A Modified P&O-MPPT based on Pythagorean Theorem and CV-MPPT for PV Systems," *2018 53rd International Universities Power Engineering Conference (UPEC)*, 2018, pp. 1-6.

[18] D. A. Jalindar and S. Tiwari, "A Modified Perturb & Observe Algorithm for MPPT With Zero Voltage Switching Buck Boost Converter in (PV) System," *2018 2nd IEEE International Conference on Power Electronics, Intelligent Control and Energy Systems (ICPEICES)*, 2018, pp. 337-342.

[19] A. Mohapatra, B. Nayak and C. Saiprakash, "Adaptive Perturb & Observe MPPT for PV System with Experimental Validation," *2019 IEEE International Conference on Sustainable Energy Technologies and Systems (ICSETS)*, 2019, pp. 257-261.

[20] M. B. Smida and A. Sakly, "Genetic based algorithm for MPPT for grid connected PV systems operating under partial shaded conditions," 7th International Conference on Modelling, Identification and Control (ICMIC), Tunisia, pp.1–6, 2015.

[21] E. P. Sarika, J. Jacob, S. Sheik Mohammed and S. Paul, "Standalone PV System with Modified VSS P&O MPPT Controller Suitable for Partial Shading Conditions," *2021 7th International Conference on Electrical Energy Systems (ICEES)*, pp. 51-55, 2021.

[22] Mahmod Mohammad AN, Mohd Radzi MA, Azis N, Shafie S, Atiqi Mohd Zainuri MA. An enhanced adaptive P&O technique for efficient MPPT under partial shading conditions. Applied Sciences. 2020 Jun 5;10(11):3912.

[23] N. Kumari, S. S. Kumar and V. Laxmi, "Modified MPPT Topology: A Comparative Analysis," *2019 IEEE 16th India Council International Conference (INDICON)*, 2019, pp. 1-4.

[24] K. O. Sarfo, W. M. Amuna, B. N. Pouliwe and F. B. Effah, "An Improved P&O MPPT Algorithm Under Partial Shading Conditions," *2020 IEEE PES/IAS PowerAfrica*, 2020, pp. 1-5.

[25] Harrag A, Messalti S. Variable step size modified P&O MPPT algorithm using GA-based hybrid offline/online PID controller. Renewable and Sustainable Energy Reviews. 2015 Sep 1;49:1247-60.

[26] R. Akkaya, A.A. Kulaksız, O. Aydogdu DSP implementation of a PV system with GA-MLP-NN based MPPT controller supplying BLDC motor drive Energy Convers. Manag., 48 (2007), pp. 210-218.

[27] C. Larbes, S. Cheikh, T. Obeidi, A. Zerguerras Genetic algorithms optimized fuzzy logic control for the MPPT in (PV) system Renew. Energy, 34 (2009), pp. 2093-2100.

[28] A.A. Kulaksız, R. Akkaya A genetic algorithm optimized ANN-based MPPT algorithm for a stand-alone PV system with induction motor drive Sol. Energy, 86 (2012), pp. 2366-2375.

[29] R. Ramaprabha, V. Gothandaraman, K. Kanimozhi, R. Divya, B.L. Mathur, MPPT using GA-optimized artificial neural network for solar PV system, in: Proceedings of the 1st International Conference on Electrical Energy Systems (ICEES), 2011, pp. 264–268.

[30] A. Messai, A. Mellit, A. Guessoum, S.A. Kalogirou, MPPT using GA optimize fuzzy logic controller and its FPGA implementation Sol. Energy, 86 (2011), pp. 265-277.

[31] A.A. Kulaksız, R. Akkaya, Training data optimization for ANNs using genetic algorithms to enhance MPPT efficiency of a stand-alone PV system Turk. J. Elec. Eng. Comput. Sci., 20 (2012), pp. 241-254.

[32] S. Mallika, RS kumar, Genetics algorithm based MPPT controller for (PV) system
Int. Electr. Eng. J. IEEJ, 4 (2013), pp. 1159-1164

[33] A. Rezaei, S.A. Gholamian Optimization of new fuzzy logic controller by genetic algorithm for MPPT in (PV) system ISESCO J. Sci. Technol., 9 (2013), pp. 9-16.

[34] P. Seena, T. Jaimol, Comparison of MPPT using GA optimized NN employing PI controller for solar PV system with using MPPT incremental conductance, in: Proceeedings of the International Conference on Power, Signals, Controls and Computation (EPSCICON), 2014, pp. 8–10.

[35] S. Hadji, F. Krim, J.P. Gaubert, Development of an algorithm of MPPT for (PV) systems using genetic algorithms, in: Proceedings of the 7th International Workshop on Systems, Signal Processing and their Applications (WOSSPA), 2011, pp. 43–46.

[36] S. Hadji, J.P. Gaubert, F. Krim, Genetic algorithms for MPPT in (PV) systems, in: Proceedings of the 2011–14th European Conference on Power Electronics and Applications (EPE 2011), 2011; pp. 1–9.

[37] R. Ramaprabha, B.L. Mathur Genetic algorithm based MPPT for partially shaded solar (PV) array Int. J. Res. Rev. Inf. Sci. (IJRRIS), 2 (2012), pp. 161-163.

[38] M. Dahmane, J. Bosche, A. EI-Hajjaji, X. Pierre, MPPT for (PV) conversion systems using genetic algorithm and robust control, in: Proceedings of the American Control conference (ACC), Washington, DC, USA, 2013, pp. 17–19.

[39] Y. Shaiek Y, MB Smida, A. Sakly, M.F. Mimouni Comparison between conventional methods and GA approach for MPPT of shaded solar PV generators Sol. Energy, 90 (2013), pp. 107-122.

[40] S. Daraban, D. Petreus, C. Morel A novel MPPT algorithm based on a modified genetic algorithm specialized on tracking the global MPP in (PV) systems affected by partial shading Energy, 74 (2014), pp. 374-388.

[41] Shankar G, Mukherjee V. MPP detection of a partially shaded PV array by continuous GA and hybrid PSO. Ain Shams Engineering Journal. 6, no. 2 (2015), pp. 471-9.

[42] DS Niranjan, S.B. Dhale, J.S. Mukherjee, T. SudhakarBabu, N. Rajasekar Solar PV array reconfiguration under partial shading conditions for maximum power extraction using genetic algorithm Renew. Sustain. Energy Rev., 43 (2015), pp. 102-110.

[43] Y.H. Liu, J.H. Chen, J.W. Huang A review of MPPT techniques for use in partially shaded conditions Renew. Sustain. Energy Rev., 41 (2015), pp. 436-453.

[44] Kota VR, Bhukya MN. A novel linear tangents based P&O scheme for MPPT of a PV system. Renewable and Sustainable Energy Reviews., 71 (2017), pp. 257-67.

[45] V. Kumar and M. Singh, "Derated Mode of Power Generation in PV System Using Modified P&O MPPT Algorithm," in *Journal of Modern Power Systems and Clean Energy*, vol. 9, no. 5, pp. 1183-1192.

[46] Owusu-Nyarko I, Elgenedy MA, Abdelsalam I, Ahmed KH. Modified variable step-size InC MPPT technique for (PV) systems. Electronics. 2021 Sep 23;10(19):2331.

[47] Yang, L.; Yunbo, Z.; Shengzhu, L.; Hong, Z. (PV) array MPPT based on improved variable step-size incremental conductance algorithm. In Proceedings of the 2017 29th Chinese Control and Decision Conference (CCDC), Chongqing, China, 28–30 May 2017.

[48] Zakzouk, N.N.E.; Elsaharty, M.A.; Abdelsalam, A.K.; Helal, AA;Williams, B.W. Improved performance low-cost incremental conductance PV MPPT technique. IET Renew. Power Gener. 2016, 10, 561–574.

[49] Liu, F.; Duan, S.; Liu, F.; Liu, B.; Kang, Y. A Variable Step Size INC MPPT Method for PV Systems. IEEE Trans. Ind. Electron. 2008, 55, 2622–2628.

[50] N. A. Rahim, A. Amir, A. Amir and J. Selvaraj, "Modified InC MPPT with direct control and dual scaled adaptive step-size method," *4th IET Clean Energy and Technology Conference (CEAT 2016)*, 2016, pp. 1-8.

[51] T. Andromeda *et al*., "Maximum Power Tracking of Solar Panel using Modified InC Method," *2018 5th International Conference on Information Technology, Computer, and Electrical Engineering (ICITACEE)*, 2018, pp. 251-255.

[52] M. H. Anowar and P. Roy, "A Modified (InC)Based (PV) MPPT Charge Controller," *2019 International Conference on Electrical, Computer and Communication Engineering (ECCE)*, 2019, pp. 1-5.

[53] U. Chauhan, A. Rani, V. singh and B. Kumar, "A Modified InC MPPT for Standalone PV System," *2020 7th International Conference on Signal Processing and Integrated Networks (SPIN)*, 2020, pp. 61-64.

[54] Hebchi M, Kouzou A, Choucha A. Improved InC algorithm for MPPT in (PV) System. In2021 18th International Multi-Conference on Systems, Signals & Devices (SSD) 2021 Mar 22, pp. 1271-1278.

[55] L. Xu, R. Cheng and J. Yang, "A Modified INC Method for PV String Under Uniform Irradiance and Partially Shaded Conditions," in *IEEE Access*, 8, (2020), pp. 131340-131351.

[56] K. L. Lian and V. Andrean, "A new MPPT method for partially shaded PV system by combining modified INC and simulated annealing algorithm," *2017 International Conference on High Voltage Engineering and Power Systems (ICHVEPS)*, 2017, pp. 388-393.

[57] M. N. Ali, K. Mahmoud, M. Lehtonen and M. M. F. Darwish, "An Efficient Fuzzy-Logic Based Variable-Step InC MPPT Method for Grid-Connected PV Systems," in *IEEE Access*, vol. 9, pp. 26420-26430, 2021.

Co-authorship Statement

I am the primary author of all the research papers compiled in composing this thesis, and my supervisors, Dr. Mohsin Jamil, and Dr. M. Tariq Iqbal are co-authors of all articles. As the lead author, did most of the research work, did the literature reviews, carried out the designs, hardware implementations, experimental setups, and analysis of the results in each of the manuscripts. I also formulate the original manuscripts and later edited each of them based on comments from the co-author and peer reviewers throughout the peer review process. Co-author Dr. Mohsin Jamil supervised all the research work, revised, and corrected each one of the manuscripts, provided research material, contributed research ideas throughout the research, and updated each of the manuscripts.

Chapter 3

An Improved Perturb and Observe Maximum Power Point Tracking Algorithm for Photovoltaic Power Systems

Preface

A version of this manuscript has been peer-reviewed, accepted in the Journal of Modern Power Systems and Clean Energy (MPCE), September 2022. I am the primary author, and I carried out most of the research work performed the literature reviews, carried out the system design, implementations, and analysis of the results. I also prepared the first draft of the manuscript and subsequently revised the final manuscript based on the feedback from the co-author and the peer review process. The Co-authors, Dr. Mohsin Jamil, and Dr. M. Tariq Iqbal supervised the research, provided the research guide, reviewed, and corrected the manuscript, and contributed research ideas to the actualization of the manuscript.

Abstract

This research aims to improve the performance of the conventional Perturb and Observe (P&O) Maximum Power Point Tracking (MPPT) algorithm. As the oscillation around the maximum power point (MPP) is the main disadvantage of this technique, we introduce a modified P&O method to conquer this handicap. The new algorithm recognizes approaching the peak of the photovoltaic (PV) array power curve and prevents oscillation around MPP. The key parameter to achieve this goal is testing the change of output power in each cycle and comparing it with the change in array terminal power of the previous cycle. If a decrease in array terminal power is seen after an increase in the previous cycle or in the opposite direction, an increase in array terminal power is seen after a decrease in the previous cycle; it means we are at the peak of the power curve so the duty cycle of the boost converter should remain the same as the previous cycle. Besides, an optimized duty cycle is introduced, which is adjusted based on the PV array operating point. Furthermore, a DC-DC boost converter powered by a solar PV array simulator is used to test the suggested concept. When irradiance changes, the proposed technique produces an average η_{MPPT} of nearly 3.1 percent greater than the conventional P&O and the incremental conductance (InC) algorithm. In addition, under strong partial shading conditions (PSC) and drift avoidance tests, the proposed technique produced an average η_{MPPT} of nearly 9 percent and 8 percent greater than the conventional algorithms, respectively.

Keywords: PV system, MPPT, P&O, Boost converter, steady-state performance.

3.1 Introduction

Solar PV is predicted to be one of the most popular renewables due to its availability, ease of installation, and near-zero maintenance. PV power generation systems are used to convert solar energy to electricity. However, PV power fluctuates depending on irradiation and temperature. Therefore, solar electricity is still more expensive than fossil fuels due to the low conversion efficiency of PV modules.

Designing an effective control algorithm plays a vital role in developing an efficient solar PV system [1]. In PV systems, it is well known that one of the main solutions to increase efficiency is the application of MPPT techniques [2]. Because the MPPT is made up of software codes, it appears to be the most cost-effective solution to increase energy throughput. MPPT ensures that the operating voltage and current remain at the MPP on the p-v characteristic curve at all times [3]. There are many papers with a variety of control techniques for PV MPPT systems; They are mainly divided into two categories: conventional and soft computing approaches. Several studies have been carried out on conventional MPPT methods such as P&O [4], [5], [6], InC algorithm [7], [8], and a hill-climbing (HC) algorithm [9], [10]. Conventional algorithms are the most used methods due to their ease of implementation, as a result of which they have become more suitable for low-cost applications. Despite their ease of use, traditional methods have demonstrated a sluggish response to changes in ambient temperature and solar radiation power. Consequently, the system's deviation from its MPP results in a power loss that is proportional to the size of the installed solar array [1].

Besides conventional algorithms, there are many other solutions, such as bioinspired algorithms, which are much more efficient in some special cases when compared to conventional ones. They are capable enough to quickly converge to a global maximum and hence can save power loss even in a partially shaded environment [11]. Particle swarm optimization (PSO) is a bioinspired

algorithm that is employed successfully in [12]. A genetic algorithm (GA) is one such algorithm that solves the obstacle of partial shading [13], [14]. Moreover, there are two artificial intelligence (AI) based algorithms, fuzzy logic-based controllers (FLBCs) and artificial neural network (ANN)-based MPPT [15], [16]. Although the mentioned algorithms show less settling time, less overshoot, and better performance about MPPT, they require data set in the beginning to train the input-output relation. In [23], [24], a sliding mode and Lyapunov function-based algorithms were presented for achieving MPPT control of a solar-PV array tied with the grid. In addition, nonlinear optimal feedback control is employed in [1] to deal with oscillations around the MPP of the system. Although there exist various techniques in the literature that try to improve the drawbacks of conventional MPPT approaches, they are substantially slower, and the implementation is still in priority when control methods are put into practice. Therefore, most scientists believe the modified conventional approaches are more popular to apply instead of the complicated modern theories [3-4]. P&O is the simplest of the traditional MPPTs and has excellent convergence [5-6]. The algorithm, however, has two significant flaws. The first is the constant oscillation that happens in the vicinity of the MPP. Second, when the irradiance (G) increases rapidly or when the irradiance is non-uniform PSC, the P&O is prone to losing its tracking orientation. Both issues contribute to a loss of power and, as a result, a reduction in tracking efficiency. As fluctuation around the MPP is the source of power loss, there are many works tried to modify the conventional algorithms in the case of PSC [17-20] and drift avoidance issues [21-22]. Complex computations and large memory requirements are the drawbacks of mentioned works. Moreover, they are not multi-purpose solutions and only consider specific issues of conventional algorithms. This paper offers a new modified P&O algorithm to compensate for the steady-state oscillation of MPP tracking. This algorithm presents a new approach to recognizing the peak power point when the stable condition arrives at the maximum of the PV array output power. In this way, when the current and

voltage of the PV array reach the optimum point, the duty cycle will remain constant, and no chattering will be produced around MPP. The conventional and modified P&Os are thoroughly benchmarked in this study under varying environmental conditions utilizing the steady state and dynamic MPPT efficiency tests, PSC tests, and drift effect tests. Those tests require the algorithm to track irradiance ramps with varying rates of change. Also, the modified P&O algorithm compares with the InC algorithm. The performance boost from the suggested method is clarified when the results for the conventional algorithms and modified P&O have been compared in all mentioned environmental conditions. In this way, the proposed algorithm can be considered a multi-purpose solution for crucial MPPT conditions.

A list of parameters used in this paper is given in Table 3.1.

TABLE 3.1

Nomenclature

Symbol	Quantity
I_{ph}	Light-generated current
I_s	Reverse saturation current
I_{sh}	Shunt resistor current
n	Ideality factor of PV cell
V_T	Thermal voltage
N_p, N_s	Parallel and series branches of PV module
R_{sh}, R_s	Shunt and series resistance of PV module
L, C	Inductor and capacitor of the DC-DC converter
P	Power of solar array
V	Voltage of the solar array
I	Current of the solar array
P	Solar array output power

P_{max}	**Solar array maximum power**
P_{out}	**DC-DC converter output power**
I_{out}	**Desired output current of DC-DC converter**
V_{out}	**Desired output voltage of DC-DC converter**
I_L	**DC-DC converter inductor current**
R	**DC-DC converter resistor**
L	**DC-DC converter inductor**
C_1	**DC-DC converter input capacitor**
C_2	**DC-DC converter output capacitor**
D	**Duty cycle**
η_{MPPT}	**MPPT algorithm's average efficiency**

3.2 Problem Statement

3.2.1 PV Array model

A comparable circuit is given in Fig. 3.1. for a PV system with N_s and N_p modules linked in series parallel. The I is the output current of the PV array, and the V is the output voltage of the PV array. By considering Kirchhoff's current law, the output current of the PV is equal to

$$I = N_p I_{ph} - N_p I_s \left(\exp\left(\frac{\frac{R_s I}{N_p} + \frac{V}{N_s}}{n V_T} \right) - 1 \right) - I_{sh} \qquad (1)$$

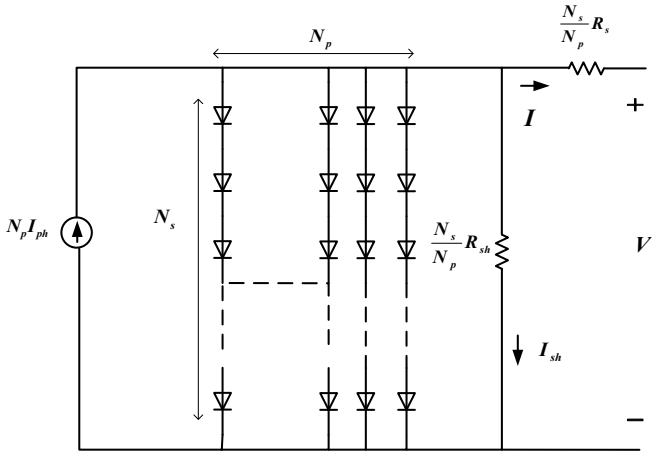

Figure 3.1: The solar array's electrical equivalent model

Where I_{ph}, I_s, N and V_T are the light generated current, reverse saturation current, ideality factor, and thermal voltage of the PV module, respectively. Moreover, considering the equivalent shunt resistor R_{sh} and the series resistor R_s of the PV module in the circuit, we can find the current flowing through the shunt resistor as (2)

$$I_{sh} = \frac{R_s I + \frac{N_p}{N_s} V}{R_{sh}} \qquad (2)$$

For simplification, assuming that $R_s << R_{sh}$. Considering the model values $R_s = 0$ and $R_{sh} = \infty$, and (1) will be determined as

$$I = N_p I_{ph} - N_p I_s \left(\exp\left(\frac{V}{n N_s V_T} \right) - 1 \right) \quad (3)$$

Therefore, the output voltage of the PV array can be calculated as

$$V = N_s n V_T \ln\left(\frac{N_p I_{ph} + N_p I_s - I - I_{sh}}{N_p I_s} \right) \quad (4)$$

3.2.2 DC-DC boost converter

A converter is the main part of the MPPT controller of the PV array, which helps to match the impedance seen from the PV device and the impedance seen from the load side. Therefore, the output voltage of PV will change according to the adjusted impedance. Many DC-DC converter topologies such as the boost topology [29], [30], the buck topology [25], single-ended primary inductor converter (SEPIC) topology [31], [32], buck-boost converters [33], and so on. The boost converters are involved in increasing the voltage. The buck converters are applied to lower the voltage. Then, buck-boost and SEPIC are competent to step up and step down the output voltage. There are also lots of studies that compare the different types of converter performance. In [29], step-up DC-DC converters in various configurations are proposed. In [25], the authors analyzed boost and SEPIC converters, considering output voltage ripple, total harmonic distortion, and power factor for both converters, and Boost converters produced better results. Besides mentioned features, boost converters are easier to use. So, the boost-type converter is frequently used because of its superior performance. For the characteristics discussed earlier, we select the boost topology to place between PV array and load. As illustrated in Figure 3.2, the main elements of a boost converter are the inductor, diode, capacitor, and switch. In this research, we use MOSFET as a

switch that can be turned on and off consistently based on the generated duty cycle. The variability in the PV voltage control process is caused by the dynamic resistance, which is obtained from the slope of its I–V characteristic curve [26], [27]. This parameter depends on the characteristics of the PV array and is highly variable with the irradiation, the temperature, and especially the PV voltage. As a result, the voltage regulation performance can be diminished when operating under irradiation and temperature change [28].

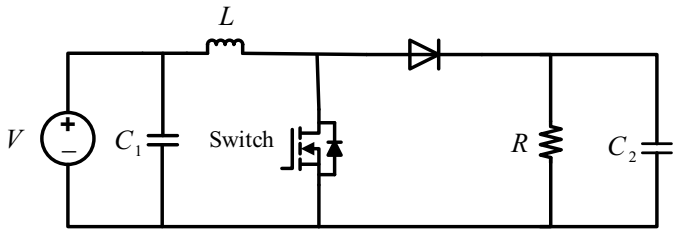

Figure 3.2: The boost converter equivalent circuit

The dynamic model of the boost converter circuit is as follows

$$\begin{cases} \dfrac{dV}{dt} = \dfrac{1}{C_1}\left(I - I_L\right) \\ \dfrac{dI_L}{dt} = \dfrac{1}{L}\left(V + \dfrac{1}{L}(D-1)V_{out}\right) \\ \dfrac{dV_{out}}{dt} = \dfrac{1}{C_2}\left(I_L - I_{out}\right) + \dfrac{1}{C_2}DI_L \end{cases} \quad (5)$$

Then,

$$\dot{x} = f(x) + g(x)D \quad (6)$$

Where D is the duty cycle of the waveform driving the switch,

$$x = \begin{bmatrix} V \\ I_L \\ V_{out} \end{bmatrix}; f(x) = \begin{bmatrix} \dfrac{1}{C_1}(I - I_L) \\ \dfrac{1}{L}(V - V_{out}) \\ \dfrac{1}{C_2}(I_L - I_{out}) \end{bmatrix}; g(x) = \begin{bmatrix} 0 \\ \dfrac{1}{L}V_{out} \\ -\dfrac{1}{C_2}I_L \end{bmatrix} \quad (7)$$

In Continuous conduction mode (CCM), the following equation relates the output voltage to the input voltage [33]:

$$V_{out} = \frac{1}{(1-D)} V \quad (8)$$

Based on

$$P = P_{out} \quad (9)$$

It is easy to extract that

$$R_{out} = R_{pv} \frac{1}{(1-D)^2} \quad (10)$$

where R_{pv} is the PV panel load; this is also a boost converter input load.

Equation (10), which is based on the equation $R_{pv} = R_{out}(1-D)^2$, shows that if D decreases/increases, R_{pv} increases/decreases; consequently, based on the I-V characteristic, the panel's current will increase, and the panel's voltage will reduce. Equivalently, as the voltage decreases/increases, the current increases/decreases, as shown in equation (4).

This demonstrates that the rate at which the duty cycle changes is always the inverse of the voltage change rate. This can be mathematically expressed as

$$\text{sign}(\dot{V}) = -\text{sign}(\dot{D}) \quad (11)$$

The output power of a PV generator is given by $P = V \times I$. The power optimization is done by forcing the system to operate at a certain point, which is defined by solving the following equation

$$\frac{dP}{dV} = 0 \quad (12)$$

3.3 Modified P&O MPPT Algorithm

3.3.1 Overview of P&O algorithm

The P&O algorithm is based on perturbing the PV array output voltage by tuning the duty cycle (perturbation step-size) of a power converter and then checking the changes in the output power of the array. If dP is positive, it means we are approaching the maximum panel power, and the perturbation must be made in the same direction. Conversely, if the output power decreases, the perturbation must be made in the reverse order. is shown $dP = 0$ that the MPP is reached. The flowchart of the P&O algorithm is displayed in Figure 3.3.

The perturbation step size plays an undeniable role in reaching the MPP as the large step size may lead to a fast-tracking response, but the amplitude of the steady-state oscillations will be high. On the other hand, if the step size has a small value, the tracking is slower, and still, a small oscillation will be seen. Nonstop oscillation around the MPP is the main drawback of the P&O algorithm. Unfortunately, this hindrance is bold because it leads to energy losses.

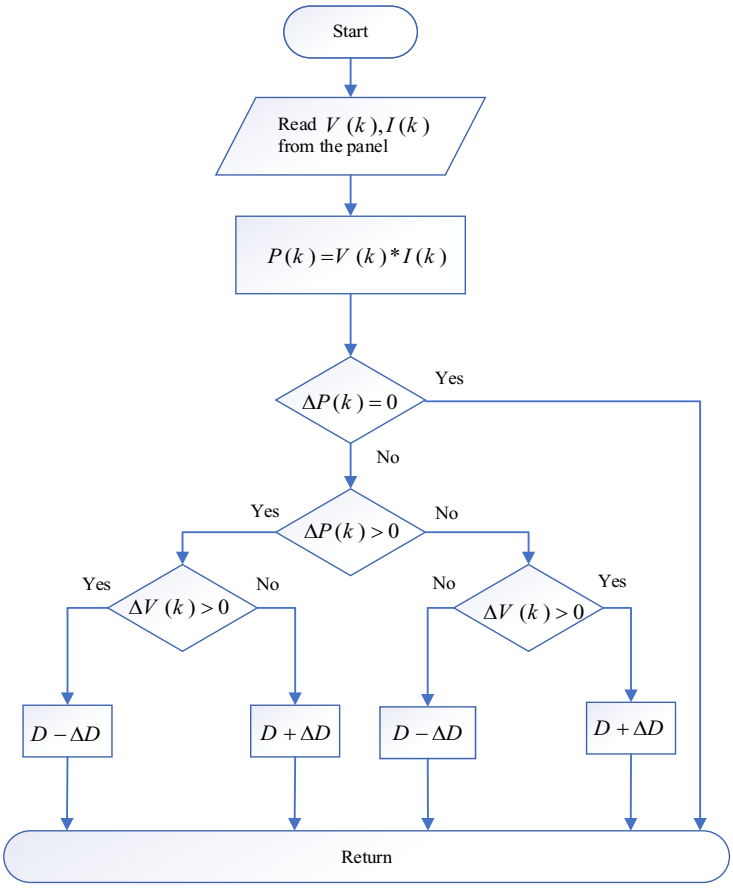

Figure 3.3: Original P&O algorithm flowchart

3.3.2 The proposed P&O algorithm

This new modified algorithm focuses on the steady-state response of PV array power output. As the oscillation around the MPP is the source of power loss, we have to reduce the fluctuation as much as possible. It is evident in Figure 3.3 that the only case that the original P&O algorithm stop oscillation is $\Delta P = 0$. For the other issues, fluctuation around the peak power point is inevitable. As the $\Delta P = 0$ rarely occurs during perturbation, we need to increase the chance of stopping the oscillation when the output power is extremely close to the climax of the power curve. For this proposal, one parameter is added to the MPPT flowchart, which is $\Delta P(\mathrm{k}-1) > 0$ to recognize when the algorithm is crossing the maximum point of the power curve. In this way, the sign of $\Delta P(\mathrm{k})$ in

each cycle will be compared to the sign of $\Delta P(\mathrm{k}-1) > 0$, that is equal to ΔP in the previous cycle. If these two signs are different, it means the PV array output power crosses the peak, and the duty cycle should not be changed. In other words, if perturbation makes a decrease (increase) in array terminal power after an increase (decrease) in the preceding cycle, it means we are crossing the peak of the power curve, so the duty cycle of the boost converter should remain the same as the previous cycle. In this manner, the steady-state oscillation will be eliminated in case of constant illumination. The flowchart of the proposed algorithm is shown in Figure 3.4. Note that the added conditions are bold in yellow color.

A positive scalar function of the state variables of the system is picked out:

$$E = \frac{1}{2}S^2 > 0 \tag{13}$$

where

$$S = \frac{dP}{dV} = I + \frac{dI}{dV}V \tag{14}$$

Then, the following condition is the sufficient condition for the global stability of the system.

$$\dot{E} = S\frac{dS}{dt} < 0, \dot{S}S < 0 \tag{15}$$

Using (3),

$$S = \frac{dP}{dV} = N_p I_{ph} - N_p I_s \left(\exp\left(\frac{V}{nN_s V_T} \right) - 1 \right) - \frac{N_p I_s}{nN_s V_T} \left(\exp\left(\frac{V}{nN_s V_T} \right) \right) \tag{16}$$

When $S = 0$, the PV system has reached its maximum output. As a result, the dynamics of the system can be split into two states: $S < 0$ and $S > 0$.

When $S < 0$, the new algorithm is divided into two types of situations: $\Delta P(\mathrm{k}-1) > 0$ and $\Delta P(\mathrm{k}-1) < 0$

.

If $\Delta P(\mathrm{k}-1) > 0$, the algorithm treats the same as the PV system reaches the MPP, so the oscillation will be removed. If $\Delta P(\mathrm{k}-1) < 0$, based on the new algorithm, $\dot{D} > 0$ and by using (7), V decreases:

$$\dot{V}_a < 0 \qquad (17)$$

As we know, the derivative of S is

$$\dot{S} = \frac{dS}{dV}\dot{V} \qquad (18)$$

Then, using (12),

$$\dot{S} = -\frac{N_p I_s}{nN_s V_T}\left(\exp\left(\frac{V}{nN_s V_T}\right) + \left(1 + \frac{1}{nN_s V_T}\right)\exp\left(\frac{V}{nN_s V_T}\right)\right)\dot{V} \qquad (19)$$

Using (14) in (16) results in $\dot{S} > 0$; thus,

$$\dot{S}S < 0 \qquad (20)$$

when $S > 0$ the new algorithm is divided into two different situations $\Delta P(\mathrm{k}-1) > 0$ and $\Delta P(\mathrm{k}-1) < 0$. If $\Delta P(\mathrm{k}-1) < 0$, the algorithm treats the same as the PV system reaches the MPP. If $\Delta P(\mathrm{k}-1) > 0$, based on the new algorithm, $\dot{D} < 0$ and by using (8), V increases:

$$\dot{V} > 0 \qquad (21)$$

Using (18) in (16) results in $\dot{S} < 0$, thus; finally,

$$\dot{S}S < 0 \qquad (22)$$

So, overall, the PV system is globally stable.

3.3.3 The proposed P&O algorithm with optimized duty cycle

In this section, the tracking efficiency is improved by considering an adjustable step size. The step size of the algorithm should be flexible by getting close to the MPP. It means that each algorithm is closer to the MPP, and the step size should be smaller. Therefore, the presented algorithm has the chance to stop as close as possible to the maximum power curve.

When the algorithm approaches the MPP to the right, the rate of approaching the MPP is optimized by multiplying the duty cycle by a coefficient that is directly proportional to the PV module's voltage and inversely proportional to its current, and it is directly proportional to the current and inversely proportional to the voltage when approaching the MPP to the left. Because the algorithm's step size reduces as it gets closer to the MPP, it helps the algorithm track the MPP more precisely. Therefore, the equations of changing the duty cycle and have to be replaced by and respectively.

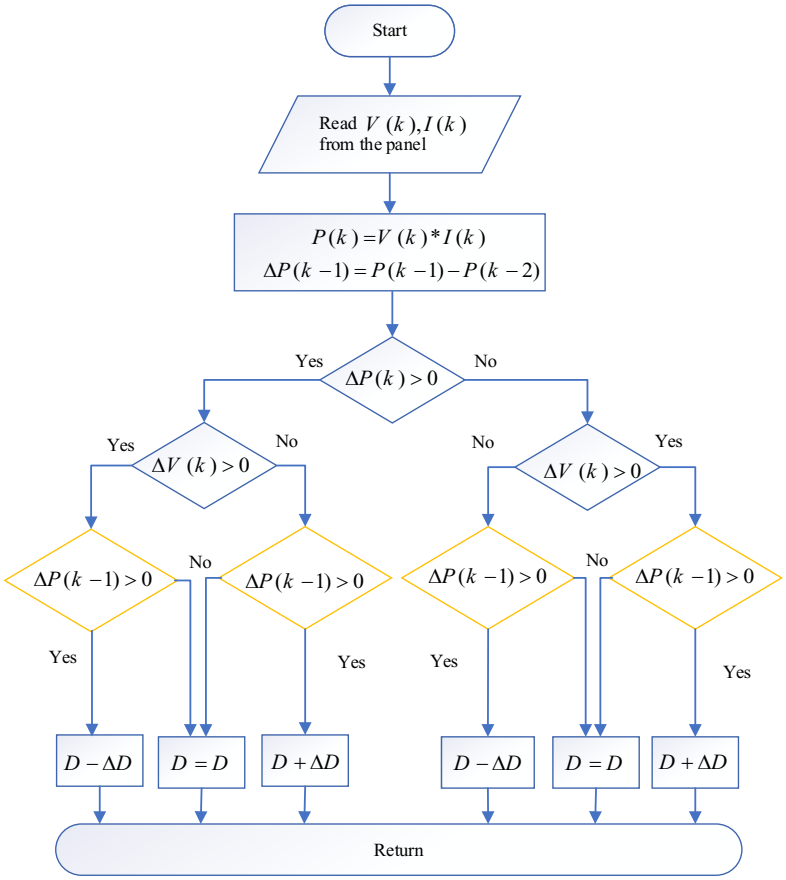

Figure 3.4: The proposed P&O algorithm flowchart

3.4 Simulation Results

This section performs a simulation on MATLAB/Simulink, which is prepared to indicate the proposed algorithm's performance. We used Trina Solar TSM-250PA05.08 in 4 parallel strings with 10 modules per series strings. Table 3.2 lists the data of the selected solar panel. The components of the boost converter were picked according to the values recommended in Table 3.3.

TABLE 3.2

Electrical Data of the TSM 250PA05.08 Module [35]

Electrical Data @ STC	Value
Peak Power (Pmax)	**250 W**
PTC Rating	**227.5 W**
Power Output Tolerance	**0/+3 %**
Maximum Power Voltage	**30.3 V**
Maximum Power Current	**8.27 A**
Open Circuit Voltage	**37.6 V**
Short Circuit Current	**8.85 A**
Module Efficiency	**15.3 %**

3.4.1 Case 1: Modified P&O algorithm

1) Irradiance sudden level change tracking performance

To confirm the performance of the modified P&O algorithm, a profile of the solar irradiation is used, which contains both step-up and step-down shapes. The irradiance values are between 700 W/m^2 and 800W/m^2, as illustrated in Figure 3.5. The irradiance starts from 720 W/m^2, lasts for 0.6 seconds at this level, then steps up to 760 W/m^2, remains at this level for 0.8 seconds, then steps down to 700 W/m^2, stay flat for 0.6 seconds. As we focused on steady-state conditions in

the proposed algorithm, the ramp up or ramp down are not considered in the irradiance profile. The simulation time is 2 sec, and the temperature is retained at a fixed value of 25℃.

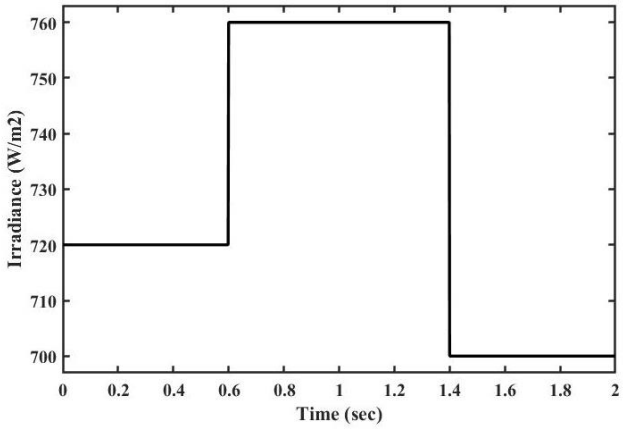

Figure 3.5: Illumination profile

TABLE 3.3
Boost Converter Components

Component	Value
Inductor	50uH
Capacitor	2mF
Maximum Power Voltage	870V
Switching Frequency	5kHz

Figure 3.6 shows the comparison of the conventional P&O technique and the proposed algorithm. The red curve is the PV output power using the original P&O algorithm, and the blue one is the result of using the modified P&O algorithm presented in this thesis. It is apparent in the enlarged images in Figure 3.6 that the tracking deviation in the introduced algorithm is minimal.

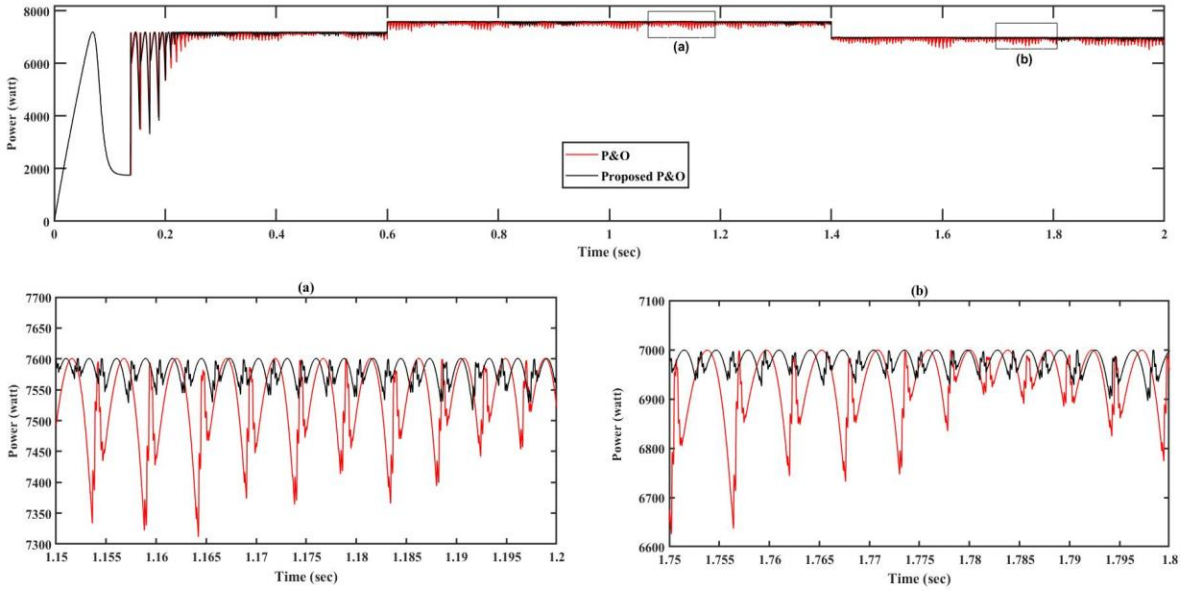

Figure 3.6: Comparison of tracking performances of proposed P&O and Original P&O under varying irradiance levels, when some parts of the graph are magnified in (a) and (b).

Another simulation is done to emphasize the performance of the introduced algorithm. Figure 3.6 depicts a contrast of power tracking by PV panel equipped with the InC MPPT and modified P&O algorithm. It is found that the modified P&O algorithm is more oscillation free than the InC MPPT.

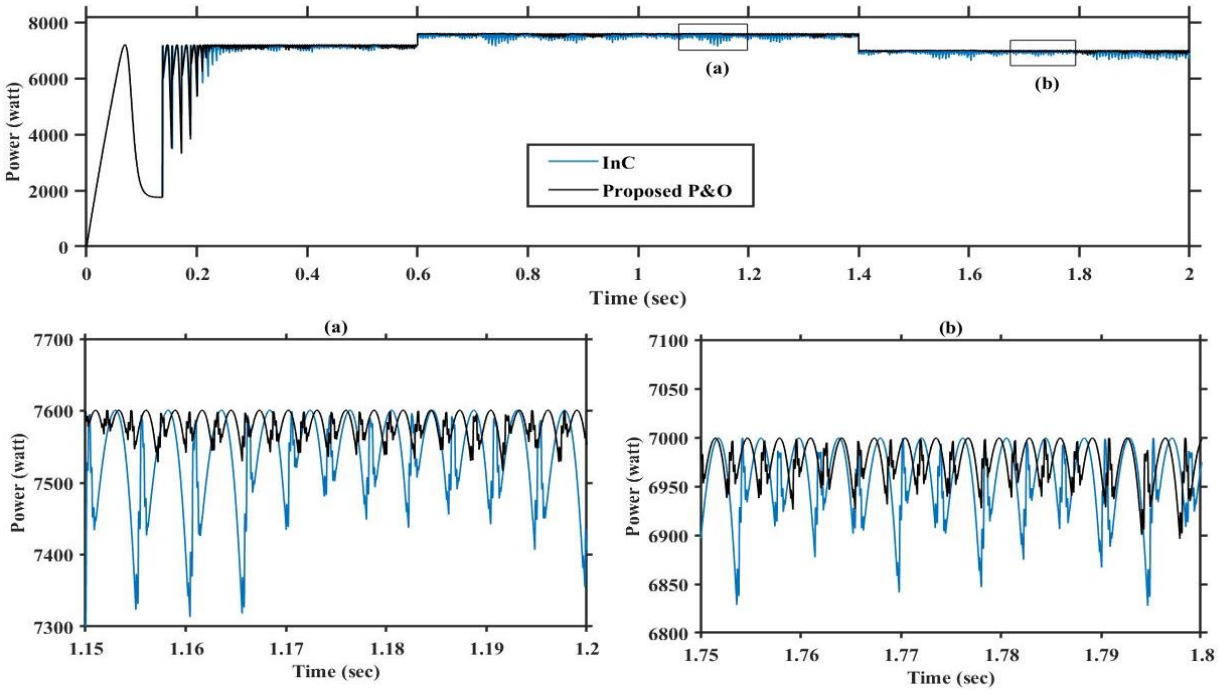

Figure 3.7: Comparison of tracking performances of proposed P&O and InC algorithm under varying irradiance levels, when some parts of the graph are magnified in (a) and (b).

The MPPT algorithm's average efficiency is measured using the MPPT efficiency formula

$$\eta_{MPPT,avg} = \frac{\int P_{out}(t)dt}{\int P_{\max}(t)dt} \qquad (23)$$

The power-voltage plot for 10 Trina modules per series of strings is illustrated in the following figure.

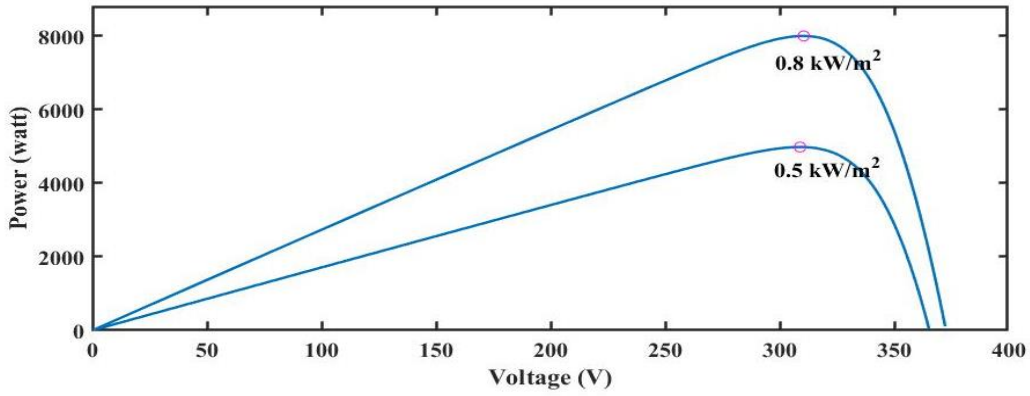

Figure 3.8: Power-voltage plot for 10 Trina modules per series strings.

It is shown in Figure 3.8 that the maximum power production for 0.8 kW/m^2 is 8000 W, and the maximum power production for 0.5 kW/m^2 is 5000 W. Now by adding the maximum power that can be produced per sample time ($2\mu s$) for determined illustration profiles in Figure 3.5, we can obtain the integration of maximum power (denominator of (23)) for the whole simulation time (2 sec). The numerator of the efficiency equation (23) will be calculated by adding the power generated by whole modules per sample time. We can easily estimate the efficiency of the MPPT algorithm by dividing two calculated amounts.

As a result, the tracking efficiencies for each MPPT are determined. After the simulation investigation, the following results are obtained.

TABLE 3.4

Irradiance Sudden Level Change Test Results

Type of MPPT	Evaluated parameters	
	Nature of tracking waveforms	Tracking efficiency (%)
Modified P&O	Less oscillatory and stable	95.27
P&O	Oscillatory	93.52
InC	Oscillatory	93.67

2) Dynamic MPPT efficiency test

The series of triangular irradiance waveforms are the best choice to determine the dynamic MPPT efficiency. In this section, two different ranges of irradiance change, i.e., slow and fast, cover the dynamic MPPT efficiency of the modified P&O algorithm. The slow insolation change is 20 W/m^2 from 700 W/m^2 to 720W/m^2, and the fast insolation change is 50 W/m^2 from 700W/m^2 to 750 W/m^2.

Figure 3.9 and Figure 3.10 show the tracking performance of both the conventional and modified P&O. Certain waveform parts are enlarged for clarity. The tracking by the modified P&O is almost perfect at the very slow change of insolation (20W/m^2), as shown in the magnified axes. This is due to the fact that the gradual ramp resembles a steady state scenario in which the variable perturbation sizing is turned on.

The typical P&O, on the other hand, exhibits significant oscillation due to the huge and fixed perturbation size.

However, because it can cope with the (slow) shift in irradiance, there is no evident loss of tracking direction. Similar results were obtained by the fast irradiance change.

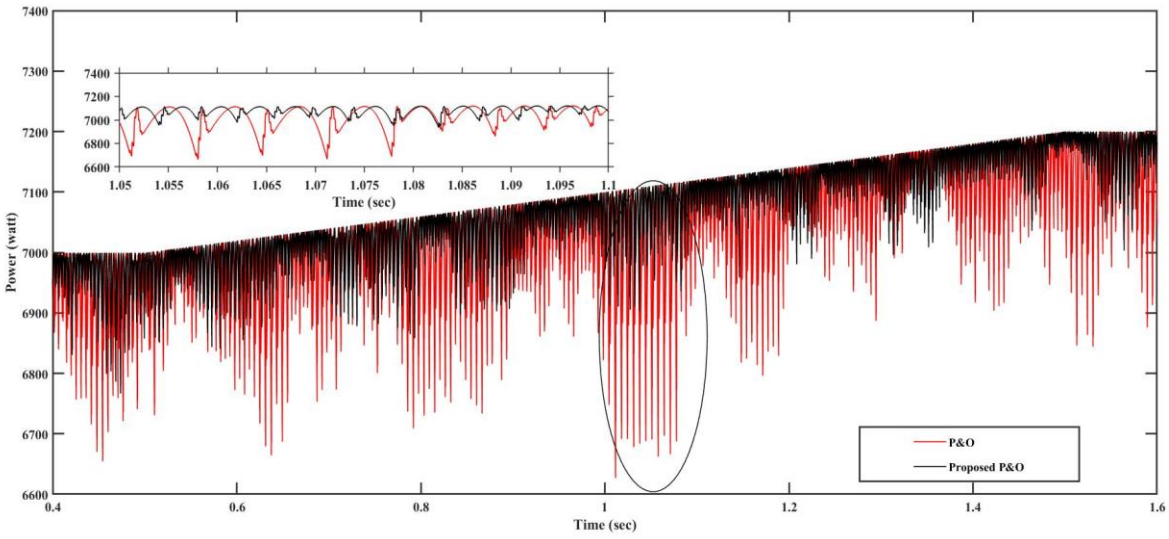

Figure 3.9: Comparison of tracking performances of proposed P&O and original P&O under slow irradiance change.

Based on mentioned dynamic irradiance change tests, the proposed method achieved an average η_{MPPT} of almost 0.5 percent higher than the conventional P&O in both slow and fast change of irradiance. On the other hand, the tracking performance of the improved P&O is highly constant.

The following table depicts the impacts of the oscillation and the loss of tracking capabilities. The average η_{MPPT} for the conventional P&O and the modified P&O in the slow ramp zone (20 $W/m^2/s$) is 96.19 percent and 96.68 percent, respectively.

When the insolation changes quickly (50 $W/m^2/s$), the conventional P&O and the modified P&O efficiencies are 96.23 percent and 96.72 percent, respectively. Although the improvement is very marginal, it will have very high impact when considering a large solar park.

TABLE 3.5

Irradiance Dynamic Level Change Test Results

Type of MPPT	Evaluated parameters	
	Slow irradiances change tracking efficiency	Fast irradiances change tracking efficiency (%)
Modified P&O	**96.68**	**96.72**
P&O	**96.19**	**96.23**

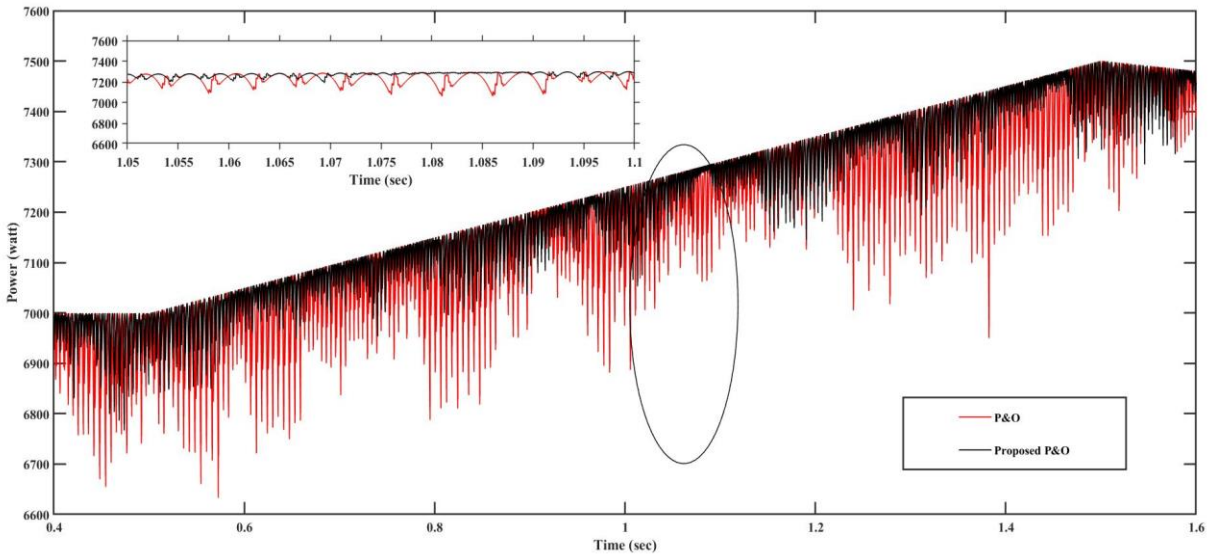

Figure 3.10: Comparison of tracking performances of proposed P&O and original P&O under fast irradiance change.

3.4.2 Case 2: Modified P&O algorithm with optimized duty cycle

In this case, the rate of approaching the MPP is optimized by multiplying the duty cycle by a coefficient that is directly proportional to the PV module's voltage and inversely proportional to its current when approaching the MPP to the right, and it is directly proportional to the current and inversely proportional to the voltage when approaching the MPP to the left. It aids the algorithm in tracking the MPP more precisely since the algorithm's step size decreases as it gets closer to the MPP. The suggested extended MPPT technique is tested in simulations and experiments to ensure

that it can deliver a satisfactory dynamic response and steady-state performance for a PV power generation system. Based on simulation results, the proposed approach obtained an average of almost 3.14 percent greater than the conventional P&O.

Another simulation is done to emphasize the performance of the introduced algorithm with an optimized duty cycle. Figure 3.12 depicts a contrast of power tracking by PV panel equipped with the InC MPPT and modified P&O algorithm. It is found that the modified P&O algorithm is more oscillation free than the InC MPPT. The suggested approach obtained an average of almost 3.13 percent greater than the InC algorithm.

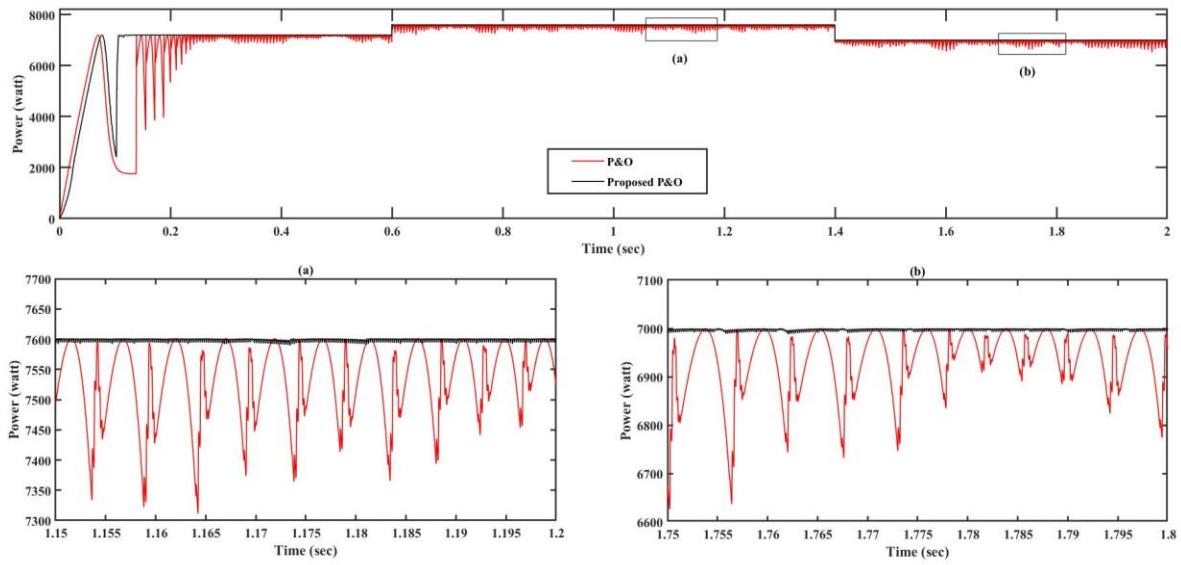

Figure 3.11: Comparison of tracking performances of proposed optimized duty cycle P&O and original P&O under varying irradiance levels, when some parts of the graph are magnified in (a) when the solar panel output power is 7600 W and (b) when the output power is 7000 W.

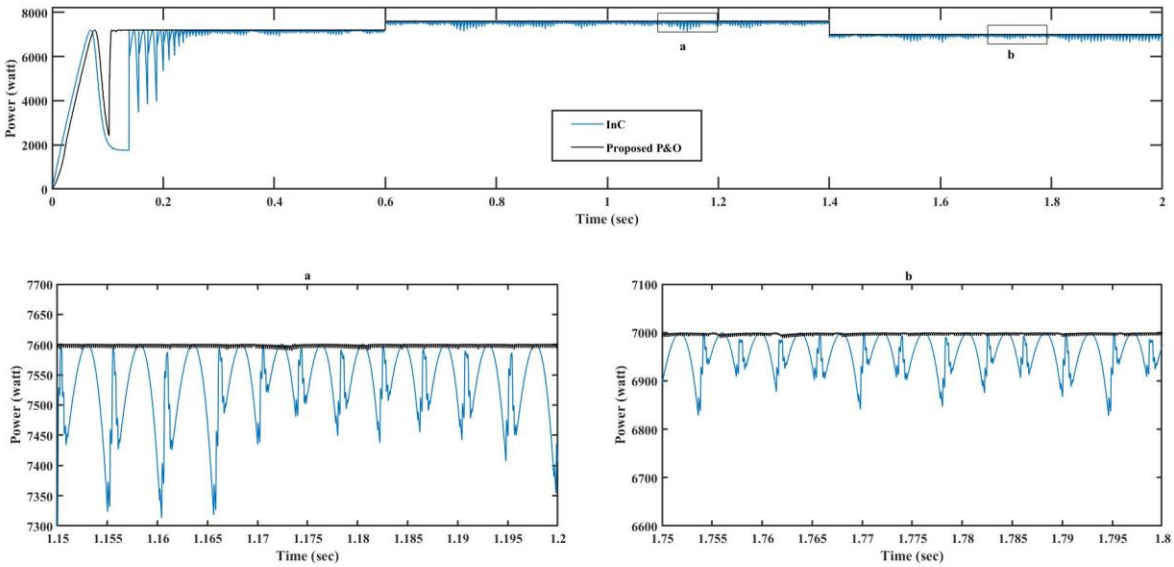

Figure 3.12: Comparison of tracking performances of proposed optimized duty cycle P&O and original InC under varying irradiance levels, when some parts of the graph are magnified in (a) and (b).

As a result, the tracking efficiencies for each MPPT are determined. After the simulation investigation, the following results are obtained.

TABLE 3.6

Optimized Duty Cycle P&O Test Results

Type of MPPT	Evaluated parameters	
	Nature of tracking waveforms	Tracking efficiency (%)
Modified P&O	Less oscillatory and stable	98.21
P&O	Oscillatory	95.07
InC	Oscillatory	95.08

3.4.3 Case 3: PSC test for modified P&O algorithm with optimized duty cycle

1) Moderate partial shading pattern

In order to test the performance of the suggested MPPT controller under non-uniform irradiance levels, three parallel strings with five modules per series strings were applied. Five PV modules that are not shaded receive 700 W/m^2 uniform irradiance, five partially shaded modules receive 300 W/m^2, and the five remaining modules receive 100 W/m^2.

Based on simulation results, the proposed approach obtained an average of almost 3.11 percent greater than the conventional P&O and InC algorithms. The following figures show the tracking time for the proposed optimized algorithm is about 0.03 sec.

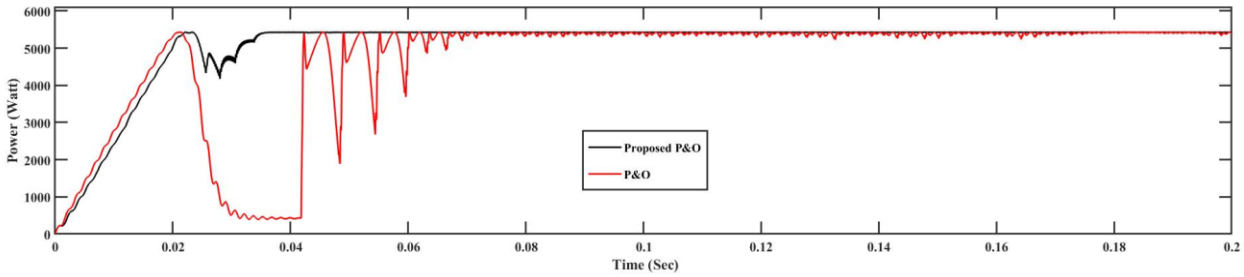

Figure 3.13: Comparison of tracking performances of proposed optimized duty cycle P&O and original P&O under partial shading condition.

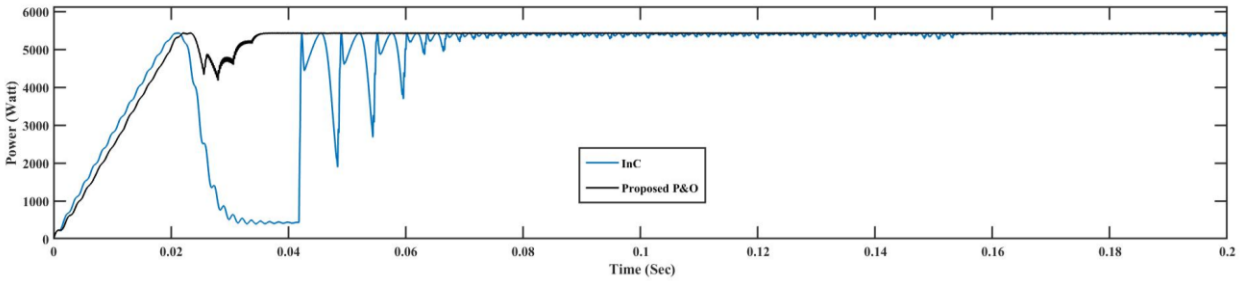

Figure 3.14: Comparison of tracking performances of proposed optimized duty cycle P&O and original InC under partial shading condition.

TABLE 3.7

Moderate PSCs Test Results

Type of MPPT	Evaluated parameters	
	Nature of tracking waveforms	Tracking efficiency (%)
Modified P&O	**Less oscillatory and stable**	**98.22**
P&O	**Oscillatory**	**95.11**
InC	**Oscillatory**	**95.11**

2) Strong partial shading pattern

In this case, five connected panels received uniform radiation conditions (750 W/m^2radiation), while five received 150 W/m^2 and five received 100 W/m^2. Based on simulation results, the suggested approach obtained an average η_{MPPT} of almost 9.06 percent greater than the conventional P&O.

Another simulation is done to emphasize the performance of the introduced algorithm with an optimized duty cycle. It is found that the modified P&O algorithm is more oscillation free than the InC MPPT. Also, the suggested approach obtained an average η_{MPPT} of almost 8.98 percent greater than the InC algorithm.

TABLE 3.8

Strong PSCs Test Results

Type of MPPT	Evaluated parameters	
	Nature of tracking waveforms	Tracking efficiency (%)
Modified P&O	Less oscillatory and stable	91.85
P&O	Oscillatory	82.79
InC	Oscillatory	82.87

As a comparison to the other modified P&O algorithms, the best efficiency among the partial shading patterns in [34] is 2 percent greater than the conventional P&O algorithm.

3.4.4 Case 4: Drift analysis for one step change in insulation

Tests of the proposed MPPT algorithm have been conducted for an insolation level step shift from 300 to 700 W/m^2in 0.1 s. This rapid change in insulation can be considered a drift issue and is popular on cloudy days. The proposed algorithm can recognize if the power increase is due to perturbation or an increase in insulation. The results of the drift test are shown in Table 3.9.

TABLE 3.9

Drift Test Results

Type of MPPT	Evaluated parameters	
	Nature of tracking waveforms	Tracking efficiency (%)
Modified P&O	Less oscillatory and stable	93.83
P&O	Oscillatory	85.43
InC	Oscillatory	85.50

3.4.5 Case 5: Modified P&O algorithm efficiency test according to EN 50530 standard

The EN 50530 MPPT efficiency test is used to evaluate the proposed algorithm in dynamic weather conditions. The solar insolation is supplied in a trapezoidal waveform with various ramp inclinations for the EN 50530 efficiency test.

The irradiance variation ramps from x% to y% of standard test conditions (STC) irradiance indicates in the following figure. Step times t_0 to t_4 are defined in Table 8.

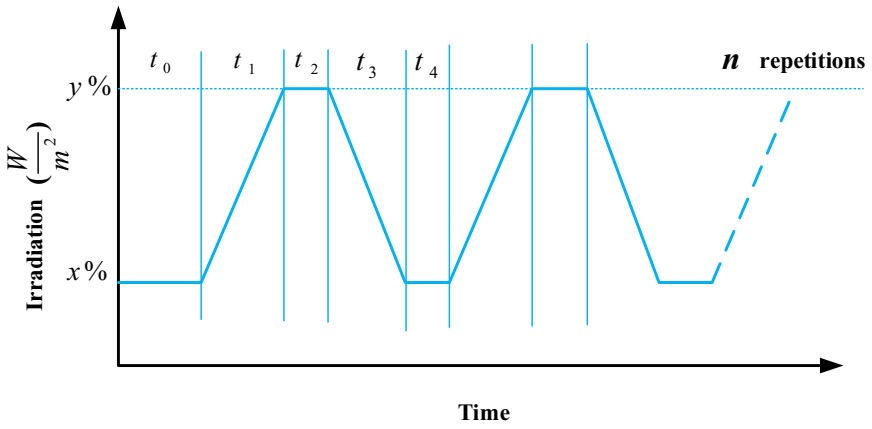

Figure 3.15: Dynamic change in insulation level for EN 50530 standard MPPT efficiency test.

The average dynamic MPPT efficiency is calculated based on (23). A summary of the dynamic MPPT efficiency test findings for the two types of sequence ramps, 10% – 50%, and 30% – 100%, can be seen in Table 3.10.

TABLE 3.10
Dynamic MPPT Test Results Based on EN 50530

Type of ramps	Step times (s)				Tracking efficiency (%)		
	t_1	t_2	t_3	t_4	Modified P&O	P&O	InC
10%-50%	0.1	0.4	0.1	0.4	77.67	52.97	52.97
	0.2	0.3	0.2	0.3	81.06	52.32	52.32
30%-100%	0.1	0.4	0.1	0.4	95.29	89.21	89.44
	0.2	0.3	0.2	0.3	96.23	89.57	89.74

3.5 Conclusion

In this research, the PV power output tracking efficiency has been studied using Matlab/Simulink. The strategy aims to reduce steady-state oscillation while minimizing the loss due to the losing direction. A modified P&O algorithm was presented to eliminate the oscillation of PV power around the peak point. The algorithm's ability to properly identify oscillation and add a boundary condition that prevents it from diverging wildly away from the MPP is critical to its effectiveness. Besides, the optimized duty cycle helps the algorithm to follow the MPPT by adjustable step sizes. By implementing the introduced technique, the average improves by nearly 3.1 percent greater than the conventional P&O and InC algorithm during sudden irradiance changes. Moreover, the modified P&O performs better than the conventional P&O algorithm in dynamic irradiance changes by enhancing the efficiency by 0.5 percent under the slow and fast irradiance changes. In addition, under strong PSC and drift avoidance tests, the proposed technique produced an average of nearly 9 percent and 8 percent greater than the conventional algorithms. By considering the results, it is confirmed that the modified P&O algorithm could track the irradiance profile with a minor deviation from MPPs under various environmental changes. Therefore, more power loss is prevented, and the tracking accuracy is increased.

Because the updated version keeps the same algorithm structure as the original, the former is simple to implement. In the future, we aim to improve the algorithm for fast convergence at the operating point.

References

[1] M. Farsi and J. Liu, "Nonlinear Optimal Feedback Control and Stability Analysis of Solar Photovoltaic Systems," IEEE Transactions on Control Systems Technology, vol. 28, no. 6, pp. 2104-2119, Nov. 2020.

[2] E. I. Batzelis, G. E. Kampitsis, S. A. Papathanassiou, and S. N. Manias, "Direct MPP calculation in terms of the single-diode PV model parameters," IEEE Transactions on Power Electron, vol. 30, no. 1, pp. 226-236, Mar. 2015.

[3] J. Ahmed and Z. Salam, "A Modified P&O MPPT Method with Reduced Steady-State Oscillation and Improved Tracking Efficiency," IEEE Transactions on Sustainable Energy, vol. 7, no. 4, pp. 1506-1515, Oct. 2016.

[4] N. Femia, G. Petrone, G. Spagnuolo, and M. Vitelli, "Optimization of perturb and observe MPPT method," IEEE Transactions on Power Electronics, vol. 20, no. 4, pp. 963-973, July 2005.

[5] H. A. Sher, A. F. Murtaza, A. Noman, K. E. Addoweesh, K. Al-Haddad, and M. Chiaberge, "A new sensorless hybrid MPPT algorithm based on fractional short-circuit current measurement and P&PO MPPT," IEEE Transactions on Sustainable Energy, vol. 6, no. 4, pp. 1426-1434, Oct. 2015.

[6] M. A. Elgendy, B. Zahawi, and D. J. Atkinson, "Assessment of perturb and observe MPPT algorithm implementation techniques for PV pumping applications," IEEE Transactions on Sustainable Energy, vol. 3, no. 1, pp. 21-33, Jan. 2012.

[7] J. H. Lee, H. Bae, and B. H. Cho, "Advanced incremental conductance MPPT algorithm with a variable step size," Proc. 12th International Power Electronics and Motion Control Conference, Aug./Sep. 2006, pp. 603-607.

[8] M. Qiang, S. Mingwei, L. Liying, and J. M. Guerrero, "A novel improved variable step-size incremental-resistance MPPT method for PV systems," IEEE Transactions on Industrial Electronics, vol. 58, no. 6, pp. 2427-2434, Jun. 2011.

[9] Weidong Xiao and W. G. Dunford, “A modified adaptive hill climbing MPPT method for photovoltaic power systems,” IEEE 35th Annual Power Electronics Specialists Conference (IEEE Cat. No.04CH37551), Aachen, Germany, Jun. 2004, pp. 1957-1963.

[10] E. Koutroulis, K. Kalaitzakis, and N. C. Voulgaris, “Development of a microcontroller-based, photovoltaic MPPT control system,” IEEE Transactions on Power Electronics, vol. 16, no. 1, pp. 46-54, Jan. 2001.

[11] R. Iftikhar, I. Ahmad, M. Arsalan, N. Naz, N. Ali, and H. Armghan, “MPPT for Photovoltaic System Using Nonlinear Controller,” International Journal of Photoenergy, vol. 2018, pp. 1-11, Apr. 2018.

[12] F. M. de Oliveira, F. R. Durand, V. D. Bacon, S. A. O. da Silva, L. P. Sampaio, and L. B. G. Campanhol, “Grid-tied photovoltaic system based on PSO MPPT technique with active power line conditioning,” IET Power Electronics, vol. 9, no. 6, pp. 1180-1191, May. 2016.

[13] M. B. Smida and A. Sakly, “Genetic based algorithm for MPPT (MPPT) for grid connected PV systems operating under partial shaded conditions,” 7th International Conference on Modelling, Identification and Control (ICMIC), Tunisia, Dec. 2015, pp.1-6.

[14] A. A. S. Mohamed, A. Berzoy, and O. A. Mohammed, “Design and Hardware Implementation of FL-MPPT Control of PV Systems Based on GA and Small-Signal Analysis,” IEEE Transactions on Sustainable Energy, vol. 8, no. 1, pp. 279-290, Jan. 2017.

[15] M. Dehghani, M. Taghipour, G. B. Gharehpetian and M. Abedi, “Optimized Fuzzy Controller for MPPT of Grid-connected PV Systems in Rapidly Changing Atmospheric Conditions,” Journal of Modern Power Systems and Clean Energy, vol. 9, no. 2, pp. 376-383, Mar. 2021.

[16] R, Kumar, N, Tadikonda, J, Kumar, RN, Mahanty, “An ANN-Based MPPT Technique for Partial Shading Photo Voltaic Distribution Generation,” In Control Applications in Modern Power Systems, Springer, Singapore. 2022, pp. 391-403.

[17] S, Rezazadeh, A, Moradzadeh, SM, Hashemzadeh, K, Pourhossein, B, Mohammadi-Ivatloo, SH, Hosseini, “A novel prime numbers-based PV array reconfiguration solution to produce maximum

energy under partial shade conditions," Sustainable Energy Technologies and Assessments, vol. 1, no. 47, pp. 101498, Oct. 2021.

[18] M. Madhukumar, T. Suresh, and M. Jamil, "Investigation of PV Integrated Grid System Under NonUniform Irradiance Conditions" Electronics, Special Issue on Power Electronics, Vol. 9, no. 9 Aug. 2020.

[19] SM, Hashemzadeh, "A new model-based technique for fast and accurate tracking of global maximum power point in photovoltaic arrays under partial shading conditions," Renewable energy, vol. 1, no. 139, pp. 1061-76, Aug. 2019.

[20] V, kumar Vethanayagam, KK, Prabhakaran, V, Balasubramanian, "A Novel Algorithm based on Voltage and Current Perturbation to track Global peak under Partial Shading Conditions," IEEE Transactions on Energy Conversio, 2022 May 27.

[21] M. Killi and S. Samanta, "Modified Perturb and Observe MPPT Algorithm for Drift Avoidance in Photovoltaic Systems," IEEE Transactions on Industrial Electronics, vol. 62, no. 9, pp. 5549-5559, Sep. 2015.

[22] V. Jately, S. Bhattacharya, B. Azzopardi, A. Montgareuil, J. Joshi and S. Arora, "Voltage and Current Reference Based MPPT Under Rapidly Changing Irradiance and Load Resistance," IEEE Transactions on Energy Conversion, vol. 36, no. 3, pp. 2297-2309, Sep. 2021.

[23] M. Rezkallah, S. K. Sharma, A. Chandra, B. Singh, and D. R. Rousse, "Lyapunov Function and Sliding Mode Control Approach for the Solar-PV Grid Interface System," IEEE Transactions on Industrial Electronics, vol. 64, no. 1, pp. 785-795, Jan. 2017.

[24] S, Golzari, F, Rashidi, HF, Farahani, "A Lyapunov function-based model predictive control for three phase grid connected photovoltaic converters" Solar Energy, vol. 15, no. 181pp. 222-233, Mar. 2019.

[25] R. F. Rajakumari and M. Deshpande, "Comparative Analysis of DC-DC Converters," 2nd International Conference on Power and Embedded Drive Control (ICPEDC), Chennai, India, Aug. 2019, pp. 504-509.

[26] J. Thongprona, K. Kirtikara, and C. Jivacate, “A method for the determination of dynamic resistance of photovoltaic modules under illumination,” Solar Energy Materials and Solar Cells, vol. 90, no. 18-19, pp. 3078-3084, Nov. 2006.

[27] A. M¨aki, S. Valkealahti, and T. Suntio, “Dynamic terminal characteristics of a photovoltaic generator,” in Proceedings 14th International Power Electronics and Motion Control Conference, Sep. 2010, pp. T12-76.

[28] A. Urtasun, P. Sanchis and L. Marroyo, “Adaptive Voltage Control of the DC/DC Boost Stage in PV Converters with Small Input Capacitor,” Solar Energy Material Solar Cells, in IEEE Transactions on Power Electronics, vol. 28, no. 11, pp. 5038-5048, Nov. 2013.

[29] M. Forouzesh, Y. P. Siwakoti, S. A. Gorji, F. Blaabjerg, and B. Lehman, “A survey on voltage boosting techniques for step-up DC-DC converters,” IEEE Energy Conversion Congress and Exposition (ECCE), Milwaukee, WI, USA, Sep. 2016, pp. 1-8.

[30] R. Kahani, M.Jamil, and M. Tariq Iqbal, "Direct Model Reference Adaptive Control of a Boost Converter for Voltage Regulation in Microgrids," Energies, Vol. 15, Issue 13, July 2022.

[31] E. Mamarelis, G. Petrone, and G. Spagnuolo, “Design of a sliding modecontrolled SEPIC for PV MPPT applications,” IEEE Transactions on Industrial Electronics, vol. 61, no. 7, pp. 3387-3398, Jul. 2014.

[32] S. J. Chiang and H. J. Shieh, “Modeling and control of PV charger system with SEPIC converter,” IEEE Transactions on Industrial Electronics, vol. 56, no. 11, pp. 4344-4353, Nov. 2009.

[33] R. Lin, Y. Chang, C. Lee, “Optimal Design of LED Array for Single-Loop CCM Buck–Boost LED Driver,” IEEE Transactions on Industrial Application, vol. 49, no. 2, 761- 768, Mar. 2013.

[34] E. P. Sarika, J. Jacob, S. Sheik Mohammed, and S. Paul, “Standalone PV System with Modified VSS P&O MPPT Controller Suitable for Partial Shading Conditions,” 2021 7th International Conference on Electrical Energy Systems (ICEES), Feb. 2021, pp. 51-55.

[35] Trina solar, “TSM-PA05.08 THE UNIVERSAL MODULE” TSM_US_June_2013_Rev C.

Chapter 4

Direct Model Reference Adaptive Control of a Boost Converter for Voltage Regulation in Microgrids

Preface

A version of this manuscript has been published in ***MDPI Energies 2022,*** *vol 15, Issue 14. I am the primary author, and I carried out most of the research work, performed the literature reviews, carried out the system design, modeling, and analysis of the results. I also prepared the first draft of the manuscript and subsequently revised the final manuscript based on the feedback from the co-author and the peer review process. The Co-authors, Dr. Mohsin Jamil, and Dr. M. Tariq Iqbal supervised the research, provided the research guide, reviewed, and corrected the manuscript, and contributed research ideas in the actualization of the manuscript.*

Abstract

In this study, we present a Direct Model Reference Adaptive Control (DMRAC) algorithm in a boost converter used in islanded micro-grids (MG) with a solar photovoltaic (PV) system. Islanded types of microgrids have very sensitive voltage and frequency variability; therefore, a robust and adaptive controller is always desired to control such variations within the MG. A DC–DC boost converter with a modified MIT rule controller is proposed in this paper, which stabilizes output voltage variations in islanded MG. Since the boost converter is a non-minimum phase, the controller design that relies only on output voltage feedback becomes challenging. Even though output voltage control can be achieved using inductor current control, such current mode controllers may also require prior knowledge of the load resistance and more states, such as output and inductor currents in feedback. Here, two control loops are used to achieve a stable output voltage; a PID controller can regulate the output voltage at a fixed level, and the outer loop is designed to implement the MIT rule for a DMRAC. To ensure that the actual system is following the desired reference model, using only an output voltage feedback sensor, a DMRAC is devised to update the PID controller parameters in real-time. Compared to a DC–DC boost converter connected to the MG, a controller, such as the one introduced in this chapter, has better performance as compared to well-tuned PID controllers. In case of load changing by ~50% of its original value, the worst-case settling time and maximum overshoot is less than ~0.1 s and 0.5 V, respectively. The MATLAB/SIMULINK is used to design and simulate the controller with different load disturbances and input voltage variances. The hardware validation is also carried out to show the performance of the proposed controller. Our results suggest that the DMRAC provides robust regulation against parameter variations.

Keywords— boost converters; adaptive control; DC–DC converter; power electronics

4.1 Introduction

MG are small-scale energy grids supplying energy to loads at the distribution level. Besides the traditional AC power grids, DC microgrids are emerging as efficient alternatives. In general, the small grids have control capabilities and can be categorized into grid-connected and islanded or isolated grids [1]. Grid-connected MGs are governed by the main power network, and their voltage and frequency are defined by it. However, for the islanded MG, due to the low system inertia and fast changes in the output power of wind and solar power sources, the frequency and voltage can experience large excursions and thus easily deviate from nominal operating conditions. Multi nano grids can also be connected to power a local network. There are few works [2,3] considering power sharing among multiple nano grids by using power management system.

When we have a DC MG, the DC–DC converters are the most significant part of the system. Many DC–DC converter topologies [4,5], such as the boost topology, the buck topology, buck-boost converters, and single-ended primary inductor converter (SEPIC) topology [5], have been discussed in the literature. DC–DC boost converters are the simplest converters for effective reproduction of output amplification for a given input voltage. Many applications have been undertaken by it, including those related to the automotive industry, power amplifications, adaptive control applications, battery power systems, robotics, wind power, and PV systems (e.g., DC MG) [6].

Many studies compare different types of converters' performances. In [7], research has been conducted over step-up DC–DC converters in various configurations. In [8], the authors analyzed boost and SEPIC converters, considering output voltage ripple, total harmonic distortion, power factor for both converters, and boost converters produced better results. Besides mentioned features, boost converters are easier to use. So, the boost-type converter is frequently used because of its superior performance. As illustrated in Figure 4.1, the main elements of a boost converter are

the inductor, diode, capacitor, and switch. In this research, we use MOSFET as a switch that can consistently turn ON and OFF based on the generated duty cycle.

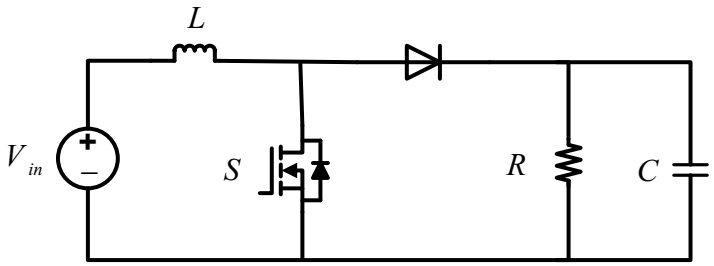

Figure. 4.1. Boost converter.

Because these converters display poor voltage regulation and inadequate dynamic response when run in an open loop, they are often equipped with closed-loop control for output voltage regulation [9]. Due to the nonlinear dynamics of boost converters and non-minimum phase (NMP) behavior, controller design for boost converters is more complex and challenging than for buck converters. Many control techniques have been presented to regulate the switch ON/OFF (duty cycle) to achieve the required output voltage. The most common controllers are linear PID controllers. The PID control design is based on linear control theory, such as the Ziegler–Nichol's method [10], the root locus approach [11], the circle-based criterion [12], the hysteresis method [13], and the bode plot [15]. These control methods perform well around the linearized model's operating points. The small-signal model of a boost converter, on the other hand, changes when the operating point changes. It is important to mention here that the duty cycle determines the poles and a right-half-plane zero and the amplitude of the frequency response. As a result, PID controllers have a hard time respecting changes in operating points, and they function poorly when the system is subjected to substantial load fluctuations.

Despite the necessity of changes in input, the Ziegler–Nichol's technique for PID tuning is an experimental one that is extensively utilized. One downside of this technique is that it necessitates

a prior understanding of plant models. A decent but not optimal system response is achieved when the controller is adjusted using the Ziegler–Nichol's technique. If the dynamics of the plant change, the transient reaction might be considerably worse. It should be noted that many plants have time-varying dynamics due to external/environmental factors, such as temperature and pressure. The controller must respond to changes in the dynamics of the plant features to provide a robust system. Nonlinear control techniques [14–17], such as fuzzy logic and sliding mode control, have recently offered good static and dynamic responsiveness. The disadvantage of the fuzzy logic technique is that all available data are needed, and the algorithm has to be trained before use. The sliding mode controller is suffering from a chattering issue.

This chapter considers a microgrid that is isolated and is displayed in Figure 4.2. DC–DC converters are used to connect a PV system and batteries to a DC bus, with the converter output controlled by a controller. The proposed DMRAC controller essentially contains two loops of voltage control rather than some previous works that just contained the adaptive loop [18,19]. The inner loop of the controller regulates the output voltage at a fixed level, which is vital for correct power injection to the MG. The outer loop implements the MIT rule for a model reference adaptive control. In other word, a specially developed controller that corrects for NMP dynamics is employed in this study by utilizing both PID control and reference model adaptive control. Additionally, the PID controller parameters are updated in real-time to ensure that the actual system is following the desired reference model even if there are uncertainties in system model parameters and load. In this way, the output voltage behavior is similar to the model, and the characteristics of the output, such as settling time, overshoot, and rising time, are manageable. Moreover, the controller does not require any current sensor feedback. All the symbols used in this work are listed in Table 4.1. The significant contributions of the proposed work are summarized as follows:

- An adaptive controller is designed to regulate the output voltage of the DC–DC converters in an isolated MG system.
- This chapter proposes a DMRAC that can adjust the parameters of the PID controller in real-time to ensure that the actual system is following the desired reference model.
- The PID controller regulates the output voltage at a fixed level, essential for correct power injection when the DC–DC boost converter is connected to the MG. The outer loop implements the MIT rule for a model reference adaptive control. Besides, no training or database is needed in this method.
- The proposed controller does not require using any current sensor, and the control scheme is only obtained using the voltage feedback of the boost converter. So, the proposed design is cost-effective.

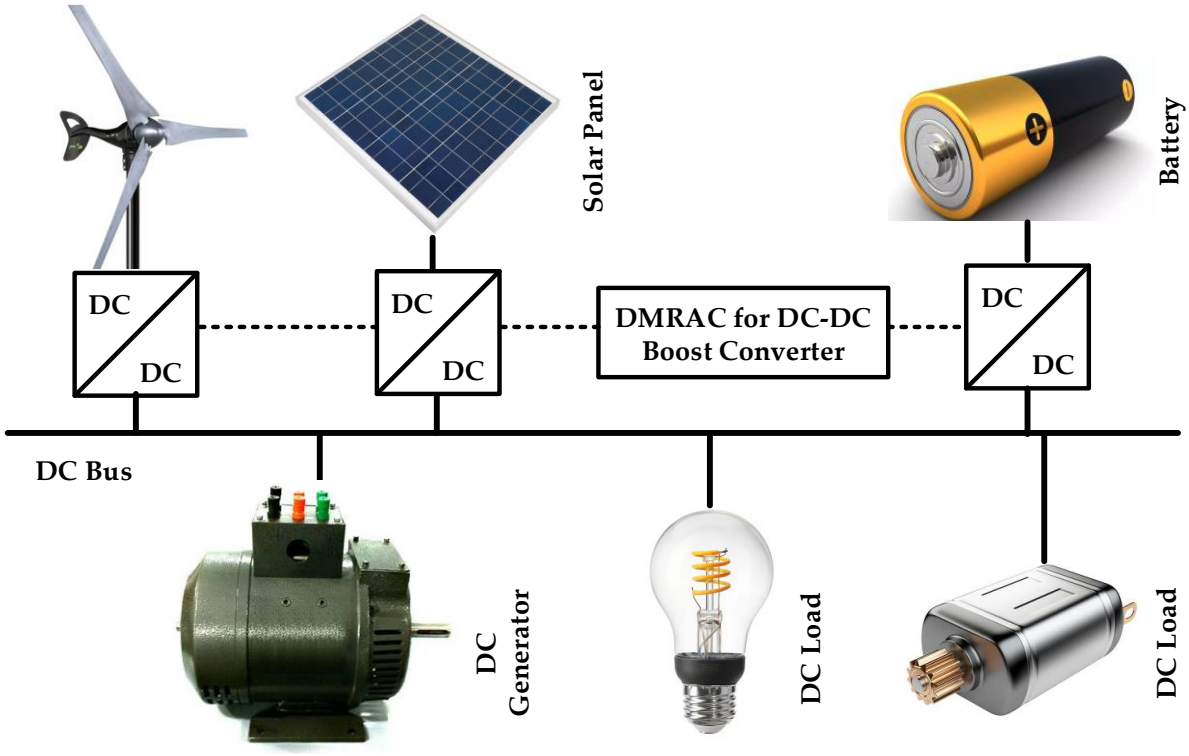

Figure. 4.2. Isolated MG diagram.

Table 4.1

Nomenclature

Symbol	Meaning
v_{in}	Input voltage
v_c	Capacitor voltage
i_l	Inductor current
d	Duty cycle
y_m	The output of the reference model
y	Plant output
u_c	Plant input
$G(s)$	Second-order transfer function
K	Known parameter
K_o	Unknown parameter
γ	Adaptation gain

4.2 DC–DC Converter Dynamic Modelling

4.2.1 Ideal dynamic model

The controller's performance depends upon the accurate modeling of the DC–DC converter. A well-established average modeling technique [17] is used to design the controller. The boost converter consists of a DC input voltage source, an inductor L, a controlled switch S, a diode, a filter capacitor C, and a load resistance R. The current in the inductor grows linearly when the switch is turned on, but the diode remains off. When the switch is turned off, the energy stored in the inductor is released to the load. As the converter's name implies, the output voltage is always greater than the input voltage. The DC–DC boost converters operate in three different modes: Continuous Conduction Mode (CCM), Discontinuous Conduction Mode (DCM), and Critical Conduction Mode (CrCM). The CCM operating mode-based DC–DC converter is considered in this research.

T is the switching period, and the switch is closed for time DT and open for $(1-D)T$, where D is the steady-state duty cycle. When the switch is on, there are two loops, one for inductor current and the other for the capacitor current. Using the KVL for the mentioned loops, the following equations can be obtained.

Defining the state vector as $x = [i_l\ v_c]^T$ and the output voltage $v_o = v_c$, the state space form during the "ON" mode can be written as follows:

$$\begin{bmatrix} \frac{di_l}{dt} \\ \frac{dv_c}{dt} \end{bmatrix} = \begin{bmatrix} 0 & 0 \\ 0 & -\frac{1}{RC} \end{bmatrix} \begin{bmatrix} i_l \\ v_c \end{bmatrix} + \begin{bmatrix} \frac{1}{L} \\ 0 \end{bmatrix} v_{in} \tag{1}$$

$$v_o = [0\ 1] \begin{bmatrix} i_l \\ v_c \end{bmatrix} \tag{2}$$

During the "OFF" mode state, the energy stored in the inductor is released to the output RC circuit through the diode.

We can derive the following state equations for the OFF mode by using KVL and KCL equations for the boost converter circuit in Figure 4.1, when the switch is off:

$$\begin{bmatrix} \frac{di_l}{dt} \\ \frac{dv_c}{dt} \end{bmatrix} = \begin{bmatrix} 0 & -\frac{1}{L} \\ \frac{1}{C} & -\frac{1}{RC} \end{bmatrix} \begin{bmatrix} i_l \\ v_c \end{bmatrix} + \begin{bmatrix} \frac{1}{L} \\ 0 \end{bmatrix} v_{in} \tag{3}$$

$$v_o = [0\ 1] \begin{bmatrix} i_l \\ v_c \end{bmatrix} i_l - \frac{V_c}{R} - C\frac{dv_c}{dt} = 0 \tag{4}$$

A state-space averaging approach is utilized to obtain a converter model across one switching period. In other words, the state-space descriptions of the two modes must be replaced with a single state-space description that approximates the behavior of the circuit across the whole time T. By using the state-space averaging technique, the averaged modified model is given by:

$$A = A_1 d + A_2(1-d) \tag{5}$$

$$B = B_1 d + B_2(1-d) \tag{6}$$

where A_1, A_2, B_1 and B_2 are given below, and d is changes in the duty cycle:

$$A_1 = \begin{bmatrix} 0 & 0 \\ 0 & -\frac{1}{RC} \end{bmatrix},\ A_2 = \begin{bmatrix} 0 & -\frac{1}{L} \\ \frac{1}{C} & -\frac{1}{RC} \end{bmatrix}$$

$$B_1 = \begin{bmatrix} \frac{1}{L} \\ 0 \end{bmatrix},\ B_2 = \begin{bmatrix} \frac{1}{L} \\ 0 \end{bmatrix}$$

Using (5) and (6), we obtain the following:

$$\begin{bmatrix} \frac{di_l}{dt} \\ \frac{dv_c}{dt} \end{bmatrix} = \begin{bmatrix} 0 & -\frac{(1-d)}{L} \\ \frac{1-d}{C} & -\frac{1}{RC} \end{bmatrix} \begin{bmatrix} i_l \\ v_c \end{bmatrix} + \begin{bmatrix} \frac{1}{L} \\ 0 \end{bmatrix} v_{in} \tag{7}$$

$$v_o = [0\ 1] \begin{bmatrix} i_l \\ v_c \end{bmatrix}$$

The boost converter's steady-state model may be calculated from Equation (7) by letting:

$$\begin{bmatrix} \frac{di_l}{dt} \\ \frac{dv_c}{dt} \end{bmatrix} = 0 \quad and \quad d = D$$

In this case, Equation (7) becomes:

$$\begin{bmatrix} 0 \\ 0 \end{bmatrix} = \begin{bmatrix} 0 & -\frac{(1-D)}{L} \\ \frac{1-D}{C} & -\frac{1}{RC} \end{bmatrix} \begin{bmatrix} i_l \\ v_c \end{bmatrix} + \begin{bmatrix} \frac{1}{L} \\ 0 \end{bmatrix} v_{in} \tag{8}$$

$$v_o = [0\ 1] \begin{bmatrix} i_l \\ v_c \end{bmatrix}$$

The steady-state relationship between v_o and v_{in} may be expressed as using (8):

$$\frac{V_o}{V_{in}} = \frac{1}{1-D} \tag{9}$$

To obtain the boost converter's transfer function, the model given by (8) must first be linearized around a particular operating point. To this end, we assume that the inductor's current I_l, capacitor voltage V_c, duty cycle D, and input voltage V_{in} determine the steady-state operating point. Now, by considering small perturbations of the operating point, the variables associated with the average model can be written as:

$$\begin{aligned} . \ i_l &= I_l + \tilde{\imath}_l \\ v_c &= V_c + \tilde{v}_c \\ v_{in} &= V_{in} + \widetilde{v_{in}} \\ d &= D + \tilde{d} \end{aligned} \tag{10}$$

where the $\tilde{\imath}_l$, $\tilde{v}_c$ and $\widetilde{v_{in}}$ are the small perturbations of the inductor current, capacitor voltage, and input voltage, respectively. Therefore, (7) becomes:

$$\frac{d}{dt}\begin{bmatrix} I_l + \tilde{\imath}_l \\ V_c + \tilde{v}_c \end{bmatrix} = \begin{bmatrix} 0 & -\frac{(1-D)}{L} \\ \frac{1-D}{C} & -\frac{1}{RC} \end{bmatrix} \begin{bmatrix} I_l \\ V_c \end{bmatrix} + \begin{bmatrix} 0 & -\frac{(1-D)}{L} \\ \frac{1-D}{C} & -\frac{1}{RC} \end{bmatrix} \begin{bmatrix} \tilde{\imath}_l \\ \tilde{v}_c \end{bmatrix} + \begin{bmatrix} 0 & \frac{\tilde{d}}{L} \\ -\frac{\tilde{d}}{C} & 0 \end{bmatrix} \begin{bmatrix} I_l \\ V_c \end{bmatrix} + \begin{bmatrix} \frac{1}{L} \\ 0 \end{bmatrix} [V_{in} + \widetilde{v_{in}}] \tag{11}$$

It is worth noting that the steady-state portion of (11) is given by:

$$\begin{bmatrix} 0 & -\frac{(1-D)}{L} \\ \frac{1-D}{C} & -\frac{1}{RC} \end{bmatrix} \begin{bmatrix} I_l \\ V_c \end{bmatrix} + \begin{bmatrix} \frac{1}{L} \\ 0 \end{bmatrix} [V_{in}] = 0$$

and:

$$\begin{bmatrix} 0 & \frac{\tilde{d}}{L} \\ -\frac{\tilde{d}}{C} & 0 \end{bmatrix} \begin{bmatrix} I_l \\ V_c \end{bmatrix} = \begin{bmatrix} \frac{V_c}{L} \\ -\frac{I_l}{C} \end{bmatrix} [\tilde{d}] \tag{12}$$

Hence, (11) is reduced to:

$$\frac{d}{dt} \begin{bmatrix} \widetilde{\imath_l} \\ \widetilde{v_c} \end{bmatrix} = \begin{bmatrix} 0 & -\frac{(1-D)}{L} \\ \frac{1-D}{C} & -\frac{1}{RC} \end{bmatrix} \begin{bmatrix} \widetilde{\imath_l} \\ \widetilde{v_c} \end{bmatrix} + \begin{bmatrix} \frac{1}{L} & \frac{V_c}{L} \\ 0 & -\frac{I_l}{C} \end{bmatrix} \begin{bmatrix} \widetilde{v_{in}} \\ \tilde{d} \end{bmatrix} \tag{13}$$

Finally, the output voltage perturbation may be expressed directly as:

$$\widetilde{v_o} = [0\ 1] \begin{bmatrix} \widetilde{\imath_l} \\ \widetilde{v_c} \end{bmatrix} \tag{14}$$

The state-space model of (13) and (14) are given by:

$$\dot{x} = Ax + Bu$$

$$y = Cx$$

$$A = \begin{bmatrix} 0 & -\frac{(1-D)}{L} \\ \frac{1-D}{C} & -\frac{1}{RC} \end{bmatrix}$$

$$B = \begin{bmatrix} \frac{1}{L} & \frac{V_c}{L} \\ 0 & -\frac{I_l}{C} \end{bmatrix}$$

$$C = [0\ 1]$$

In this research, we design a controller to generate duty cycle correction $\tilde{d}$ in such a way that the output voltage remains constant. In this regard, we consider the transfer function given in (15)

using the state transition matrix, which may be expressed as follows in terms of the converter's parameters:

$$\frac{\widetilde{v_o}(s)}{\tilde{d}(s)} = \frac{(1-D)V_o - (LI_l)s}{(LC)s^2 + \frac{L}{R}s + (1-D)^2} \tag{15}$$

4.2.2 Parasitic realization in boost converter dynamic model

The goal of analyzing ideal/lossless components and leaving parasitic elements out, as we have before, is to simplify model development and to determine the fundamental features of the switching system. Nevertheless, parasitic elements and losses need to be considered for improving model accuracy, analyzing system efficiency, and studying dynamic behavior. As a result of including the parasitic elements, nonlinear current and voltage waveforms are generated, and this complicates the process of developing a model. The schematic in Figure 4.3 shows a simplified equivalent circuit for the DC–DC boost converter with parasitic elements. A capacitance C and inductor L can be considered as an output filter. An analysis of capacitor equivalent series resistance (ESR), R_C, and inductor DC resistance, R_L, is performed.

Per switching cycle, the boost converter has two modes in CCM. Again, the switch is closed for time DT and open for $(1-D)T$, where D is the steady-state duty cycle. Defining the state vector as $x = [i_l \; v_c]^T$ and the output voltage $v_o = v_c$, and writing the KVL and KCL for loops in Figure 4.3, we can obtain the state space (ss) form for "ON" and "OFF" modes of the converter. During the "ON" mode state, the ss form will be:

$$\begin{bmatrix} \frac{di_l}{dt} \\ \frac{dv_c}{dt} \end{bmatrix} = \begin{bmatrix} -\frac{R_L}{L} & 0 \\ 0 & -\frac{1}{(R_C+R)C} \end{bmatrix} \begin{bmatrix} i_l \\ v_c \end{bmatrix} + \begin{bmatrix} \frac{1}{L} \\ 0 \end{bmatrix} v_{in} \tag{16}$$

$$v_o = [0 \; \frac{R}{R+R_C}] \begin{bmatrix} i_l \\ v_c \end{bmatrix}$$

During the "OFF" mode state, ss form is:

$$\begin{bmatrix} \frac{di_l}{dt} \\ \frac{dv_c}{dt} \end{bmatrix} = \begin{bmatrix} (-\frac{R_L}{L}) - \frac{RR_C}{L(R+R_C)} & -\frac{R}{L(R+R_C)} \\ \frac{R}{(R_C+R)C} & -\frac{1}{(R_C+R)C} \end{bmatrix} \begin{bmatrix} i_l \\ v_c \end{bmatrix} + \begin{bmatrix} \frac{1}{L} \\ 0 \end{bmatrix} v_{in} \quad (17)$$

$$v_o = [\frac{RR_C}{(R+R_C)} \ \frac{1}{R+R_C}] \begin{bmatrix} i_l \\ v_c \end{bmatrix}$$

Using (5) and (6), we obtain the following:

$$\begin{bmatrix} \frac{di_l}{dt} \\ \frac{dv_c}{dt} \end{bmatrix} = \begin{bmatrix} (-\frac{R_L}{L}) - \frac{(1-d)^2RR_C}{L(R+R_C)} & -\frac{(1-d)R}{L(R+R_C)} \\ \frac{R}{(R_C+R)C} & -\frac{1}{(R_C+R)C} \end{bmatrix} \begin{bmatrix} i_l \\ v_c \end{bmatrix} + \begin{bmatrix} \frac{1}{L} \\ 0 \end{bmatrix} v_{in} \quad (18)$$

$$v_o = [\frac{(1-d)RR_C}{(R+R_C)} \ \frac{1}{R+R_C}] \begin{bmatrix} i_l \\ v_c \end{bmatrix}$$

Now, applying perturbation, this will result in the small signal model as:

$$\frac{d}{dt}\begin{bmatrix} \tilde{\imath}_l \\ \tilde{v}_c \end{bmatrix} = \begin{bmatrix} (-\frac{R_L}{L}) - \frac{(1-d)^2RR_C}{L(R+R_C)} & -\frac{(1-D)R}{L(R+R_C)} \\ \frac{(1-D)R}{(R_C+R)C} & -\frac{1}{(R_C+R)C} \end{bmatrix} \begin{bmatrix} \tilde{\imath}_l \\ \tilde{v}_c \end{bmatrix} + \begin{bmatrix} \frac{1}{L} & \frac{v_o}{L} + \frac{(1-DRR_CI_L)}{L(R+R_C)} \\ 0 & -\frac{RI_L}{C(R+R_C)} \end{bmatrix} \begin{bmatrix} \widetilde{v_{in}} \\ \tilde{d} \end{bmatrix} \quad (19)$$

$$v_o = \begin{bmatrix} \frac{(1-D)RR_C}{(R+R_C)} & \frac{C}{R+R_C} \end{bmatrix} \begin{bmatrix} \tilde{\imath}_l \\ \tilde{v}_c \end{bmatrix} + \begin{bmatrix} 0 - \frac{RR_CI_L}{R+R_C} \end{bmatrix} \begin{bmatrix} \widetilde{v_{in}} \\ \tilde{d} \end{bmatrix}$$

$$\frac{\widetilde{v_o}(s)}{\tilde{d}(s)} =$$

$$\frac{s\left[\left(\frac{(1-D)RR_C}{(R+R_C)}\right)\left(\frac{v_o}{L}+\frac{(1-D)RR_CI_L)}{L(R+R_C)}\right)-\frac{R^2I_L}{C(R+R_C)^2}\right]+\left(\frac{v_o}{L}+\frac{(1-D)RR_CI_L)}{L(R+R_C)}\right)\left[\left(\frac{(1-D)RR_C}{C(R+R_C)^2}\right)+\left(\frac{R^2(1-D)}{C(R+R_C)^2}\right)\right]-\frac{R^2I_L}{C(R+R_C)^2}\left(\frac{R_L}{L}+\left(\frac{(1-D)^2RR_C}{L(R+R_C)}\right)\right)+\frac{(1-D)^2R}{LC(R+}}{s^2+s\left[\left(\frac{R_L}{L}\right)+\frac{(1-d)^2RR_C}{L(R+R_C)}+\frac{1}{(R_C+R)C}\right]+\left[\frac{R_L}{L}+\left(\frac{(1-D)^2RR_C}{L(R+R_C)}\right)\right]\left[\frac{1}{(R_C+R)C}\right]+\frac{(1-D)^2R^2}{CL(R+R_C)^2}} \quad (20)$$

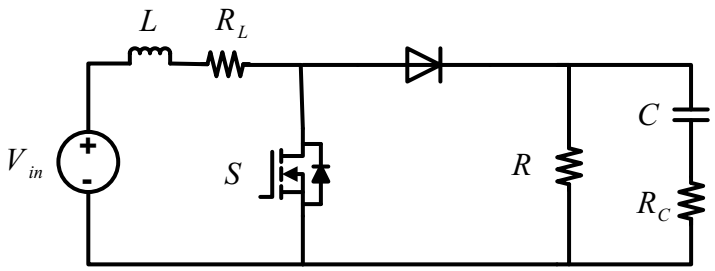

Figure 4.3. Boost converter considering parasitic components.

4.3 Controller Design and Simulation

4.3.1 Model reference adaptive controller

Adaptive control is a popular control strategy for developing sophisticated control systems with higher performance and accuracy [20]. The DMRAC is a direct adaptive method with adjustable controller settings and an adjusting mechanism. Adaptive controllers are far more successful at dealing with unknown parameter fluctuations and environmental changes than the well-known and easily structured fixed gain PID controllers. The outer loop, or regular feedback loop, and the inner loop, or parameter adjustment loop, make up an adaptive controller. This work designs the adaptive controller with a DMRAC scheme using the MIT rule to control a DC–DC boost converter.

The MRAC is designed using an adaptive control approach that adjusts the controller settings such that the output of the real plant follows the output of a reference model with the same reference input.

The reference model is used to simulate the adaptive control system's ideal response to the reference input. A controller is generally characterized by various parameters that may be changed. Only one parameter is utilized to define the control law in this article. The amount of adaption gain mostly determines the value. The adjustment mechanism component is used to change the controller's settings so that the real plant can follow the reference model. The adjusting mechanism can be developed using mathematical techniques, such as the MIT rule, Lyapunov theory, and the

theory of augmented error. However, our work focuses on the MIT rule to guarantee the stability of the control system as well as conversance of tracking error to zero.

Figure 4.4 depicts the DMRAC system's fundamental block diagram. As indicated in the diagram, y_m represents the output of the reference model, whereas y is the output of the real plant, with ε denoting the difference between them.

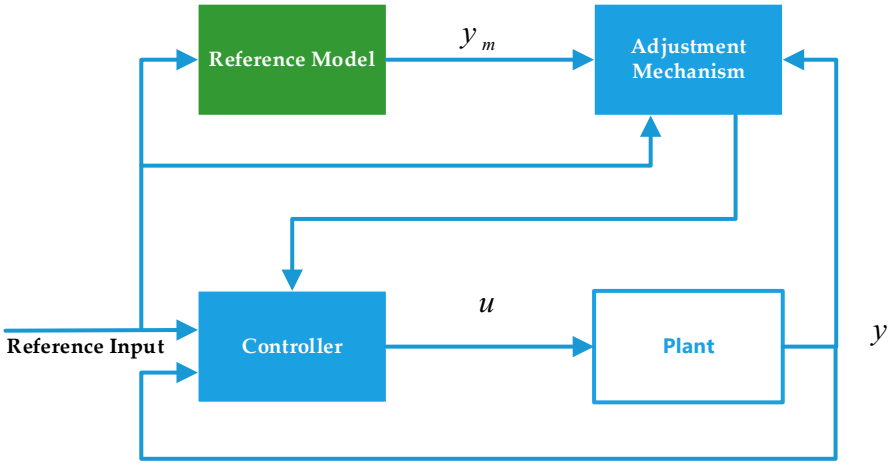

Figure 4.4. Direct MRAC system.

$$\varepsilon(t) = y(t) - y_m(t) \tag{21}$$

The MIT rule was initially created in 1960 by Massachusetts Institute of Technology (MIT) academics and was used to construct aviation autopilot systems. For every system, the MIT rule may be used to build a controller with the DMRAC scheme.

A cost function is defined as follows in this rule:

$$J(\theta) = \varepsilon^2/2 \tag{22}$$

where ε is the difference between the plant's outputs and the model's outputs, and θ is the variable parameter.

The parameter is changed in such a way that the cost function may be reduced to zero. As a result, the change in the θ parameter is maintained in the direction of J's negative gradient, i.e.:

$$\frac{d\theta}{dt} = -\gamma \frac{\partial J}{\partial \theta} \tag{23}$$

From (22):

$$\frac{d\theta}{dt} = -\gamma e \frac{\partial \varepsilon}{\partial \theta} \tag{24}$$

The partial derivative phrase $\frac{\partial \varepsilon}{\partial \theta}$ is referred to as the system's sensitivity derivative. This phrase describes how the error changes as a function of the parameter θ. Equation (23) shows how the parameter changes over time, allowing the cost function $J(\theta)$ to be lowered to zero. Here γ is a positive number that represents the controller's adaptation gain.

Assume the process is linear, with the transfer function $KG(s)$, where K is an unknown parameter and $G(s)$ is a known second-order transfer function. Our objective is to create a controller that will allow our process to monitor the reference model using the transfer function $G_m(s) = K_o G(s)$, where K_o is a known parameter.

From (21):

$$\varepsilon(s) = KG(s)U(s) - K_o G(s)U_c(s) \tag{25}$$

Furthermore, (15) can be written as follows:

$$\widetilde{v_o}(s) = R \frac{(1-D)V_o - (LI_l)s}{(RLC)s^2 + Ls - R(1-D)^2} \tilde{d}(s) \tag{26}$$

where R in (26) can be considered as K in (25) and $\tilde{d}(s)$ is the $U(s)$. Moreover, R can be considered a system uncertainty.

Defining a PID control law, $\theta = k_p, k_i, k_d$. Therefore $u(t)$ is as follows:

$$u(t) = k_p e(t) + k_i \int e(t)dt + k_d \dot{e(t)} \tag{27}$$

where: k_p is the proportional gain; k_i is the integral gain; k_d is the derivative gain; y is the plant output; and $e(t) = r(t) - y(t)$, with $r(t)$ as the input of the reference model.

The representation of the PID controller in Laplace domain is:

$$U(s) = k_p E(s) + \frac{1}{s} k_i E(s) + s k_d E(s) \tag{28}$$

Therefore, the Laplace domain of the system output will be as follows:

$$Y(s) = G(s)U(s) = G(s)[k_p E(s) + \tfrac{1}{s} k_i E(s) + s k_d E(s)] \tag{29}$$

As $e(t) = r(t) - y(t)$, it is clear that:

$$Y(s) = G(s)[R(s) - Y(s)][k_p + \tfrac{1}{s} k_i + s k_d] \tag{30}$$

Then we can obtain:

$$Y(s)[1 + G(s)[k_p + \frac{1}{s} k_i + s k_d]] = G(s)R(s)[k_p + \frac{1}{s} k_i + s k_d] \tag{31}$$

$$Y(s) = \frac{G(s)R(s)[k_p + \frac{1}{s} k_i + s k_d]}{[1 + G(s)[k_p + \frac{1}{s} k_i + s k_d]]} \tag{32}$$

Now the time domain of the system output can be written as:

$$y(t) = \frac{g(t)r(t)[p k_p + k_i + p^2 k_d]}{[1 + g(t)[p k_p + k_i + p^2 k_d]]} \tag{33}$$

According to (21):

$$\varepsilon(t) = \frac{g(t)r(t)\left[p k_p + k_i + p^2 k_d\right]}{\left[1 + g(t)\left[p k_p + k_i + p^2 k_d\right]\right]} - \frac{{\omega_n}^2}{p^2 + 2\xi\omega_n p + {\omega_n}^2} r(t) \tag{34}$$

Derivative of (34) over PID parameters, is as follows:

$$\frac{\partial \varepsilon(t)}{\partial k_p} = \frac{g(t)ep}{\left[1 + g(t)\left[p k_p + k_i + p^2 k_d\right]\right]}$$

$$\frac{\partial \varepsilon(t)}{\partial k_i} = \frac{g(t)e}{\left[1 + g(t)\left[p k_p + k_i + p^2 k_d\right]\right]}$$

$$\frac{\partial \varepsilon(t)}{\partial k_d} = \frac{g(t)ep^2}{\left[1 + g(t)\left[p k_p + k_i + p^2 k_d\right]\right]} \tag{35}$$

For the sake of ensuring that the tracking error is perfect, we will assume the time behavior of this close loop process is equal to the time behavior of the close loop reference model, as follows:

$$\frac{g(t)}{\left[1+g(t)\left[pk_p+k_i+p^2k_d\right]\right]}=\frac{{\omega_n}^2}{p^2+2\xi\omega_n p+{\omega_n}^2} \tag{36}$$

Now the gradient method described in (24) is applied to find the expressions of the control parameters:

$$\begin{aligned}
\frac{dk_p}{dt} &= -\gamma_p\varepsilon(t)\frac{p{\omega_n}^2}{p^2+2\xi\omega_n p+{\omega_n}^2}e(t)\\
\frac{dk_i}{dt} &= -\gamma_i\varepsilon(t)\frac{{\omega_n}^2}{p^2+2\xi\omega_n p+{\omega_n}^2}e(t)\\
\frac{dk_d}{dt} &= -\gamma_d\varepsilon(t)\frac{p^2{\omega_n}^2}{p^2+2\xi\omega_n p+{\omega_n}^2}e(t)
\end{aligned} \tag{37}$$

4.3.2 Stability and robustness analysis

Lyapunov stability theory was introduced in [21]. Lyapunov proposed two methods of demonstrating stability in his original work of 1892. The first method developed the solution into a sequence, which then proved to be convergent within parameters. Another approach, known as the Lyapunov stability criterion or direct method, uses an analogy of the potential function of classical dynamics with the Lyapunov function V(x). For a system as $\dot{x}=f(x)$, if the Lyapunov function has three following conditions:

$$V(x)=0 \text{ if and only if } x=0$$

$$V(x)>0 \text{ if and only if } x\neq 0$$

$$\dot{V}(x)<0$$

The system is stable in the sense of Lyapunov. By considering (22) as the Lyapunov function, the mentioned equation can be rewritten as:

$$V(\theta) = \varepsilon^2/2 \tag{38}$$

where ε is the error equation in (21), the second term of the error equation is the output of the model reference, and the first term is the output of the DC–DC boost converter, which can be obtained from (15).

Now the derivative of the Lyapunov equation is:

$$\dot{V}(\theta) = \varepsilon\dot{\varepsilon} \tag{39}$$

By considering the derivative of error term in Equation (39), we reach the following equation:

$$\dot{V}(\theta) = (\varepsilon)\frac{d\varepsilon}{d\theta}\frac{d\theta}{dt} \tag{40}$$

Therefore, by substituting Equations (35) and (37):

$$\dot{V}(k_p) = (\varepsilon)(y_m ep)(-\gamma_p \varepsilon y_m ep) = -\gamma_p \varepsilon^2 {y_m}^2 e^2 p^2$$

$$\dot{V}(k_i) = (\varepsilon)(y_m e)(-\gamma_i \varepsilon y_m e) = -\gamma_i \varepsilon^2 {y_m}^2 e^2$$

$$\dot{V}(k_d) = (\varepsilon)(y_m ep^2)(-\gamma_d \varepsilon y_m ep^2) = -\gamma_d \varepsilon^2 {y_m}^2 e^2 p^4 \tag{41}$$

From (41), it is easy to claim that the derivative of the Lyapunov equation is negative in (39), which is the third condition of Lyapunov stability.

4.4 Simulation Results

Simulink is an extension to MATLAB that allows you to create dynamic models in Windows. The benefit is that models are inserted as block diagrams once the target system's matching mathematical equations are established. To simulate an electrical system, such as a DC–DC converter, one must enter equations for various blocks in the system and use icons in Simulink to create an analogous block diagram. Individual icon settings can be defined for the process. Finally, an equation solver and simulation duration are selected. A Simulink model can readily be

constructed, as shown in the flowchart in Figure 4.5, referring to the model reference adaptive controller block diagram in Figure 4.4.

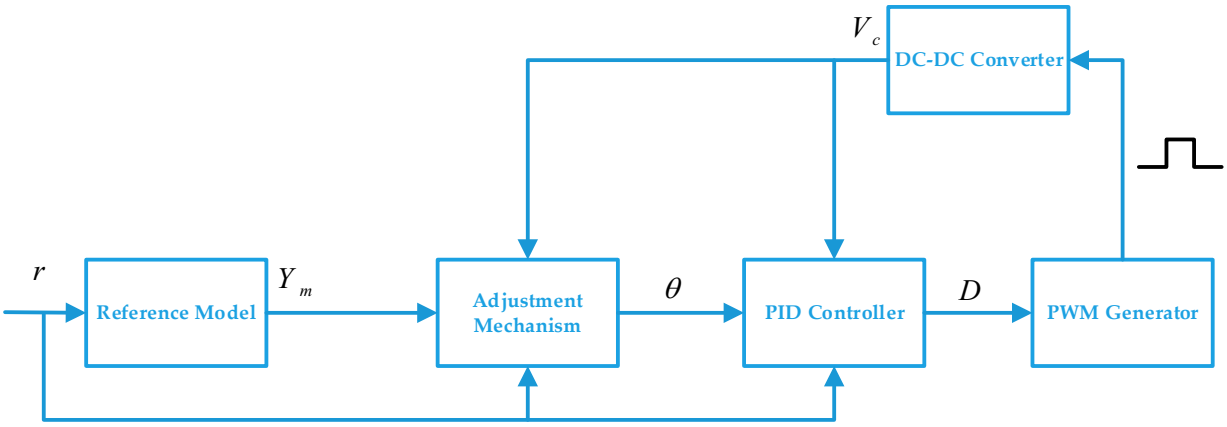

Figure. 4.5. The flowchart of the controller method.

In this simulation, the inductor is $L = 1.3 \times 10^{-3}$ H, the capacitor is $C = 6.5 \times 10^{-3}$ F, the resistor is $R = 100\ \Omega$, and the input voltage source is considered to be $V_{in} = 5$ V. Therefore, the transfer function of the boost converter, which gives the output voltages in terms of duty ratio, is:

$$\frac{\widetilde{v_o}(s)}{\tilde{d}(s)} = \frac{(1-0.5)15 - (1.3\times10^{-3})(45)s}{(1.3\times10^{-3})(6.5\times10^{-3})s^2 + \frac{1.3\times10^{-3}}{100}s - (0.5)^2} \tag{42}$$

where the reference input is 15 V, and the model reference block of the adaptive method is a first order transfer function with a pole far enough from the origin. The mentioned block is shown in Figure 4.6.

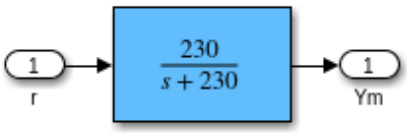

Figure 4.6. Model reference Simulink block.

The model is a first-order system with a pole lying on the left-hand side of the complex plane. Figure 4.7 below shows the model reference block's step response.

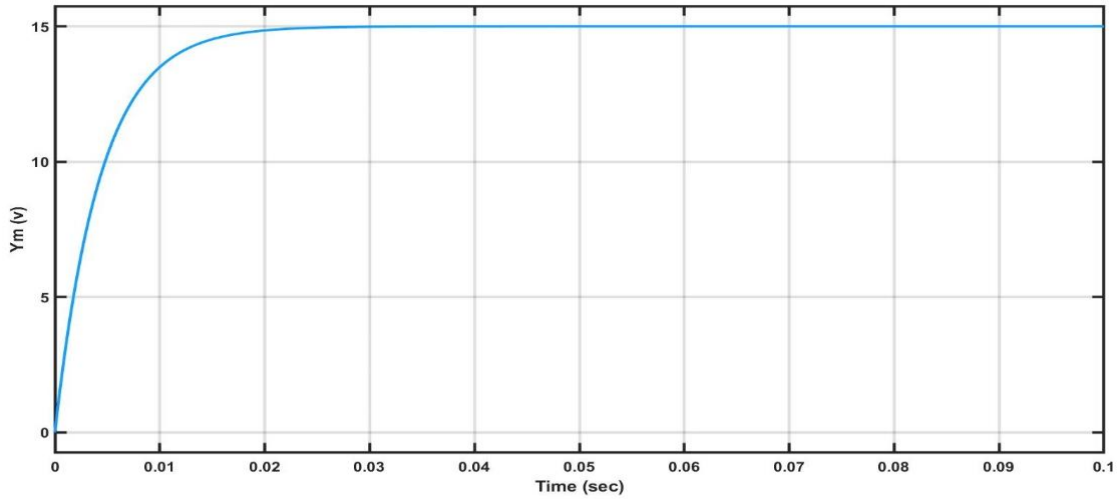

Figure 4.7. Model reference block output.

The adjustment mechanism block, illustrated in Figure 4.8 below, has two inputs: the error and the output of the model reference block, and only has one output, θ, which multiplies the PID parameters to adjust the controller.

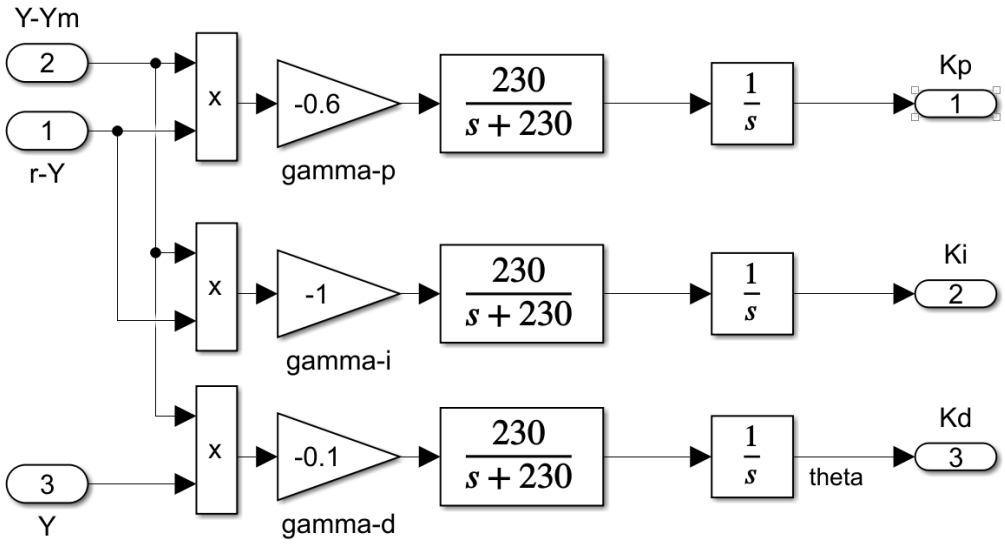

Figure 4.8. Adjustment mechanism block.

The controller block is a PID controller tuned using automated tuning of Simulink to determine the initial condition of PID parameters. Figure 4.9 below shows some more details of the controller block, where the Y_p stands for the capacitor voltage V_C.

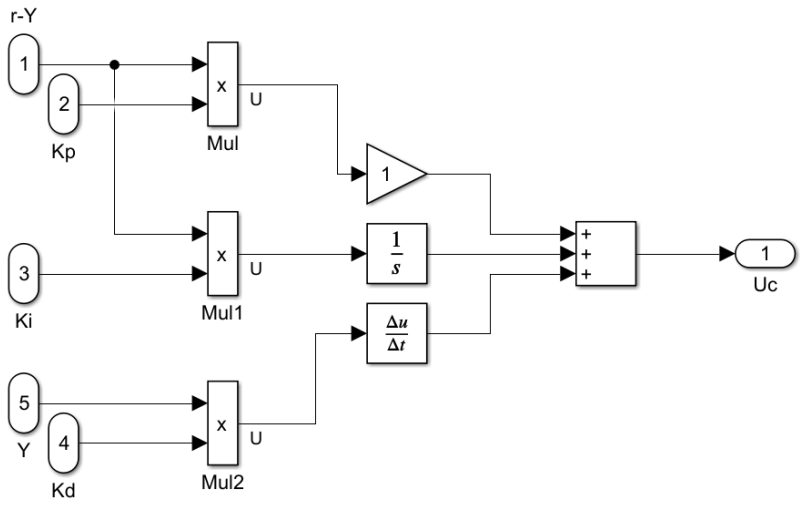

Figure 4.9. Controller block.

Finally, a PWM generator is used to produce pulses based on the controller output. The pulses are vital as an input of the switching component.

Simulations were carried out to verify the controller's capabilities for DC–DC converters that achieve voltage regulation. The switching frequency is considered 2 kHz. As load variation is expected in a typical MG, the proposed controller's effectiveness and robustness are validated through load variations. The transient response of the step-up converter is illustrated in Figure 4.10a when the reference voltage is V = 15 V. The output signal reaches the reference value set at ~ 0.04 s. The overshoot is ~ 0.03 V which is negligible. In the case of the change in load (from R = 100 Ω to R = 150 Ω), the worst-case settling time shown in Figure 4.10a (in the right figure magnifier) was obtained as ~0.1 s with a maximum overshoot of ~0.5 V. The adjustment

parameter is being adapted by the load changes in Figure 4.10b, and the control signal is changed as a consequence of adjustment parameter changes in Figure 4.10c.

The control signal generates the desired value of the duty cycle, which is updated by the MIT rule to obtain the desired voltage and connect it to the Pulse Width Modulator (PWM). This duty cycle change changes the output voltage to reduce the error signal to zero.

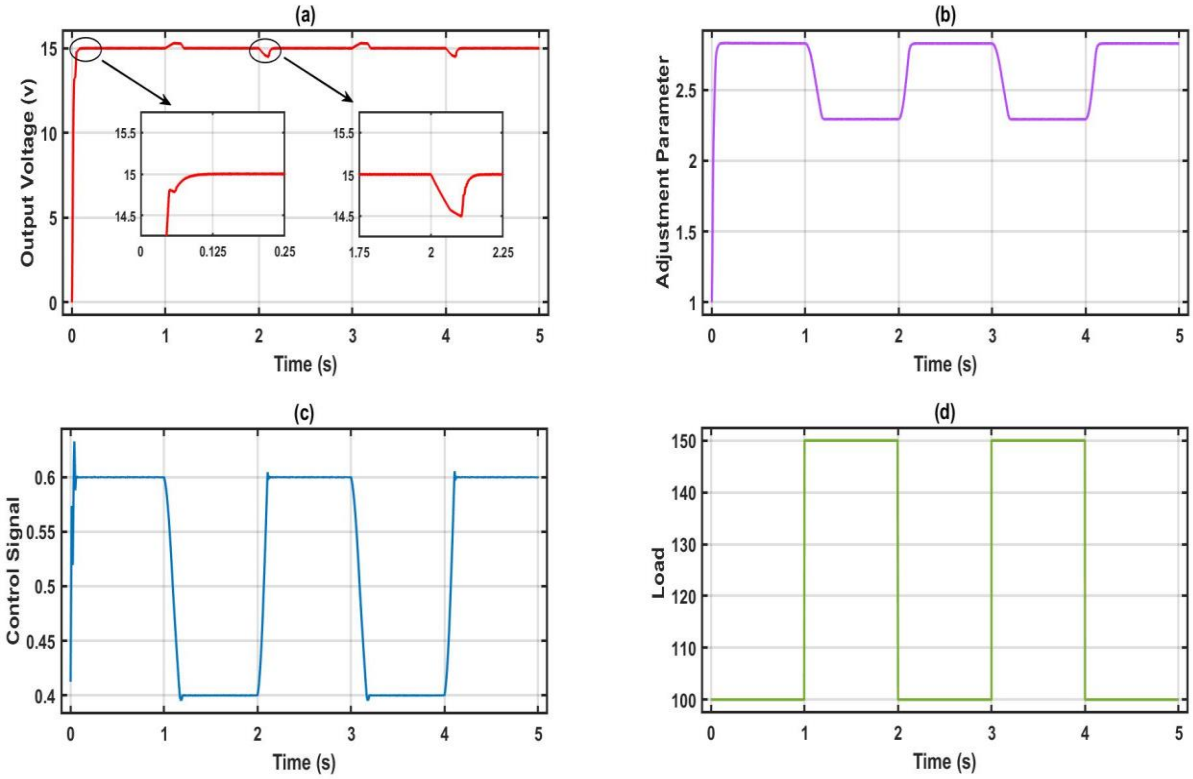

Figure 4.10. Simulation results: (**a**) The DC–DC converter transient output voltage and the responses to the load changes from 100 Ω to 150 Ω (and vice-versa), (**b**) PID controller adjustment coefficient, (**c**) control signal waveform for the load changes, and (**d**) load resistance changes from 100 Ω to 150 Ω (and vice-versa).

In the other case, as the output of the PV system that is connected to a DC–DC converter in the considered MG is not stable, the input voltage of the DC–DC converter is changed, and the results are shown in Figure 4.11. The input voltage is changed by 2 V from 8 V to 10 V (and vice-versa), and the worst overshoot response is less than ~1 V. It means that the maximum overshoot in the effect of input voltage changing is less than ~6.6%.

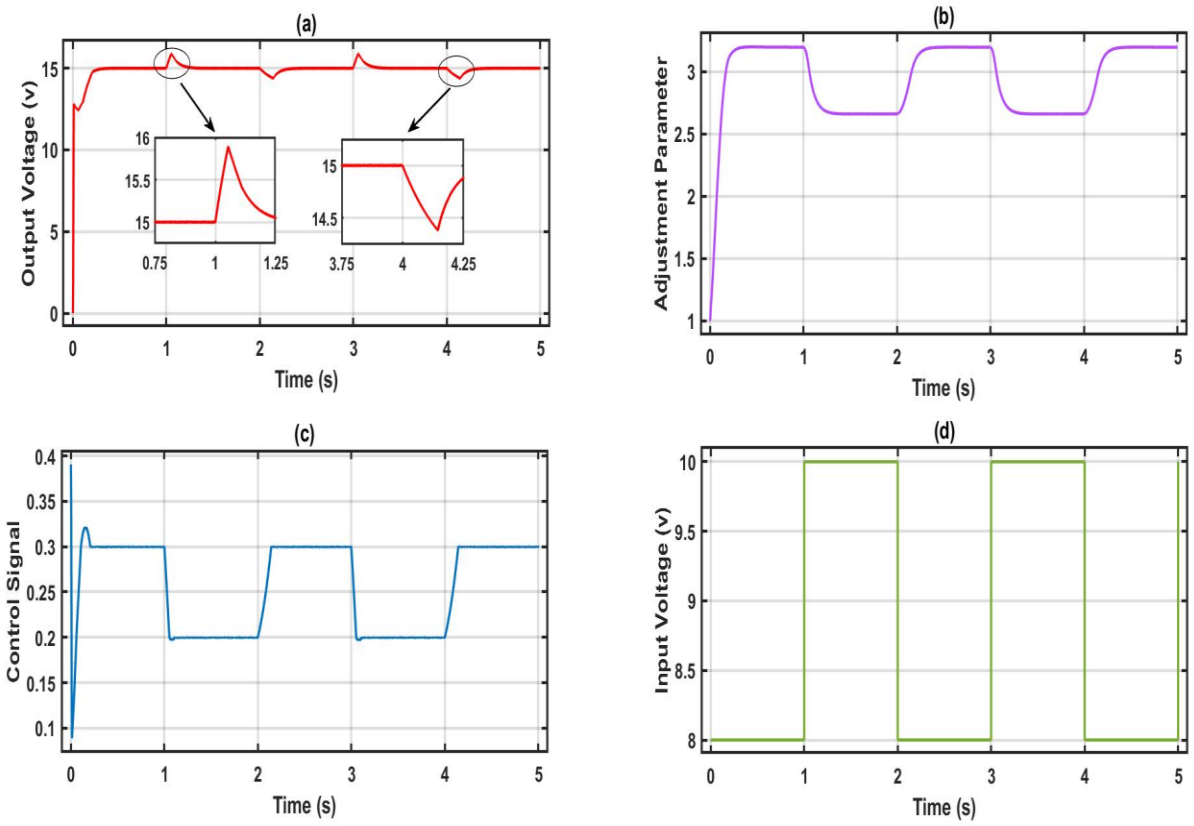

Figure 4.11. Simulation results: (**a**) The DC–DC converter transient output voltage and the responses to the input voltage changes from 8 V to 10 V (and vice-versa), (**b**) PID controller adjustment coefficient, (**c**) control signal waveform for the input voltage changes and (**d**) input voltage changes from 8 V to 10 V (and vice-versa).

As shown in [22], the lowest overshoot in 15 V setpoint, among three different PID tuning methods, namely the Ziegler–Nichol's frequency-domain method, damped oscillation method, and Good Gain method, is 34%, and the fastest rise time is 1.5 ms. Therefore, it is evident from the simulation results that the proposed algorithm has better performance in dealing with the maximum overshoot issues. Moreover, comparing the proposed method with nonlinear methods, such as the improved sliding mode controller presented in [23], shows that the output's overshoot of DMRAC is still negligible.

The bode plot of the DMRAC is presented in Figure 4.12, where the model reference is as shown in Figure 4.7 and the adjustment parameters shown in Figure 11d. The following figure shows the gain margin is 8.44 dB and the phase margin is 65.3 deg.

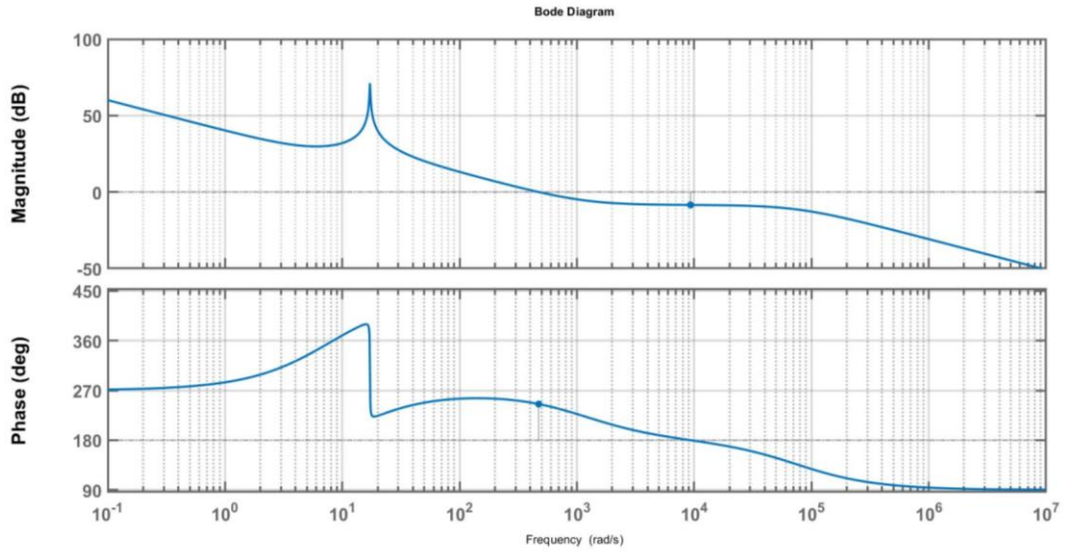

Figure 4.12. Bode plot of the closed loop DMRAC for the boost converter. The blue dot in magnitude plot shows the gain margin (8.44 dB), and the blue dot in phase plot shows the phase margin (65.3 deg).

4.5 Experimental Result

A hardware implementation is conducted to evaluate the controller's performance in the real world. The Arduino Uno is used to interface Simulink's DMRAC controller and the DC–DC boost converter circuit to implement hardware in the loop. It is worth mentioning that the analog input pins of Arduino Uno are limited to 5 V, so a voltage divider circuit is used to reduce the feedback output voltage. Therefore, it is inevitable to revise the feedback voltage in Simulink. Figure 4.13 shows the designed Simulink to create an embedded system on Arduino Uno. Figure 4.14a illustrates the setup connectivity between Simulink and the DC–DC boost converter. The components used to implement the experimental test are shown in Figure 4.14b. The components used to build the circuit are listed in Table 4.2.

Table 4.2.

Hardware Description

Device/Component	Model/Value
Arduino	Uno
Capacitor	330 µF
Inductor	250 µH
Load resistor	330 Ω
Voltage divider resistors	100 Ω, 220 Ω
Mosfet	IRLZ44 N
Diode	In4004

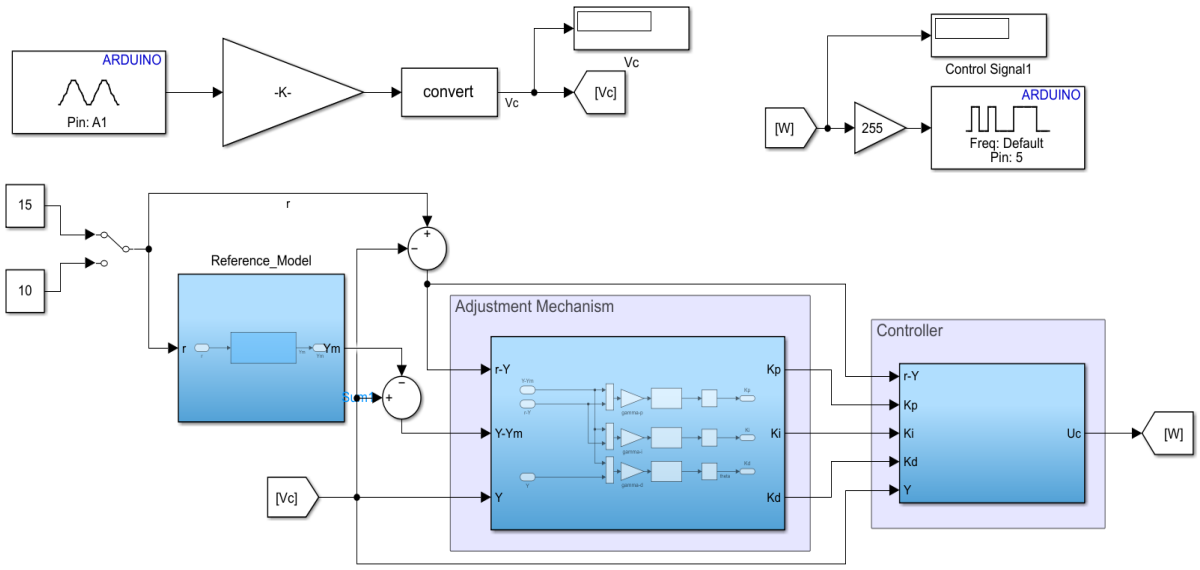

Figure 4.13. The designed Simulink to create an embedded system on Arduino Uno.

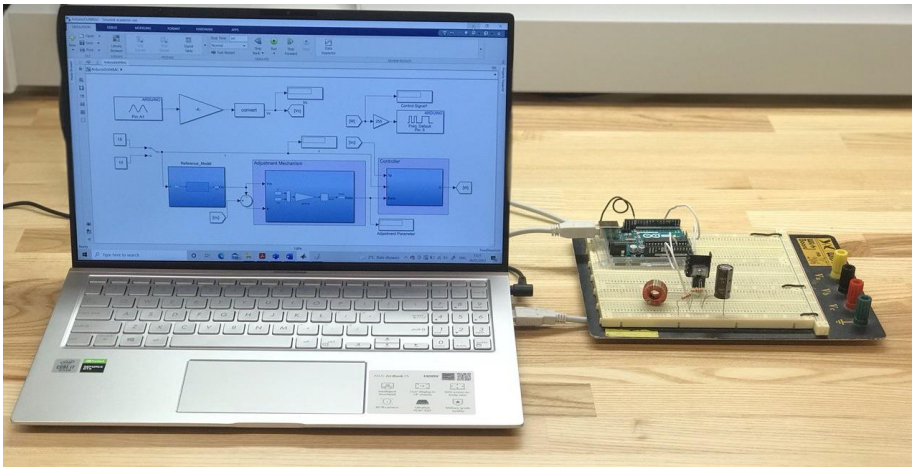

(a)

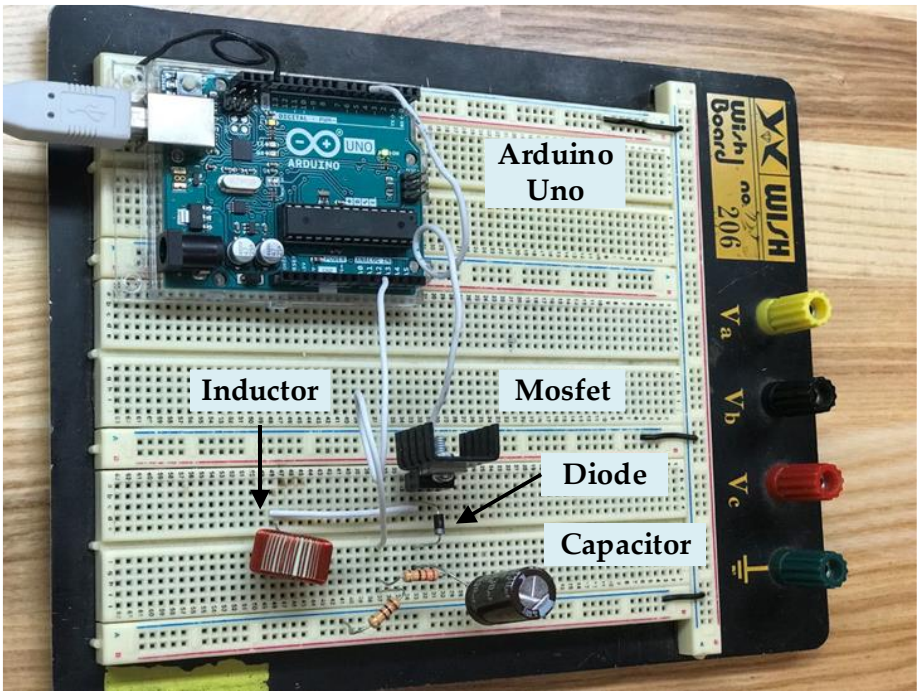

(b)

Figure 4.14. (**a**) Set up connectivity between Simulink and target hardware, (**b**) hardware implementation.

Figure 4.15a shows the transient output response of the boost converter for the reference voltage of 15 V. The effect of input voltage changes from 8 V to 10 V (and vice-versa) is shown in Figure 4.15b. In Figure 4.15c, we can see how the output voltage changes with the presence of a change in voltage reference from 15 V to 10 V (and vice-versa). In all cases, the settling time is about 0.2

s. Moreover, it is evident in Figure 4.15a, c that the system is tracking the reference voltage with almost no overshoot.

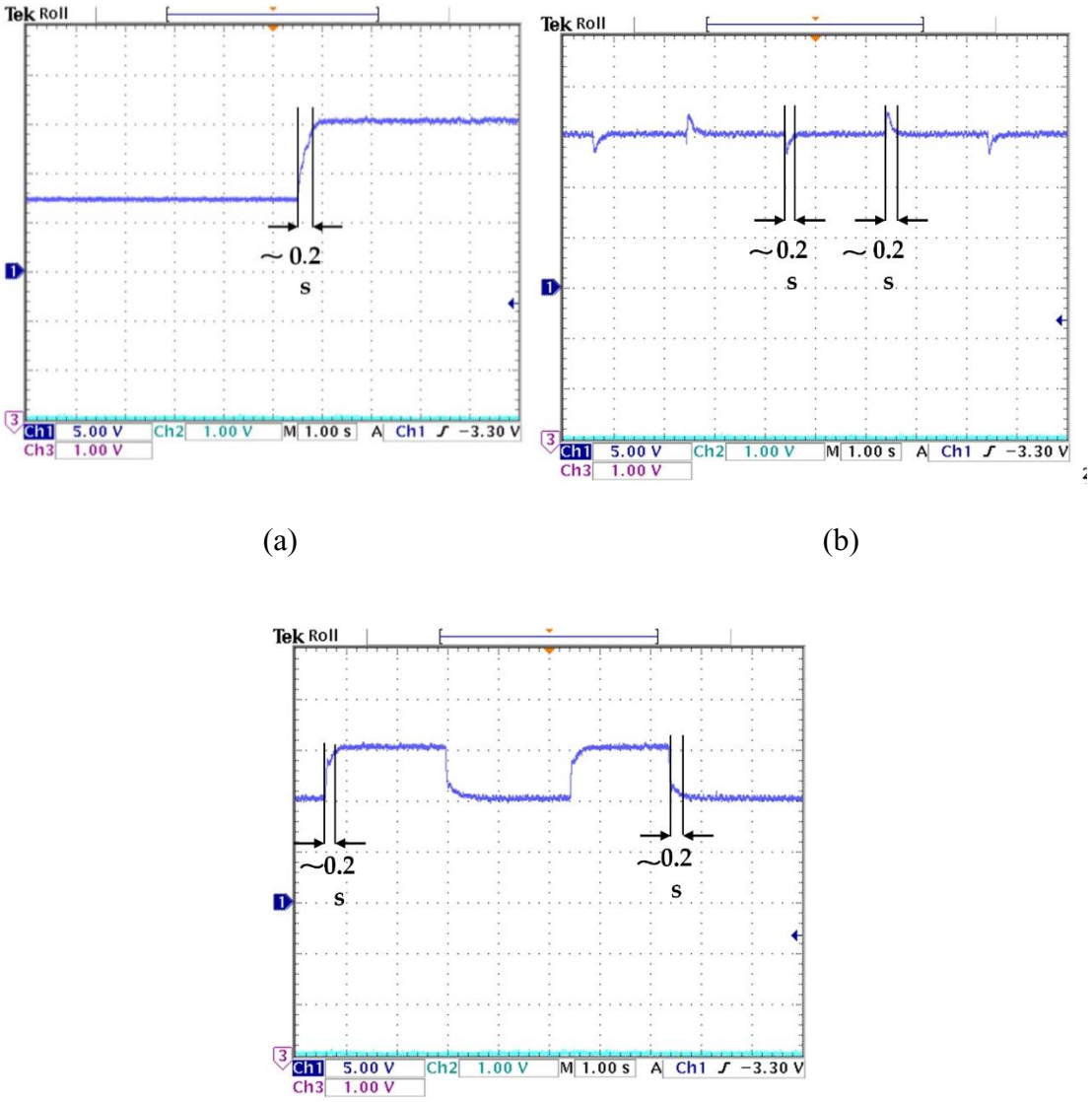

Figure 4.15. Oscilloscope output results: (**a**) Transient output response of the boost converter for the reference voltage of 15 V, (**b**) output response waveform of input voltage changes from 8 V to 10 V (and vice-versa), and (**c**) the output voltage changes with the presence of a change in voltage reference from 15 V to 10 V (and vice-versa) implementation.

4.6 Conclusion

This work presents an adaptive controller to regulate the output voltage of the DC–DC converters that exist in an isolated MG. Since the converter system is a non-minimum phase, the controller design that relies only on output voltage feedback becomes challenging. Even though output voltage control can be achieved using inductor current control, such current mode controllers may also require prior knowledge of the load resistance and more states, such as output and inductor currents in feedback. In this work, the output voltage is stabilized by two control loops. A PID controller regulates the output voltage at a fixed level, and the outer loop implements the MIT rule for DMRAC. The DMRAC updates the PID controller parameters in real-time to ensure that the existing system tracks the desired reference model, using only an output voltage feedback sensor. The proposed controller and the model are tested in MATLAB/SIMULINK for load disturbances. The load was changed by ~50% of its original value, and the worst-case settling time and maximum overshoot were less than ~0.1 s and 0.5 V, respectively, as compared to well-tuned PID controllers. The hardware validation is also carried out to show the performance of the proposed controller. Our results suggest that the DMRAC provides robust regulation against parameter variations. Therefore, it is suitable to use in any isolated MG.

The control scheme is implemented with a single output voltage feedback sensor, so no additional sensing circuitry was required.

The limitation of the proposed design is that the time delay effect on stability was not studied. Additionally, the simulation parameters were ideal. In future research work, the mentioned limitations will be addressed.

REFERENCES

1. Maneesh, K, and Barjeev, T. A state of art review of microgrid control and integration aspects. In *IEEE International conference IICPE*, *Proceedings of the 2016 7th India International Conference on Power Electronics (IICPE), Patiala, India, 17–19 November 2016;* IEEE: New York, NY, USA, 2016; pp. 1–6.
2. Zakir, M.; Arshad, A.; Sher, H.A.; Lehtonen, M. An Optimal Power Management System Based on Load Demand and Resources Availability for PV Fed DC-Microgrid with Power-Sharing among Multiple Nanogrids. In Proceedings of the 2021 IEEE PES Innovative Smart Grid Technologies Europe *(*ISGT Europe), Espoo, Finland, 18–21 October 2021; pp. 1–5.
3. Zakir, M.; Sher, H.A.; Arshad, A.; Lehtonen, M. A fault detection, localization, and categorization method for PV fed DC-microgrid with power-sharing management among the nano-grids. *Int. J. Electr. Power Energy Syst.* **2022**, *137*, 107858.
4. Forouzesh, M.; Siwakoti, Y.P.; Gorji, S.A.; Blaabjerg, F.; Lehman, B. A survey on voltage boosting techniques for step-up DC-DC converters. In Proceedings of the IEEE Energy Conversion Congress and Exposition (ECCE), Milwaukee, WI, USA, 2016; pp. 1–8.
5. Mamarelis, E.; Petrone, G.; Spagnuolo, G. Design of a sliding mode controlled SEPIC for PV MPPT applications. *IEEE Trans. Ind. Electron.* **2014**, *61*, 3387–3398.
6. Yanarates, C.; Zhou, Z. Design and Cascade PI Controller-Based Robust Model Reference Adaptive Control of DC-DC Boost Converter. *IEEE Access* **2022**, *10*, 44909–44922.
7. Young, M. *The Technical Writer's Handbook*; University Science: Mill Valley, CA, USA, 1989.
8. Rajakumari R. F.; Deshpande, M. Comparative Analysis of DC-DC Converters. In Proceedings of the 2nd International Conference on Power and Embedded Drive Control (ICPEDC), Chennai, India, 2019; pp. 504–509.
9. Zaitu, R. *Voltage Mode Boost Converter Small Signal Control Loop Analysis Using the TPS61030*; Application Report; Texas Instruments: Dallas, TX, USA, 2007.

10. Perry, A.G.; Feng, G.; Liu, Y.F.; Sen, P.C. A design method for PI-like fuzzy logic controller for DC-DC converter. I*EEE Trans. Ind. Electron.* **2007**, *54*, 2688–2695.
11. Aldo, B.; Corsanini, D.; Landi, A.; Sani, L. Circle based Criteria for performance evaluation of controlled DC-DC Switching Converters. *IEEE Trans. Ind. Electron.* **2006**, *53*, 1862–1869.
12. Zhang, J.; Shu-Hung Chung, H.; Lo, W.L. and Ron Hui, S.Y. Implementation technique for design of switching Regulators Using Genetic Algorithm. *IEEE Trans. Power Electron.* **2001**, *16*, 752–763.
13. Hung, J.Y.; Gao, W.; Hung, J.C. Variable structure control: A survey. *IEEE Trans. Ind. Electron.* **1993**, *40*, 2–22.
14. Tang, K.L., and Mulholland, R.J. Comparing Fuzzy logic with classical controller design. *IEEE Trans. Syst. Man Cybern.* **1987**, *6*, 1085–1087.
15. Nelms, R.M.; Guo, L.; Hung, J.H. Digital Controller design for Buck and Boost Converters Using Root Locus Technique. In Proceedings of the 29th Annual Conference of the IEEE Industrial Electronics Society, Roanoke, VA, USA, 2003; Volume 2, pp. 1864–1869.
16. Rashid, U.; Jamil, M.; Gilani, S.O.; Niazi, I.K. LQR based Training of Adaptive Neuro-Fuzzy Controller. In Proceedings of the 25th Italian Workshop on Neural Networks, Salerno, Italy, 20–22 May 2015; pp. 311–322.
17. Schmidt S, Richter M, Oberrath J, Mercorelli P. Control oriented modeling of DCDC converters. *IFAC-Pap. Line* **2018**, *51*, 331–336.
18. Kumar, M.; Tyagi, B. Design of A Model Reference Adaptive Controller (MRAC) for DC-DC Boost Converter for Variations in Solar Outputs using modified MIT Rule in an Islanded Microgrid. In Proceedings of the 2020 IEEE International Conference on Power Electronics, Smart Grid and Renewable Energy (PESGRE2020), Cochin, India, 2–4 January 2020; pp. 1–6.
19. Raj, R.N.; Purushothaman, K.V.; Singh, N.A. Adaptive TSK-type neural fuzzy controller for boost DC-DC converter. In Proceedings of the 2017 IEEE International Conference on Circuits and Systems (ICCS), Thiruvananthapuram, India, 20–21 December 2017; pp. 441–446.

20. Awais, M.; Khan, L.; Ahmad, S.; Jamil, M. Feedback-Linearization-Based Fuel-Cell Adaptive-Control Paradigm in a Microgrid Using a Wavelet-Entrenched Neuro-Fuzzy Framework. *Energies* **2021**, *14*, 1850.
21. Lyapunov, A.M. The General Problem of the Stability of Motion. Ph.D Thesis, University Kharkov, Kharkiv, Ukraine, 1892. (In Russian)
22. Ibrahim, O.; Yahaya, N.Z.; Saad, N. Comparative studies of PID controller tuning methods on a DC-DC boost converter. In Proceedings of the International Conference on Intelligent and Advanced Systems (ICIAS), Kuala Lumpur, Malaysia, 15–17 August 2016; pp. 1–5.
23. Liu, S.; Liu, X.; Jiang, S.; Zhao, Z.; Wang, N.; Liang, X.; Zhang, M.; Wang, L. Application of an Improved STSMC Method to the Bidirectional DC–DC Converter in Photovoltaic DC Microgrid. *Energies* **2022**, *15*, 1636.

Chapter 5

Super-Fast Sliding Mode Control of a Boost Converter for Voltage Tracking in Microgrids

Preface

*A version of this manuscript will be submitted in **MDPI Energies October 2022**. As the primary author, I carried out most of the research work, performed the literature reviews, carried out the system design, modeling, and analysis of the results. I also prepared the first draft of the manuscript. The co-authors, Dr. Mohsin Jamil, and Dr. M. Tariq Iqbal supervised the research, provided the research guide, reviewed, and corrected the manuscript, and contributed research ideas in the actualization of the manuscript.*

Abstract

In this study, we present a super-fast sliding mode (SFSM) controller algorithm in a boost converter used in islanded microgrids (MG) with a solar photovoltaic (PV) system. Islanded types of microgrids have very sensitive voltage and frequency variability; therefore, a robust and fast controller is always desired to control such variations within the MG. A dc-dc boost converter with a modified sliding surface is proposed in this paper, which stabilizes inductor current and output voltage variations in islanded MG. Since the boost converter is a non-minimum phase, the controller design becomes challenging. Even though output voltage control can be achieved using inductor current control, such current mode controllers may also require prior knowledge of the load resistance and more states such as output and inductor currents in feedback. Here, an integral term is introduced into the SFSM controller as an additional controlled state variable. Compared to a DC-DC boost converter connected to the MG, a controller such as the one introduced in this paper is more successful in dealing with unknown parameter fluctuations and disturbance changes. The MATLAB/SIMULINK is used to design and simulate the controller with different load disturbances and input voltage variances. The hardware validation is also carried out to show the performance of the proposed controller. Our results suggest that the SFSM provides robust regulation against parameter variations.

Keywords— boost converters; adaptive control; DC-DC converter; power electronics

5.1 Introduction

MG are small-scale energy grids supplying energy to loads at the distribution level. In general, the small grids have control capabilities and can be categorized into grid connected and islanded or isolated grids [1]. Grid-connected MGs are governed by the main power network and their voltage and frequency are defined by it. However, for the islanded MG, due to the low system inertia and fast changes in the output power of wind and solar power sources, the frequency and voltage can experience large excursions and thus easily deviate from nominal operating conditions.

When we have a DC MG, the DC-DC converters are the most significant part of system. Many DC-DC converter topologies [2, 3], such as the boost topology, the buck topology, buck-boost converters, single-ended primary inductor converter (SEPIC) topology [3], have been discussed in the literature. The boost converters are involved in increasing the voltage. The buck converters are applied to lower the voltage. Then, buck-boost and SEPIC are competent to do both operations, i.e., step up and step down the output voltage. Boost converters are used as front-end converters for battery sources, photovoltaic solar systems, and fuel cells to get greater output voltage than the input DC voltage.

Many studies compare the different types of converters' performance. In [4], research has been done over step-up DC-DC converters in various configurations. In [5], the authors analyzed boost and SEPIC converters, considering output voltage ripple, total harmonic distortion, power factor for both converters, and Boost converters produced better results. Besides mentioned features, boost converters are easier to use. So, the boost-type converter is frequently used because of its superior performance. As illustrated in Figure 5.1, the main elements of a boost converter are the inductor, diode, capacitor, and switch. In this research, we use MOSFET as a switch that can consistently turn ON and OFF based on the generated duty cycle.

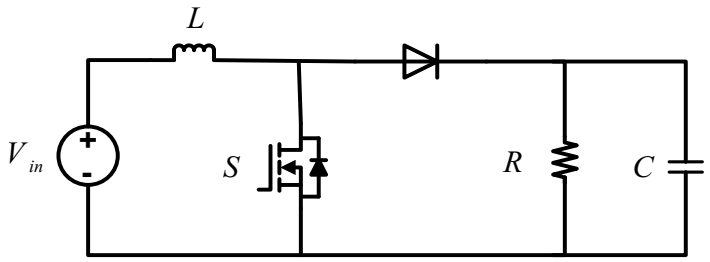

Fig. 5.1. Boost converter.

Because these converters display poor voltage regulation and inadequate dynamic response when run in an open loop, they are often equipped with closed-loop control for output voltage regulation [6]. The DC-DC boost converters operate in three different modes: Continuous Conduction Mode (CCM), Discontinuous Conduction Mode (DCM), and Critical Conduction Mode (CrCM). The CCM operating mode-based DC-DC converter is considered in this research. With the CCM, boost type converters have the right-half-plane-zero (RHPZ) characteristic in the duty-cycle to output voltage function [7]. Dynamically, this results in sluggish response of the system, particularly when the mode of control is solely based on control of the output voltage, i.e., voltage-mode control.

The converter's performance depends upon the applied control strategy linked to ON/OFF switching states. Many control techniques have been presented to regulate the switch ON/OFF (duty cycle) to achieve the required output voltage. The most common controllers are linear PID controllers. A linearized small-signal model of the DC-DC converter is used, which depends upon the standard frequency response methods. The PID control design is based on linear control theory, such as the Ziegler-Nichols method [8], the root locus approach [9], the circle-based criterion [10], the hysteresis method [11], the bode plot, and so on. These control methods perform well around the linearized model's operating points. The small-signal model of a boost converter, on the other hand, changes when the operating point change. It is important to mention here that the duty cycle

determines the poles and a right-half-plane zero and the amplitude of the frequency response. As a result, PID controllers have a hard time respecting changes in operating points, and they function poorly when the system is subjected to substantial load fluctuations.

Despite the necessity of changes in input, the Ziegler-Nichols technique for PID tuning is an experimental one that is extensively utilized. One downside of this technique is that it necessitates a prior understanding of plant models. A decent but not optimal system response is achieved when the controller is adjusted using the Ziegler-Nichols technique. If the dynamics of the plant change, the transient reaction might be considerably worse. It should be noted that many plants have time-varying dynamics due to external/environmental factors such as temperature and pressure. The controller must respond to changes in the dynamics of the plant features to provide a robust system. Numerous investigations have been conducted into the possibility of applying various types of nonlinear controllers to power converters, each with the same goal of improving their controllability. Nonlinear control techniques [12-19] such as fuzzy logic, sliding mode control and adaptive strategy have recently offered good static and dynamic responsiveness. Despite their unique advantages, most of the above controllers are unsuitable for power converters due to their inefficiency or complexity, or they have a slow dynamic response and require complicated control circuits.

The aim of this paper is to propose a SFSM controller based on indirect sliding-mode control (ISC) in pulse width modulation (PWM). When applied to boost converters, this controller can provide good large-signal performance with fast dynamical responses. In order to provide a comprehensive description of the proposed SFSM controller, various theoretical and practical aspects of the controller are discussed. Simulations are presented to demonstrate that the proposed controller works well in wide operating conditions while validating the theoretical design.

The main goal of proposing a nonlinear controller for boost converters is to provide fast response for converters that they cannot meet with nonlinear voltage types of controllers or any sliding mode (SM) controllers. A summary of the salient features of the proposed controller is as follows:

- The dynamical responses of the proposed controller are fast when compared to the conventional SM controller.
- The SFSM is equipped by the inherent robust features of SM controller.
- The proposed controller is stable across a wide range of operating conditions.
- The settling time varies only slightly under a wide range of operating conditions.
- Voltage overshoots are relatively low.

Table 5.1

Nomenclature

Symbol	Meaning
v_{in}	Input voltage
v_c	Capacitor voltage
i_l	Inductor current
d	Duty cycle
y_m	The output of the reference model
y	Plant output
u_c	Plant input
$G(s)$	Second-order transfer function

5.2 DC–DC Converter Dynamic Modelling

5.2.1 Ideal dynamic model

The controller's performance depends upon the accurate modeling of the DC–DC converter. A well-established average modeling technique [17] is used to design the controller. The boost converter consists of a DC input voltage source, an inductor L, a controlled switch S, a diode, a filter capacitor C, and a load resistance R. The current in the inductor grows linearly when the switch is turned on, but the diode remains off. When the switch is turned off, the energy stored in the inductor is released to the load. As the converter's name implies, the output voltage is always greater than the input voltage. The DC–DC boost converters operate in three different modes: CCM, DCM, and CrCM. The CCM operating mode-based DC–DC converter is considered in this research.

T is the switching period, and the switch is closed for time DT and open for $(1-D)T$, where D is the steady-state duty cycle. When the switch is on, there are two loops, one for inductor current and the other for the capacitor current. Using the KVL for the mentioned loops, the following equations can be obtained.

Defining the state vector as $x = [i_l\ v_c]^T$ and the output voltage $v_o = v_c$, the state space form during the "ON" mode can be written as follows:

$$\begin{bmatrix} \frac{di_l}{dt} \\ \frac{dv_c}{dt} \end{bmatrix} = \begin{bmatrix} 0 & 0 \\ 0 & -\frac{1}{RC} \end{bmatrix} \begin{bmatrix} i_l \\ v_c \end{bmatrix} + \begin{bmatrix} \frac{1}{L} \\ 0 \end{bmatrix} v_{in} \tag{1}$$

$$v_o = [0\ 1] \begin{bmatrix} i_l \\ v_c \end{bmatrix} \tag{2}$$

During the "OFF" mode state, the energy stored in the inductor is released to the output RC circuit through the diode.

We can derive the following state equations for the OFF mode by using KVL and KCL equations for the boost converter circuit in Figure 5.1, when the switch is off:

$$\begin{bmatrix} \frac{di_l}{dt} \\ \frac{dv_c}{dt} \end{bmatrix} = \begin{bmatrix} 0 & -\frac{1}{L} \\ \frac{1}{C} & -\frac{1}{RC} \end{bmatrix} \begin{bmatrix} i_l \\ v_c \end{bmatrix} + \begin{bmatrix} \frac{1}{L} \\ 0 \end{bmatrix} v_{in} \tag{3}$$

$$v_o = [0\ 1] \begin{bmatrix} i_l \\ v_c \end{bmatrix} i_l - \frac{V_c}{R} - C\frac{dv_c}{dt} = 0 \tag{4}$$

A state-space averaging approach is utilized to obtain a converter model across one switching period. In other words, the state-space descriptions of the two modes must be replaced with a single state-space description that approximates the behavior of the circuit across the whole time T. By using the state-space averaging technique, the averaged modified model is given by:

$$A = A_1 d + A_2(1-d) \tag{5}$$

$$B = B_1 d + B_2(1-d) \tag{6}$$

where A_1, A_2, B_1 and B_2 are given below, and d is changes in the duty cycle:

$$A_1 = \begin{bmatrix} 0 & 0 \\ 0 & -\frac{1}{RC} \end{bmatrix},\ A_2 = \begin{bmatrix} 0 & -\frac{1}{L} \\ \frac{1}{C} & -\frac{1}{RC} \end{bmatrix}$$

$$B_1 = \begin{bmatrix} \frac{1}{L} \\ 0 \end{bmatrix},\ B_2 = \begin{bmatrix} \frac{1}{L} \\ 0 \end{bmatrix}$$

Using (5) and (6), we obtain the following:

$$\begin{bmatrix} \frac{di_l}{dt} \\ \frac{dv_c}{dt} \end{bmatrix} = \begin{bmatrix} 0 & -\frac{(1-d)}{L} \\ \frac{1-d}{C} & -\frac{1}{RC} \end{bmatrix} \begin{bmatrix} i_l \\ v_c \end{bmatrix} + \begin{bmatrix} \frac{1}{L} \\ 0 \end{bmatrix} v_{in} \tag{7}$$

$$v_o = [0\ 1] \begin{bmatrix} i_l \\ v_c \end{bmatrix}$$

The boost converter's steady-state model may be calculated from (7) by letting:

$$\begin{bmatrix} \frac{di_l}{dt} \\ \frac{dv_c}{dt} \end{bmatrix} = 0 \quad and \quad d = D$$

In this case, (7) becomes:

$$\begin{bmatrix} 0 \\ 0 \end{bmatrix} = \begin{bmatrix} 0 & -\frac{(1-D)}{L} \\ \frac{1-D}{C} & -\frac{1}{RC} \end{bmatrix} \begin{bmatrix} i_l \\ v_c \end{bmatrix} + \begin{bmatrix} \frac{1}{L} \\ 0 \end{bmatrix} v_{in} \tag{8}$$

$$v_o = [0\ 1] \begin{bmatrix} i_l \\ v_c \end{bmatrix}$$

The steady-state relationship between v_o and v_{in} may be expressed as using (8):

$$\frac{V_o}{V_{in}} = \frac{1}{1-D} \tag{9}$$

To obtain the boost converter's transfer function, the model given by (8) must first be linearized around a particular operating point. To this end, we assume that the inductor's current I_l, capacitor voltage V_c, duty cycle D, and input voltage V_{in} determine the steady-state operating point. Now, by considering small perturbations of the operating point, the variables associated with the average model can be written as:

$$\begin{aligned} i_l &= I_l + \tilde{\imath}_l \\ v_c &= V_c + \tilde{v}_c \\ v_{in} &= V_{in} + \widetilde{v_{in}} \\ d &= D + \tilde{d} \end{aligned} \tag{10}$$

where the $\tilde{\imath}_l$, $\tilde{v}_c$ and $\widetilde{v_{in}}$ are the small perturbations of the inductor current, capacitor voltage, and input voltage, respectively. Therefore, Equation (7) becomes:

$$\frac{d}{dt}\begin{bmatrix} I_l + \tilde{\imath}_l \\ V_c + \tilde{v}_c \end{bmatrix} = \begin{bmatrix} 0 & -\frac{(1-D)}{L} \\ \frac{1-D}{C} & -\frac{1}{RC} \end{bmatrix} \begin{bmatrix} I_l \\ V_c \end{bmatrix} + \begin{bmatrix} 0 & -\frac{(1-D)}{L} \\ \frac{1-D}{C} & -\frac{1}{RC} \end{bmatrix} \begin{bmatrix} \tilde{\imath}_l \\ \tilde{v}_c \end{bmatrix} + \begin{bmatrix} 0 & \frac{\tilde{d}}{L} \\ -\frac{\tilde{d}}{C} & 0 \end{bmatrix} \begin{bmatrix} I_l \\ V_c \end{bmatrix} + \begin{bmatrix} \frac{1}{L} \\ 0 \end{bmatrix} [V_{in} + \widetilde{v_{in}}] \tag{11}$$

It is worth noting that the steady-state portion of (11) is given by:

$$\begin{bmatrix} 0 & -\frac{(1-D)}{L} \\ \frac{1-D}{C} & -\frac{1}{RC} \end{bmatrix} \begin{bmatrix} I_l \\ V_c \end{bmatrix} + \begin{bmatrix} \frac{1}{L} \\ 0 \end{bmatrix} [V_{in}] = 0$$

and:

$$\begin{bmatrix} 0 & \frac{\tilde{d}}{L} \\ -\frac{\tilde{d}}{C} & 0 \end{bmatrix} \begin{bmatrix} I_l \\ V_c \end{bmatrix} = \begin{bmatrix} \frac{V_c}{L} \\ -\frac{I_l}{C} \end{bmatrix} [\tilde{d}] \tag{12}$$

Hence, (11) is reduced to:

$$\frac{d}{dt} \begin{bmatrix} \widetilde{i_l} \\ \widetilde{v_c} \end{bmatrix} = \begin{bmatrix} 0 & -\frac{(1-D)}{L} \\ \frac{1-D}{C} & -\frac{1}{RC} \end{bmatrix} \begin{bmatrix} \widetilde{i_l} \\ \widetilde{v_c} \end{bmatrix} + \begin{bmatrix} \frac{1}{L} & \frac{V_c}{L} \\ 0 & -\frac{I_l}{C} \end{bmatrix} \begin{bmatrix} \widetilde{v_{in}} \\ \tilde{d} \end{bmatrix} \tag{13}$$

Finally, the output voltage perturbation may be expressed directly as:

$$\widetilde{v_o} = [0\ 1] \begin{bmatrix} \widetilde{i_l} \\ \widetilde{v_c} \end{bmatrix} \tag{14}$$

The state-space model of (13) and (14) are given by:

$$\dot{x} = Ax + Bu$$

$$y = Cx$$

$$A = \begin{bmatrix} 0 & -\frac{(1-D)}{L} \\ \frac{1-D}{C} & -\frac{1}{RC} \end{bmatrix}$$

$$B = \begin{bmatrix} \frac{1}{L} & \frac{V_c}{L} \\ 0 & -\frac{I_l}{C} \end{bmatrix}$$

$$C = [0\ 1]$$

In this research, we design a controller to generate duty cycle correction $\tilde{d}$ in such a way that the output voltage remains constant. In this regard, we consider the transfer function given in (15)

using the state transition matrix, which may be expressed as follows in terms of the converter's parameters:

$$\frac{\widetilde{v_o}(s)}{\tilde{d}(s)} = \frac{(1-D)V_o - (LI_l)s}{(LC)s^2 + \frac{L}{R}s + (1-D)^2} \tag{15}$$

5.2.2 Parasitic realization in boost converter dynamic model

The goal of analyzing ideal/lossless components and leaving parasitic elements out, as we have before, is to simplify model development and to figure out the fundamental features of the switching system. Nevertheless, parasitic elements and losses need to be considered for improving model accuracy, analyzing system efficiency, and studying dynamic behavior. As a result of including the parasitic elements, nonlinear current and voltage waveforms are generated, and this complicates the process of developing a model. The schematic in Figure 5.2 shows a simplified equivalent circuit for the DC–DC boost converter with parasitic elements. A capacitance C and inductor L can be considered as an output filter. An analysis of capacitor equivalent series resistance (ESR), R_C, and inductor DC resistance, R_L, is performed.

Per switching cycle, the boost converter has two modes in CCM. Again, the switch is closed for time DT and open for $(1-D)T$, where D is the steady-state duty cycle. Defining the state vector as $x = [i_l \; v_c]^T$ and the output voltage $v_o = v_c$, and writing the KVL and KCL for loops in Figure 5.2, we can obtain the state space (ss) form for "ON" and "OFF" modes of the converter. During the "ON" mode state, the ss form will be:

$$\begin{bmatrix} \frac{di_l}{dt} \\ \frac{dv_c}{dt} \end{bmatrix} = \begin{bmatrix} -\frac{R_L}{L} & 0 \\ 0 & -\frac{1}{(R_C+R)C} \end{bmatrix} \begin{bmatrix} i_l \\ v_c \end{bmatrix} + \begin{bmatrix} \frac{1}{L} \\ 0 \end{bmatrix} v_{in} \tag{16}$$

$$v_o = [0 \; \frac{R}{R+R_C}] \begin{bmatrix} i_l \\ v_c \end{bmatrix}$$

During the "OFF" mode state, ss form is:

$$\begin{bmatrix} \frac{di_l}{dt} \\ \frac{dv_c}{dt} \end{bmatrix} = \begin{bmatrix} (-\frac{R_L}{L}) - \frac{RR_C}{L(R+R_C)} & -\frac{R}{L(R+R_C)} \\ \frac{R}{(R_C+R)C} & -\frac{1}{(R_C+R)C} \end{bmatrix} \begin{bmatrix} i_l \\ v_c \end{bmatrix} + \begin{bmatrix} \frac{1}{L} \\ 0 \end{bmatrix} v_{in} \quad (17)$$

$$v_o = [\frac{RR_C}{(R+R_C)} \ \frac{1}{R+R_C}] \begin{bmatrix} i_l \\ v_c \end{bmatrix}$$

Using Equations (5) and (6), we obtain the following:

$$\begin{bmatrix} \frac{di_l}{dt} \\ \frac{dv_c}{dt} \end{bmatrix} = \begin{bmatrix} (-\frac{R_L}{L}) - \frac{(1-d)^2RR_C}{L(R+R_C)} & -\frac{(1-d)R}{L(R+R_C)} \\ \frac{R}{(R_C+R)C} & -\frac{1}{(R_C+R)C} \end{bmatrix} \begin{bmatrix} i_l \\ v_c \end{bmatrix} + \begin{bmatrix} \frac{1}{L} \\ 0 \end{bmatrix} v_{in} \quad (18)$$

$$v_o = [\frac{(1-d)RR_C}{(R+R_C)} \ \frac{1}{R+R_C}] \begin{bmatrix} i_l \\ v_c \end{bmatrix}$$

Now, applying perturbation, this will result in the small signal model as:

$$\frac{d}{dt}\begin{bmatrix} \tilde{\imath_l} \\ \tilde{v_c} \end{bmatrix} = \begin{bmatrix} (-\frac{R_L}{L}) - \frac{(1-d)^2RR_C}{L(R+R_C)} & -\frac{(1-D)R}{L(R+R_C)} \\ \frac{(1-D)R}{(R_C+R)C} & -\frac{1}{(R_C+R)C} \end{bmatrix} \begin{bmatrix} \tilde{\imath_l} \\ \tilde{v_c} \end{bmatrix} + \begin{bmatrix} \frac{1}{L} & \frac{v_o}{L} + \frac{(1-DRR_CI_L)}{L(R+R_C)} \\ 0 & -\frac{RI_L}{C(R+R_C)} \end{bmatrix} \begin{bmatrix} \widetilde{v_{in}} \\ \tilde{d} \end{bmatrix} \quad (19)$$

$$v_o = \begin{bmatrix} \frac{(1-D)RR_C}{(R+R_C)} & \frac{C}{R+R_C} \end{bmatrix} \begin{bmatrix} \tilde{\imath_l} \\ \tilde{v_c} \end{bmatrix} + \begin{bmatrix} 0 - \frac{RR_CI_L}{R+R_C} \end{bmatrix} \begin{bmatrix} \widetilde{v_{in}} \\ \tilde{d} \end{bmatrix}$$

$$\frac{\widetilde{v_o}(s)}{\tilde{d}(s)} =$$

$$\frac{s\left[\left(\frac{(1-D)RR_C}{(R+R_C)}\right)\left(\frac{v_o}{L}+\frac{(1-D)RR_CI_L)}{L(R+R_C)}\right)-\frac{R^2I_L}{C(R+R_C)^2}\right]+\left(\frac{v_o}{L}+\frac{(1-D)RR_CI_L)}{L(R+R_C)}\right)\left[\left(\frac{(1-D)RR_C}{C(R+R_C)^2}\right)+\left(\frac{R^2(1-D)}{C(R+R_C)^2}\right)\right]-\frac{R^2I_L}{C(R+R_C)^2}\left(\frac{R_L}{L}+\left(\frac{(1-D)^2RR_C}{L(R+R_C)}\right)\right)+\frac{(1-D)^2R}{LC(R+}}{s^2+s\left[\left(\frac{R_L}{L}\right)+\frac{(1-d)^2RR_C}{L(R+R_C)}+\frac{1}{(R_C+R)C}\right]+\left[\frac{R_L}{L}+\left(\frac{(1-D)^2RR_C}{L(R+R_C)}\right)\right]\left[\frac{1}{(R_C+R)C}\right]+\frac{(1-D)^2R^2}{CL(R+R_C)^2}} \quad (20)$$

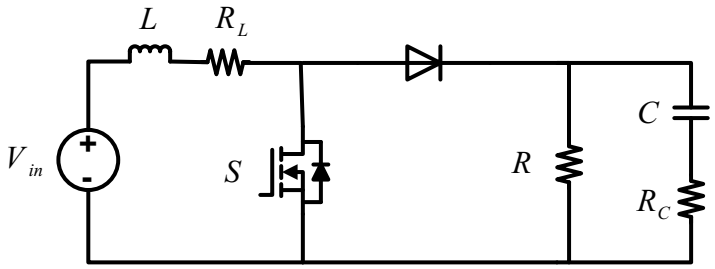

Figure 5.2. Boost converter considering parasitic components.

5.3 Controller Design and Simulation

5.3.1 Super-Fast Sliding Mode Controller

Many works have been done to apply the SM controller to the DC-DC converters [21-24]. The main issue with all mentioned works is having a slow dynamical response. Both the output voltage error and the inductor-current error are controlled in the proposed SFSM controller. It is possible to accurately regulate the output voltage by adopting the output-voltage error as a state variable, and the inductor-current error allows the inductor current to follow the desired reference inductor current closely. Like conventional current-mode controllers, RHPZ converters need to monitor and track the inductor-current reference in order to maintain dynamic response [25].

The logic state of power switch can be represented by the switching function u = 1/2(1 + sign(S)), where u represents the logic state of the switch.

A linear combination of three state variables is used as the sliding surface of the proposed controller, i.e.,

$$S = \alpha_1 x_1 + \alpha_2 x_2 + \alpha_3 x_3 \qquad (21)$$

where α1, α2, and α3 represents the sliding coefficients.

As a controlled state variable, we are using the current error x_1, the voltage error x_2, and the integral of the current and voltage errors x_3, which is expressed as follows:

$$\begin{cases} x_1 = i_{\text{ref}} - i_L \\ x_2 = V_{\text{ref}} - v_o \\ x_3 = \int [i_{\text{ref}} x_1 + V_{\text{ref}} x_2] dt \end{cases} \quad (22)$$

Inductor current i_L is the instantaneous current through the inductor.

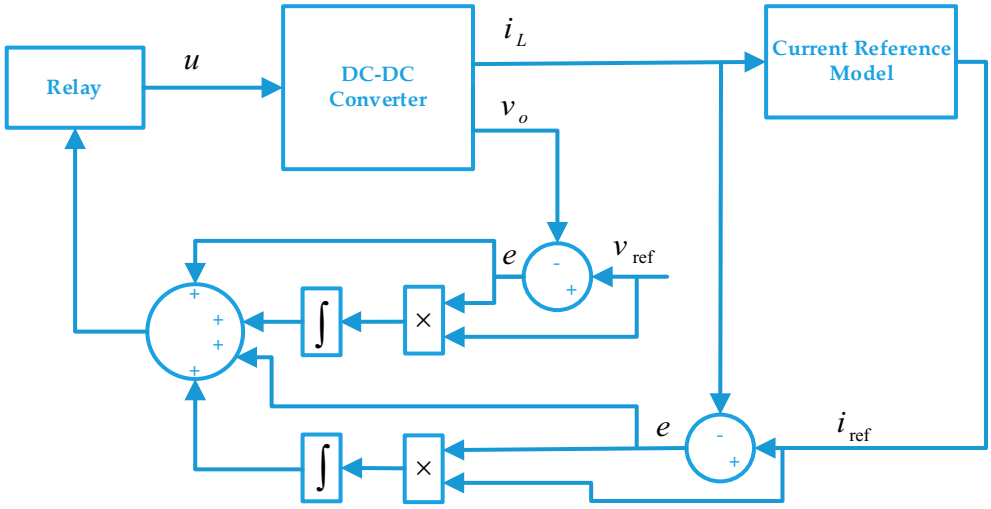

Fig. 5.3. SFSM control system.

Figure 5.3 depicts the SFSM system's fundamental block diagram. As indicated in the diagram, v_{ref} represents the voltage reference, whereas v_o is the output of the real plant, with e denoting the difference between them. Also, i_{ref} indicates the inductor current reference model. It is possible to have both steady-state voltage errors and inductor current errors, such that $v_o \neq v_{ref}$ and $i_L \neq i_{ref}$. For reducing these steady-state errors, an integral term x_3 has been introduced into the SFSM current controller as an additional controlled state variable. This is commonly known as integral SM control [26], and the application of this material in power converters has attracted some recent attention [27]– [29]. Although the integral term reduced the steady-state error, cause

longer transient response. The terms i_{ref} and v_{ref} which are presented in term x_3, will compensate the mentioned drawback, and make a faster algorithm.

5.3.2 Stability Analysis

Lyapunov stability theory was introduced in [30]. Lyapunov proposed two methods of demonstrating stability in his original work of 1892. The first method developed the solution into a sequence, which then proved to be convergent within parameters. Another approach, known as the Lyapunov stability criterion or direct method, uses an analogy of the potential function of classical dynamics with the Lyapunov function $V(x)$. For a system as $\dot{x} = f(x)$, if the Lyapunov function has three following conditions:

$$V(x) = 0 \text{ if and only if } x = 0$$

$$V(x) > 0 \text{ if and only if } x \neq 0$$

$$\dot{V}(x) < 0$$

The system is stable in the sense of Lyapunov.

By considering the following function as the Lyapunov function,

$$V = S^2 \tag{28}$$

the mentioned equation can be rewritten as

When $S > 0$,

$$\dot{S} = -\alpha_1 \frac{V_{in}}{L} - \alpha_2 \frac{v_o}{RC} + \alpha_3 (k+1)(v_{\text{ref}} - v_o) - i_L < 0 \tag{29}$$

When $S < 0$,

$$\dot{S} = \alpha_1 \left(\frac{v_o}{L} - \frac{V_{in}}{L}\right) + \alpha_2 \left(\frac{i_C}{C}\right) + \alpha_3 (k+1)(v_{\text{ref}} - v_o) - i_L > 0 \tag{30}$$

Now, by defining the coefficient α_1, α_2, and α_3 such that the equations (29) and (30) are valid, the system is stable in the sense of Lyapunov.

5.4 Simulation Results

Simulink is an extension to Matlab that allows you to create dynamic models in Windows. The benefit is that models are inserted as block diagrams once the target system's matching mathematical equations are established. To simulate an electrical system, such as a DC-DC converter, one must enter equations for various blocks in the system and use icons in Simulink to create an analogous block diagram. Individual icon settings can be defined for the process. Finally, an equation solver and simulation duration are selected.

In this simulation, the inductor is $L = 0.16 \times 10^{-3}\ H$, the capacitor is $C = 0.1 \times 10^{-3}\ F$, the resistor is $R = 100\ \Omega$, and the input voltage source is considered to be $V_{in} = 100\ V$. Therefore, the transfer function of the boost converter, which gives the output voltages in terms of duty ratio, is:

$$\frac{\widetilde{v_o}(s)}{\tilde{d}(s)} = \frac{(1-0.5)100-(0.16\times10^{-3})(10)s}{(0.16\times10^{-3})(0.1\times10^{-3})s^2+\frac{0.166\times10^{-3}}{100}s-(0.5)^2} \quad (35)$$

Where the reference input is 100V, and the model reference block of the inductor current is a 1st order transfer function with a pole far enough from the origin. The mentioned block is shown in the following equation:

$$\frac{i_{ref}}{I_L} = \frac{1}{0.001s+1} \quad (36)$$

The model is a first-order system with a pole laying on the left-hand side of the complex plane. The feedback loop with the sliding mode controller coefficients illustrated in Figure 4.4 below.

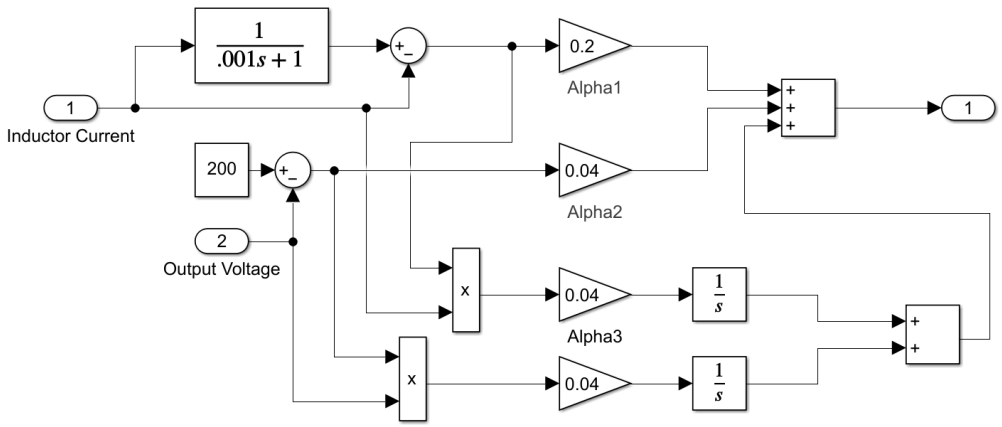

Fig. 5.4. Feedback loop

Finally, the whole Simulink diagram of the DC-DC boost converter system and the designed controller is shown in Figure 5.5. As shown in Figure 5.5, there is a PWM generator to produce pulses which is vital as an input of the switching component.

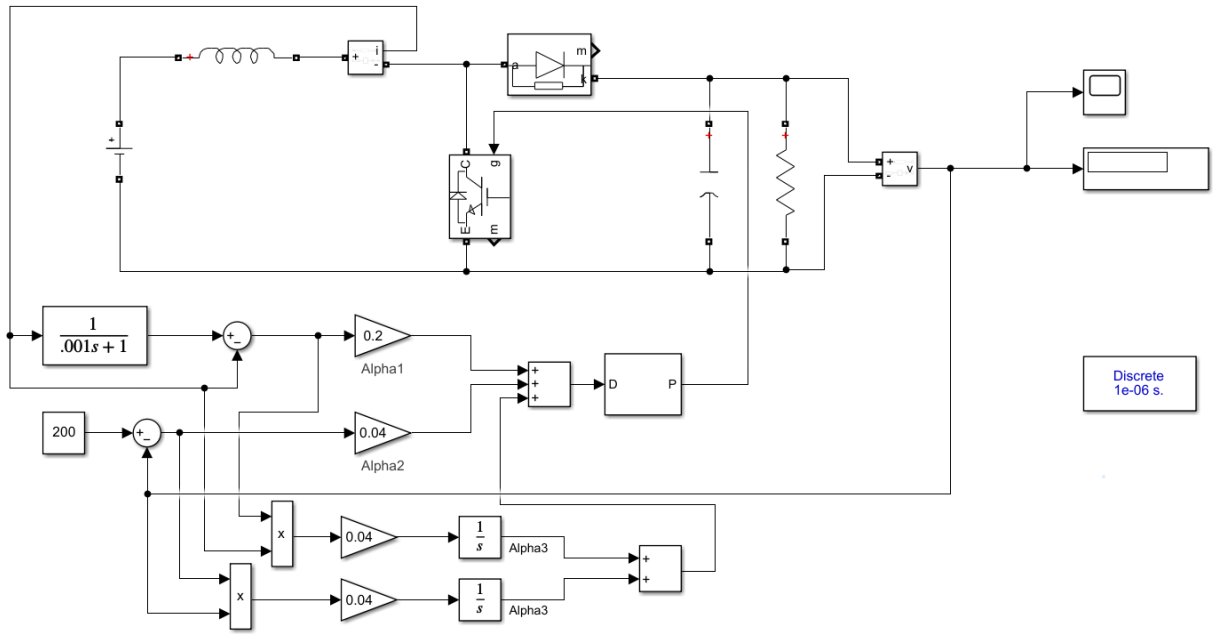

Fig. 5.5. The Simulink Block diagram of the Boost converter and the SFSM controller

Simulations were carried out to verify the controller's capabilities for dc-dc converters that achieve voltage regulation. The switching frequency is considered 2kHz. As load variation is expected in

a typical MG, the proposed controller's effectiveness and robustness are validated through load variations. The transient response of the step-up converter is illustrated in Figure 5.6a when the reference voltage is V = 200V. The output signal reaches the reference value set at ~ 0.02s. The overshoot is ~ 60V. In the case of the change in load (from R = 100Ω to R = 150 Ω), the worst-case settling time shown in Figure 5.6a (in the right figure magnifier) was obtained as ~0.0.3s with a maximum overshoot of ~60V.

The control signal generates the desired value of the duty cycle, which is updated by the introduced sliding mode to obtain the desired voltage and connect it to the PWM. This duty cycle change changes the output voltage to reduce the error signal to zero.

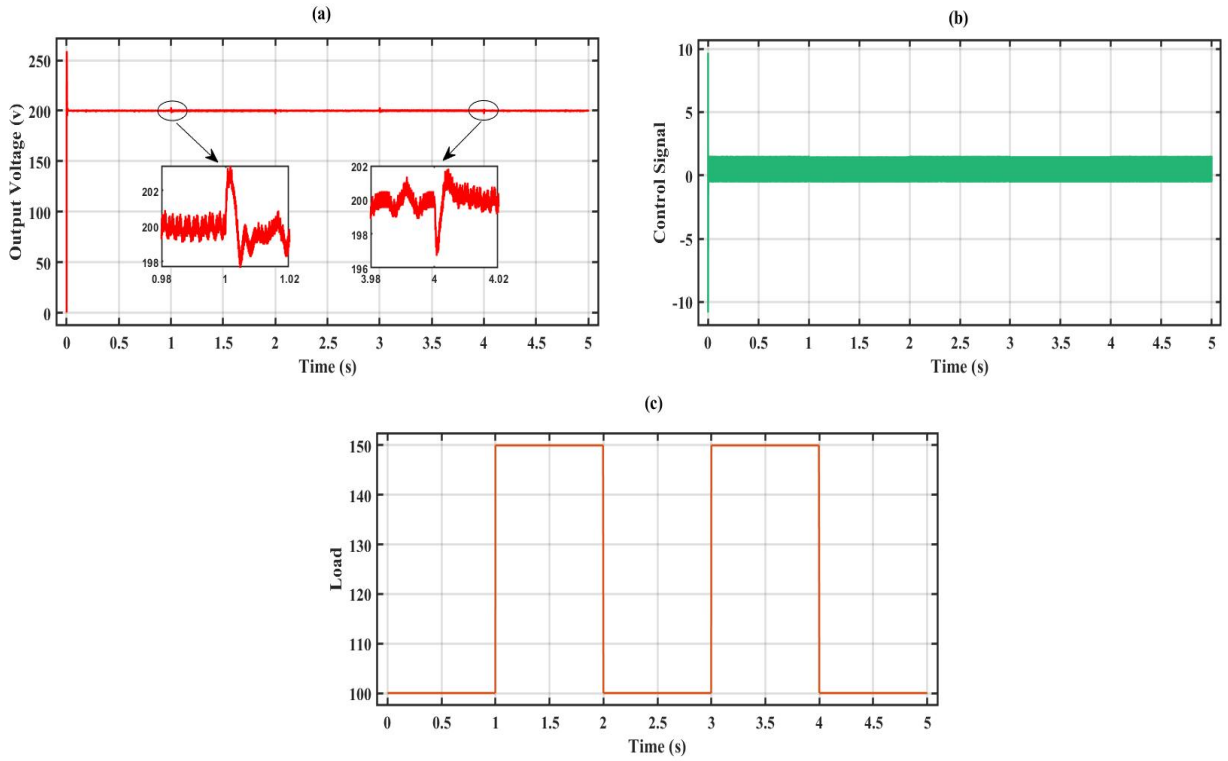

Fig. 5.6. Simulation results: (a) The DC-DC converter transient output voltage and the responses to the load changes from 100Ω to 150Ω (and vice-versa), (b) Control signal waveform for the load changes, and (c) Load resistance changes from 100Ω to 150Ω (and vice-versa).

In the other case, as the output of the PV system is connected to a DC-DC converter in the considered MG is not stable, the input voltage of the DC-DC converter is changed, and the results are shown in Figure 5.7. The input voltage is changed by 20 V from 100V to 120V (and vice-versa), and the worst overshoot response is less than ~8V. It means that the maximum overshoot in the effect of input voltage changing is less than ~4%.

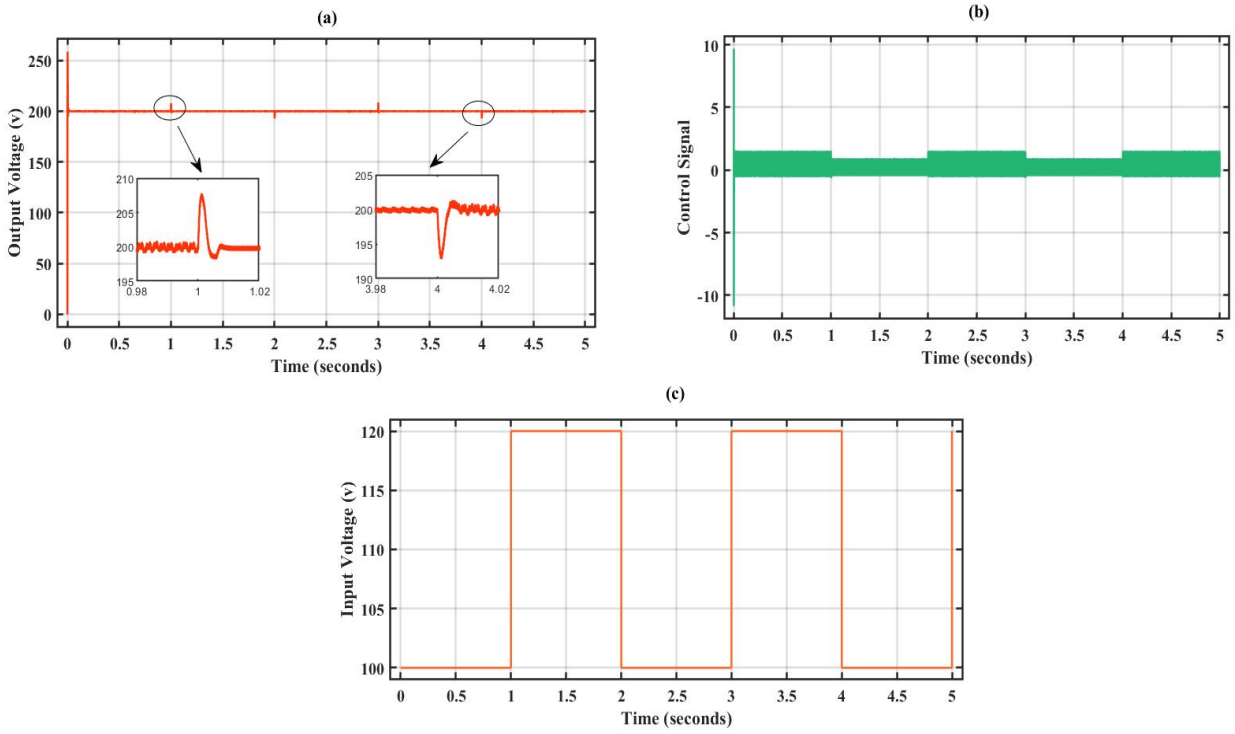

Fig. 5.7. Simulation results: (a) The DC-DC converter transient output voltage and the responses to the input voltage changes from 100V to 120V (and vice-versa), (b) Control signal waveform for the input voltage changes, and (c) Input voltage changes from 100V to 120V (and vice-versa).

5.5 Conclusion

This work presents a super-fast sliding mode controller to regulate the output voltage of the DC-DC converters that exist in an isolated MG. The output voltage control can be achieved using inductor current control. With this controller, boost converters are capable of providing large-

signal performance and fast dynamics. A variety of operating conditions can be handled by the proposed controller. Regardless of the operating conditions, settling time varies only slightly.

The proposed controller and the model are tested in MATLAB/SIMULINK for load disturbances. The load was changed by ~50% of its original value, and the worst-case settling time and maximum overshoot were less than 0.01 s and 4%, respectively, as compared to well-tuned PID controllers. The control scheme is implemented with a single output voltage feedback sensor, so no additional sensing circuitry was required.

The limitation of the proposed design is that the time delay effect on stability was not studied. Additionally, the simulation parameters were ideal. In future research work, the mentioned limitations will be addressed.

References

[1] Maneesh, K, and Barjeev, T. A state of art review of microgrid control and integration aspects. *IEEE International conference IICPE*, 2016. p. 1–6.

[2] Forouzesh, M.; Siwakoti, Y. P.; Gorji, S. A.; Blaabjerg, F. and Lehman, B. A survey on voltage boosting techniques for step-up DC-DC converters. IEEE Energy Conversion Congress and Exposition (ECCE), Milwaukee, WI, USA, 2016. P. 1-8.

[3] Mamarelis, E.; Petrone, G.; and Spagnuolo, G. Design of a sliding mode controlled SEPIC for PV MPPT applications. *IEEE Transactions on Industrial Electronics* 2014; 61(7): 3387-3398.

[4] Young, M. *The Technical Writer's Handbook,* Mill Valley, CA: University Science, 1989.

[5] Rajakumari R. F. and Deshpande, M. Comparative Analysis of DC-DC Converters. 2nd International Conference on Power and Embedded Drive Control (ICPEDC), Chennai, India, 2019. p. 504-509.

[6] Zaitu, R. Voltage Mode Boost Converter Small Signal Control Loop Analysis Using the TPS61030. Application Report, Texas Instruments, 2007.

[7] F. A. Himmelstoss, J. W. Kolar, and F. C. Zach, "Analysis of a smith predictor-based control concept eliminating the right-half plane zero of continuous mode boost and buck-boost DC/DC converters," in Proc. Int.Conf. IECON, Nov. 1991, pp. 423–428.

[8] Perry, A. G.; Feng, G.; Liu, Y. F. and Sen, P. C. A design method for PI-like fuzzy logic controller for DC-DC converter. *IEEE Transactions on Industrial Electronics* 2007; 54(5): 2688-2695.

[9] Aldo, B.; Corsanini, D.; Landi, A. and Sani, L. Circle based Criteria for performance evaluation of controlled DC-DC Switching Converters. *IEEE Transactions on Industrial Electronics* 2006; 53(6): 1862-1869.

[10] Zhang, J.; Shu-Hung Chung, H.; Lo, W. L. and Ron Hui, S. Y. Implementation technique for design of switching Regulators Using Genetic Algorithm. *IEEE Transactions on power electronics* 2001; 16(6): 752-763.

[11] Hung, J. Y.; Gao, W. and Hung, J. C. Variable structure control: A survey. *IEEE Transactions on Industrial Electronics* 1993; 40(1): 2-22.

[12] Tang, K.L., and Mulholland, R. J. Comparing Fuzzy logic with classical controller design. *IEEE Transactions on Systems, Man and cybernetics* 1987; 6: 1085-1087.

[13] Nelms, R. M.; Guo, L.; Hung, J, H. Digital Controller design for Buck and Boost Converters Using Root Locus Technique. In proc. 29th Annual Conference of the IEEE Industrial Electronics Society, Roanoke, VA, 2003; 2: 1864-1869.

[14] Rashid, U.; Jamil, M.; Gilani, S. O. and Niazi, I. K. LQR based Training of Adaptive Neuro-Fuzzy Controller. 25th Italian Workshop on Neural Networks, 2015. p. 311-322.

[15] E. Figueres, G. Garcera, J. M. Benavent, M. Pascual, and J. A. Martinez, "Adaptive two-loop voltage-mode control of DC–DC switching converters," IEEE Trans. Ind. Electron., vol. 53, no. 1, pp. 239–253, Feb. 2006.

[16] K. H. Cheng, C. F. Hsu, C. M. Lin, T. T. Lee, and C. Li, "Fuzzy neural sliding-mode control for DC–DC converters using asymmetric Gaussian membership functions," IEEE Trans. Ind. Electron., vol. 54, no. 3, pp. 1528–1536, Jun. 2007.

[17] M. Castilla, L. G. de Vicuna, J. M. Guerrero, J. Matas, and J. Miret, "Sliding-mode control of quantum series-parallel resonant converters via input–output linearization," IEEE Trans. Ind. Electron., vol. 52, no. 2, pp. 566–575, Apr. 2005.

[18] E. Vidal-Idiarte, L. Martinez-Salamero, J. Calvente, and A. Romero, "An H∞ control strategy for switching converters in sliding-mode current control," IEEE Trans. Power Electron., vol. 21, no. 2, pp. 553–556, Mar. 2006.

[19] Kahani R, Jamil M, Iqbal MT. Direct Model Reference Adaptive Control of a Boost Converter for Voltage Regulation in Microgrids. Energies. 2022 Jul 12;15(14):5080.

[20] Schmidt S, Richter M, Oberrath J, Mercorelli P. Control oriented modeling of DCDC converters. IFAC-Papers Online, 2018; 51(2): 331-336.

[21] Y. He and F. L. Luo, “Sliding-mode control for DC–DC converters with constant switching frequency,” Proc. Inst. Electr. Eng.—Control Theory and Applications, vol. 153, no. 1, pp. 37–45, Jan. 2006.

[22] Y. He and F. L. Luo, “Design and analysis of adaptive sliding-mode like controller for DC–DC converters,” Proc. Inst. Electr. Eng.—Electric Power Applications, vol. 153, no. 3, pp. 401–410, May 2006.

[23] S. C. Tan, Y. M. Lai, and C. K. Tse, “A unified approach to the design of PWM based sliding mode voltage controller for basic DC–DC converters in continuous conduction mode,” IEEE Trans. Circuits Syst. I, Reg. Papers, vol. 53, no. 8, pp. 1816–1827, Aug. 2006.

[24] S. C. Tan, Y. M. Lai, C. K. Tse, and L. Martinez-Salamero, “Special family of PWM-based sliding mode voltage controllers for basic DC–DC converters in discontinuous conduction mode,” IET Elect. Power Appl., vol. 1, no. 1, pp. 64–74, Jan. 2007.

[25] Tan SC, Lai YM, Chi KT, Martínez-Salamero L, Wu CK. A fast-response sliding-mode controller for boost-type converters with a wide range of operating conditions. IEEE Transactions on Industrial Electronics. 2007 Nov 19;54(6):3276-86.

[26] V. Utkin, J. Guldner, and J. X. Shi, Sliding Mode Control in Electromechanical Systems. London, U.K.: Taylor & Francis, 1999.

[27] G. Escobar, R. Ortega, H. Sira-Ramirez, J. P. Vilain, and I. Zein, “An experimental comparison of several nonlinear controllers for power converters,” IEEE Control Syst. Mag., vol. 19, no. 1, pp. 66–82, Feb. 1999.

[28] S. K. Mazumder, A. H. Nayfeh, and D. Borojevi´c, “Robust control of parallel DC–DC buck converters by combining integral-variable-structure and multiple-sliding-surface control schemes,” IEEE Trans. Power Electron., vol. 17, no. 3, pp. 428–437, May 2002.

[29] H. Sira-Ramirez, “On the generalized PI sliding mode control of DC-DC power converters: A tutorial,” Int. J. Control, vol. 76, no. 9/10, pp. 1018–1033, 2003.

[30] Lyapunov, A. M. The General Problem of the Stability of Motion (In Russian), Doctoral dissertation, University Kharkov, English translation, 1892.

Chapter 6

Conclusion and Future Work

6.1 Conclusion

In this study, Matlab/Simulink has been used to examine the tracking efficiency of photovoltaic (PV) power production. The plan is to minimize the loss caused by the losing direction while minimizing steady-state oscillation. To stop PV power from fluctuating around the peak, a redesigned perturb and observe (P&O) algorithm was provided. The efficacy of the algorithm depends on its capacity to correctly identify oscillation and add a boundary condition that stops it from drifting drastically away from the maximum power point (MPP). Additionally, the algorithm can follow the maximum power point tracking (MPPT) with customizable step sizes thanks to the optimized duty cycle. Implementing the suggested method results in an average improvement over the incremental conductance (InC) algorithm and traditional P&O of roughly 3.1 percent for abrupt irradiance fluctuations.

Additionally, by increasing efficiency by 0.5 percent for both slow and fast irradiance changes, the improved P&O algorithm outperforms the traditional P&O method in dynamic irradiance changes. Furthermore, under strong partial shading circumstances (PSC) and drift avoidance tests, the new technique outperformed the standard algorithms on average by approximately 9% and 8%, respectively. By taking into account the findings, it is confirmed that under a variety of environmental changes, the improved P&O algorithm may monitor the irradiance profile with a slight departure from MPPs. As a result, additional power loss is reduced, and tracking precision

is improved. The original algorithm's structure is preserved in the modified version, making the former easier to implement.

In the second phase of the research, we offer an adaptive controller to adjust the output voltage of the DC-DC converters of PV systems. It becomes difficult to create a controller that just uses output voltage feedback since the converter system is a non-minimum phase. Although inductor current control can be used to regulate output voltage, other states, such as output and inductor currents in feedback, may also be necessary for these current mode controllers. Two control loops in this study steady the output voltage. The output voltage is fixed using a PID controller, and the outer loop implements the direct model reference adaptive controller (DMRAC) MIT rule.

Using only an output voltage feedback sensor, the DMRAC adjusts the PID controller parameters in real-time to make sure the current system tracks the desired reference model.

In MATLAB/SIMULINK, the proposed controller and the model are tested for load disturbances. The load was altered by about 50% of its initial amount, and when compared to properly tuned PID controllers, the worst-case settling time and maximum overshoot were less than 0.1 s and 0.5 V, respectively. A hardware validation is also done to demonstrate how well the suggested controller performs. Our findings imply that the DMRAC offers reliable regulation against parameter changes. It can therefore be used in any isolated micro-grid (MG).

A single output voltage feedback sensor is used to accomplish the control strategy; therefore, no additional sensing circuitry was required.

Finally, a super-fast sliding mode controller presented for DC-DC output voltage tracking with fast dynamical responses. The proposed controller and the model are tested in MATLAB/SIMULINK for load disturbances. The load was changed by ~50% of its original value, and the worst-case settling time and maximum overshoot were less than 0.01 s and 4%, respectively.

6.2 Research Contribution/Problem Solutions

The contribution of this research work for the modified P&O MPPT algorithm is summarised below.

1. A novel MPPT algorithm with a set of features such as: improving the efficiency of conventional P&O algorithm by 0.5 percent for both slow and fast irradiance changes, and improving the efficiency of the traditional methods on average by about 9% and 8% under strong partial shading situations (PSC) and drift avoidance tests, respectively.
2. An adaptive controller is designed to regulate the output voltage of the DC–DC converters in a PV system.
3. This thesis proposes a novel output voltage regulation approach that can adjust the parameters of the PID controller in real-time to ensure that the actual system is following the desired reference model.
4. We used Trina Solar TSM-250PA05.08 in 4 parallel strings with 10 modules per series strings in the simulations on MATLAB/Simulink, which is prepared to indicate the proposed algorithm's performance.
5. The average for the conventional P&O and the modified P&O in the slow ramp zone (20 $W/m^2/s$) is 96.19 percent and 96.68 percent, respectively. When the insolation changes quickly (50 $W/m^2/s$), the conventional P&O and the modified P&O efficiencies are 96.23 percent and 96.72 percent, respectively.
6. The EN 50530 MPPT efficiency test is used to evaluate the proposed algorithm in dynamic weather conditions.

7. Tests of the proposed MPPT algorithm have been conducted for an insolation level step shift from 300 to 700 W/m^2 in 0.1 s.

For the output voltage regulation of the PV systems, the following solutions are considered.

1. Simulations were carried out to verify the controller's capabilities for DC–DC converters that achieve voltage regulation. The switching frequency is considered 2 kHz.
2. The input voltage is changed by 2 V from 8 V to 10 V (and vice-versa), and the worst overshoot response is less than ∼1 V. It means that the maximum overshoot in the effect of input voltage changing is less than ∼6.6%.
3. The Arduino Uno is used to interface Simulink's DMRAC controller and the DC–DC boost converter circuit to implement hardware in the loop.

6.3 Future Work

As a part of future work, we aim to improve the introduced MPPT algorithm for fast convergence at the operating point. Besides the response time, the efficiency can also be improved. Moreover, it is still possible to consider the algorithms in case of cost, hardware implementation, and applications. In addition, the computations should not be that complex to lead to large memory requirements. Also, the industry still needs a general solution for different cases of environmental conditions. So, the future modified algorithms should have high efficiency in different ambient factors, such as high temperature. Not just limited to the slow and fast irradiation changes, PSC, and drift effects.

Moreover, time delay effect can be considered for the proposed DMRAC and super-fast sliding mode controller. Additionally, the simulation parameters were ideal. In future research work, the mentioned limitations should be addressed. It will be also better to consider more load and input voltage variations for these controllers.

Articles in Refereed Publications

- **R. Kahani**, M. Jamil, MT. Iqbal, "A Novel Dynamic MPPT Algorithm for Photovoltaic Power Systems" *Journal of Modern Power Systems and Clean Energy (MPCE)*, September 2022.
- **R. Kahani**, M. Jamil, MT. Iqbal, "Direct Model Reference Adaptive Control of a Boost Converter for Voltage Regulation in Microgrids". *Energies*, 12;15(14):5080, July 2022.
- **R. Kahani**, M. Jamil, MT. Iqbal, " Super-Fast Sliding Mode Control of a Boost Converter for Voltage Tracking in Microgrids". Submitted in *Energies*, October 2022.
- **R. Kahani**, M. Jamil, MT. Iqbal, " Maximum Power Point Tracking (MPPT) Modified Algorithms Survey". Submitted in the *Journal of Renewable and Sustainable Energy Reviews,* October 2022.

Regional Conference Publications

- **R. Kahani** and M. Jamil, "Designing a Model Reference Adaptive Controller for a DC-DC Boost Converter" *the 30th Annual Newfoundland Electrical and Computer Engineering Conference (NECEC), 2021.*